FACULDADE DE ENGENHARIA DA UNIVERSIDADE DO PORTO

Real-Time Overwater Wireless Network Design

Miguel José Gutiérrez Gaitán

Doctoral Program in Electrical and Computer Engineering

Advisor: Prof. Dr. Luís Miguel Pinho de Almeida

Co-Advisor: Dr. Pedro Miguel Salgueiro dos Santos

Co-Advisor: Dr. Pedro Miranda de Andrade de Albuquerque d'Orey

February 6, 2023

Real-Time Overwater Wireless Network Design

Miguel José Gutiérrez Gaitán

Doctoral Program in Electrical and Computer Engineering

Approved by:

President: Prof. Dr. Jaime dos Santos Cardoso
Referee: Dr. Svetlana Girs
Referee: Dr. Thomas Watteyne
Referee: Prof. Dr. Rui Lopes Campos
Advisor: Prof. Dr. Luís Miguel Pinho de Almeida
Co-Advisor: Dr. Pedro Miguel Salgueiro dos Santos
Co-Advisor: Dr. Pedro Miranda de Andrade de Albuquerque d'Orey

February 6, 2023

Abstract

This dissertation addresses various communication and networking challenges that arise when dealing with the design of *real-time* wireless networked systems operating *over water* environments. The end goal is to build up a comprehensive and tailored *cross-layer* framework that considers physical, data link, and network layer elements for improved real-time and overwater wireless communication performance *by design*. In this direction, we first focus on mitigating distinctive physical factors in overwater RF propagation (e.g. tides, intertidal zones) to then address upper-layers design considerations related to the improvement of traffic *schedulability*, i.e. the ability of the network to satisfy explicit timing constraints (e.g. packet deadlines). In particular, due to the layered structure of these research challenges, we organize our studies into two separate action domains: *i*) *overwater*, involving physical layer factors of communication, and *ii*) *real-time*, which entails both data link and network layers aspects.

In terms of *overwater* communication, special emphasis has been placed on investigating the impact of tides on link quality, and how tailored design strategies can help mitigate such an issue. To this aim, we first investigate overwater RF propagation from the perspective of channel modeling and characterization to then capitalize this understanding into novel design methods that effectively improve link quality (e.g. received power). Specifically, we propose an approach that uses a tidal-informed two-ray propagation model to provide both static (e.g. sensor nodes) and mobile nodes (e.g. autonomous vessels) with better design options for antenna height and positioning. We also present a novel methodology for path loss prediction based on the non-trivial integration of the two-ray propagation model with precise location-dependent hydrodynamics (i.e. tidal model). A key aspect of this methodology is the ability to account for a reflective surface of varying altitude and permittivity as a function of the tide. This feature is crucial for an accurate path loss estimation over water environments with characteristic *intertidal zones*.

In terms of *real-time* communication, we aim to improve the real-time performance of globally time-synchronized wireless mesh networks (e.g. TSCH-based). Within this context, we endorse the idea of judicious *gateway designation* for enhanced traffic schedulability at system's design time. Concretely, we introduce the concept of *network centrality* from social network analysis (SNA) as an effective heuristic for gateway designation that facilitates real-time communication. We also generalize this idea to multiple gateways with the aid of the unsupervised learning method of *spectral clustering*. More importantly, we propose a novel metric termed *minimal overlap centrality* which conveniently exploits the relationship between path node-overlaps and gateway designation for improved network schedulability. In similar fashion, we propose a novel scheme termed *minimal-overlap routing* based on a new greedy heuristic for path-overlap minimization. This strategy increases traffic schedulability regardless of the gateway designation criterion.

In a nutshell, this dissertation offers various, novel, and effective *cross-layer* insights and methods aiming to improve the wireless communication performance of real-time overwater wireless networked systems *by design*. We summarize our major achievements in this direction as follows:

- On the *overwater* action domain, we pioneered research studies on the large-scale fading impact of *tides* and *intertidal zones* in short and medium range *shore-to-shore* and *shore-to-vessel* RF communication links. This understanding led us to propose novel methods for link design and link-quality prediction able to mitigate/anticipate changes due to tides of up to 20 dB. Notably, our experimental measurements using commodity technologies (e.g. LoRa, WiFi) in different overwater settings (e.g. estuaries, marinas) showed major trends of the received power in agreement with the proposed methods.
- On the *real-time* side, we brought to the forefront a new dimension in the design of real-time wireless sensor networks (RT-WSNs), complementing the more common approaches based on real-time scheduling or routing. Specifically, we introduced the idea of *centrality-driven gateway designation* and proposed a new metric resorting to the minimization of path overlaps. We showed by simulations that our novel *minimal-overlap* centrality achieves up to 50% better traffic schedulability than traditional metrics in SNA. Likewise, a *minimal-overlap* routing was proposed to enhance schedulability regardless of gateway designation.

We claim these original research findings constitute initial but promising results towards our end goal of building up a comprehensive cross-layer design framework specifically proposed to improve wireless communication performance in real-time and overwater networked systems.

Keywords: Wireless Networks, Real-Time Communication, Internet of Things.

This work was partially supported by National Funds through FCT/MCTES (Portuguese Foundation for Science and Technology), within the CISTER (UIDB/04234/2020), within the AQUAMON project (PTDC/CCI-COM/30142/2017), and by FCT and the ESF (European Social Fund) through the Regional Operational Programme (ROP) Norte 2020, under PhD grant 2020.06685.BD.

Resumo

Esta dissertação aborda vários desafios de comunicação e networking que surgem quando se trata do design de sistemas em rede sem fios *em tempo real* que operam *sobre ambientes de água*. O objetivo final é construir uma estrutura abrangente e personalizada de *camadas cruzadas* que considere elementos das camadas física, de ligação de dados e rede para um melhor desempenho de comunicação sem fios em tempo real e sobre-água *por design*. Neste sentido, focamo-nos primeiro na mitigação de fatores físicos distintivos na propagação de RF sobre a água (por exemplo, marés, zonas inter-marés) para, em seguida, abordar considerações de conceção de camadas superiores relacionadas com a melhoria do *escalonamento* do tráfego, ou seja, a capacidade da rede para satisfazer restrições explícitas de tempo (p. ex., prazos de pacote). Em particular, devido à estrutura em camadas destes desafios de investigação, organizamos os nossos estudos em dois domínios de ação separados: i) *sobre a água*, envolvendo fatores de camada física de comunicação, e ii) *em tempo real*, o que implica tanto aspetos das camadas de ligação de dados e rede.

Em termos de comunicação *sobre a água*, foi dada especial ênfase à investigação do impacto das marés na qualidade das ligações e à forma como estratégias de design adaptadas podem ajudar a mitigar tal problema. Para este objetivo, primeiro investigamos a propagação de RF sobre a água na perspetiva da modelação e caracterização de canais para depois capitalizar este entendimento em novos métodos de design que melhorem efetivamente a qualidade das ligações (por exemplo, o poder recebido). Especificamente, propomos uma abordagem que utiliza um modelo de propagação de dois raios informado pelas marés para fornecer tanto os nós estáticos (p. ex., os nós dos sensores) como os nóns móveis (p. ex., veículos autónomos) com melhores opções de conceção para a altura e posicionamento da antena. Apresentamos também uma nova metodologia para a previsão da perda de caminhos baseada na integração não trivial do modelo de propagação de dois raios com hidrodinâmica precisa dependente da localização (ou seja, modelo de maré). Um aspeto chave desta metodologia é a capacidade de ter em consideração uma superfície refletora de altitude e permissividade variáveis em função da maré. Esta característica é crucial para uma estimativa precisa da perda de caminho sobre ambientes de água com zonas inter-marés características.

Em termos de comunicação *em tempo real*, pretendemos melhorar o desempenho em tempo real das redes mesh sem fios sincronizadas globalmente (por exemplo, baseadas em TSCH). Neste contexto, apoiamos a ideia de designação de gateway criteriosa para uma maior escalonabilidade de tráfego no tempo de conceção do sistema. Concretamente, introduzimos o conceito de *centralidade da rede* a partir da análise das redes sociais (ARS) como uma heurística eficaz para a designação de gateway que facilita a comunicação em tempo real. Generalizamos também esta ideia a múltiplas portas de entrada com a ajuda do método de aprendizagem não supervisionado do *agrupamento espectral*. Mais importante ainda, propomos uma nova *centralidade de sobreposição mínima*, que convenientemente explora a relação entre sobreposições de caminho e a designação do gateway para uma melhor escalonabilidade da rede. Da mesma forma, propomos um novo esquema denominado *encaminhamento de sobreposição mínima* baseado numa nova heurística

gananciosa para a minimização da sobreposição de caminhos. Esta estratégia aumenta a escalonabilidade do tráfego, independentemente do critério de designação do gateway.

Em resumo, esta dissertação oferece vários, novos e eficazes insights e métodos de *camadas cruzadas* com o objetivo de melhorar o desempenho da comunicação de sistemas em rede sem fios em tempo real por design. Resumimos as nossas principais contribuições neste sentido:

- No domínio da ação *sobre a água*, fomos pioneiros em estudos de investigação sobre o impacto em larga escala das *marés* e das *zonas inter-marés* em curto e médio alcance das ligações de comunicação RF de *costa a terra* e de *terra-a-embarcação*.Este entendimento levou-nos a propor novos métodos de conceção de ligações e previsão de qualidade de ligação capazes de mitigar/antecipar mudanças devido a marés de até $\sim$ 20 dB. Nomeadamente, as nossas medições experimentais utilizando tecnologias de mercadorias (p. ex., LoRa, Wi-Fi) em diferentes configurações sobre a água (p. ex., estuários, marinas) mostraram grandes tendências do poder recebido de acordo com os métodos propostos.

- Do lado em *tempo real*, trouxemos para a vanguarda uma nova dimensão no design de redes de sensores sem fios em tempo real (RT-WSNs), complementando as abordagens mais comuns baseadas em agendamento ou encaminhamento em tempo real. Especificamente, introduzimos a ideia de *designação de gateway orientada por centralidade* e propusemos uma nova métrica recorrendo à minimização das sobreposições de caminhos. Mostrámos por simulações que a nossa nova centralidade de *sobreposição mínima* alcança até 50% melhor escalonabilidade de tráfego do que as métricas tradicionais no ARS. Da mesma forma, foi proposto um encaminhamento de sobreposição mínima para aumentar a agendabilidade, independentemente da designação de gateway.

Afirmamos que estes resultados originais da investigação constituem resultados iniciais, mas promissores, para o nosso objetivo final de construir um quadro abrangente de design de camada cruzada especificamente proposto para melhorar o desempenho da comunicação sem fios em sistemas em rede em tempo real e sobre a água.

Palavras-chave: Redes Sem Fios, Comunicação em Tempo Real, Internet das Coisas.

Acknowledgments

The first place in these acknowledgments is for sure for **Luís Almeida**, my PhD advisor. To him, my most heartfelt gratitude and admiration. Not only because of his continuous guidance and support as a supervisor but also for his friendly style, always responsive and constructive, offering clever feedback, and showing tremendous empathy and flexibility.

I'd also like to thank my co-supervisors, **Pedro Santos**, and **Pedro d'Orey**, for their genuine and useful support at different stages of my PhD path. I've been extremely lucky to count on such quality and mature (co-)advice, complementing points of view, and confidence.

To **Thomas Watteyne** and his team at INRIA Paris, France, for their very warm welcome during my stay there, and for showing me an inspiring approach to doing research.

To all my co-authors who somehow have enriched these studies with their valuable perspectives and skills. To **Diego Dujovne** and **Alejandro Figueroa** from Chile, who inspired me to look at new research directions and opportunities. To **Antonio Casimiro**, **José Cecilio**, and **Marta Rodrigues** for their professionalism and teamwork within the context of the AQUAMON project. To **João Sousa** and **Manuel Ribeiro** from LSTS at FEUP, for facilitating us with their cutting-edge equipment and applied use-case insights. To **Patrick Yomsi** and **Luis Pinto** for being two key mentors at the beginning of my research career. To **Ramiro Sámano-Robles** for his constant trust in my abilities and for teaching me complementary visions for my research work.

Special thanks, of course, to **Eduardo Tovar** who first recruited me and then continuously offered me excellent conditions for doing research. To **Sandra**, **Filipe**, **Marwin**, **Cristiana** and **Inês**, for their extraordinarily valuable administrative support.

To all my friends and colleagues at **CISTER** with whom I shared uncountable discussions about (PhD-) life and more. To those I met at the very beginning, **Shashank**, **João**, **Mubarak**, **Ishfaq**, **Aftab**, **Konstantinos**, **Geoffrey**, **Michele**, **Ali**, **Lukas**, **Claudio**, **Harrison**, etc., and to those who then were becoming friends over the years, **Radha**, **Javier**, **Yillian**, **Giann**, **Jatin**, **Enio**, **Laerte**, **Gowhar**, **Yousef**, and **Jingjing**. And to those recently arrived, **Abdul**, **Alam**, **Mohammad**, **Saeid**, **Luis Javier**, **Reydel**, **Sergio** and **Shardul**. To all of you, my gratitude.

To the ones who were or are part of the **DaRTES** crew, **Aqsa**, **Zahid**, **Livio**, **Dimpi**, **Yimin**, **Barikisu**, **Danilo**, **Ottavio**, **Diogo**, and many more, for making my time there enjoyable.

And finally, to my family, for all the precious time I took from yours. I love you.

Miguel Gutiérrez Gaitán

«Everyone must leave something behind when he dies [...]. A child or a book or a painting or a house or a wall built or a pair of shoes made. Or a garden planted. Something your hand touched some way so your soul has somewhere to go when you die, and when people look at that tree or that flower you planted, you're there. **It doesn't matter what you do [...], so long as you change something from the way it was before you touched it into something that's like you after you take your hands away**. The difference between the man who just cuts lawns and a real gardener is in the touching [...]. The lawn-cutter might just as well not have been there at all; the gardener will be there a lifetime»

Extracted from the novel *"Fahrenheit 451"*
(Ray Bradbury, 1953)

Thesis Publications

Journal Articles

[1] M. G. Gaitán, L. Almeida, P. d'Orey, P. Santos and T. Watteyne, "Minimal-Overlap Centrality for Multi-Gateway Designation in Real-Time TSCH Networks", in **ACM Transactions on Embedded Computing Systems** (Under Review).

[2] M. G. Gaitán, P. d'Orey, J. Cecilio, M. Rodrigues, P. Santos, L. Pinto, A. Oliveira, A. Casimiro and L. Almeida, "Modeling LoRa Communications in Estuaries for IoT Environmental Monitoring Systems", in **IEEE Sensors Journal 2022**.

[3] M. G. Gaitán, D. Dujovne, J. Zuñiga, A. Figueroa and L. Almeida, "Multi-Gateway Designation for Real-Time TSCH Networks using Spectral Clustering and Centrality", in **IEEE Embedded Systems Letters 2022**.

Conference Papers

[4] M. G. Gaitán, P. d'Orey, P. Santos, M. Ribeiro, L. Pinto, L. Almeida and J. Sousa, "Wireless Radio Link Design to Improve Near-Shore Communication with Surface Nodes on Tidal Waters", in **IEEE OCEANS 2021**.

[5] M. G. Gaitán, P. Santos, L. Pinto and L. Almeida, "Optimal Antenna-Height Design for Improved Capacity on Over-water Radio Links affected by Tides", in **IEEE OCEANS 2020**.

[6] M. G. Gaitán, P. Santos, L. Pinto and L. Almeida, "Experimental Evaluation of the Two-Ray Model for Near-Shore WiFi-based Network Systems Design", in **IEEE VTC2020-Spring**.

[7] M. G. Gaitán, L. Pinto, P. Santos and L. Almeida, "On the Two-Ray Model Analysis of Overwater Links with Tidal Variations", in **INForum 2019**.

Workshop Papers

[8] M. G. Gaitán, P. d'Orey, P. Santos and L. Almeida, "Minimal-Overlap Centrality-Driven Gateway Designation for Real-Time TSCH Networks", in **RAGE 2022** Workshop, co-located with DAC 2022. **[Best Paper Award]**.

[9] M. G. Gaitán, L. Almeida, T. Watteyne, P. d'Orey, P. Santos and D. Dujovne, "Joint Scheduling, Routing and Gateway Designation in Real-Time TSCH Networks", in **JRWRTC 2022** Workshop, co-located with RTNS 2022.

[10] P. d'Orey, M. G. Gaitán, P. Santos, M. Ribeiro, J. Sousa and L. Almeida, "Empirical Evaluation of Short-Range WiFi Vessel-to-Shore Overwater Communications", in **ACM WINTECH'22 Workshop**, co-located with ACM MobiCom 2022.

[11] M. G. Gaitán, L. Almeida, P. Santos and P. Yomsi, "EDF Scheduling and Minimal-Overlap Shortest-Path Routing for Real-Time TSCH Networks", in **NG-RES 2021** Workshop, co-located with HiPEAC 2021.

WORK-IN-PROGRESS PAPER

[12] M. G. Gaitán, L. Almeida, A. Figueroa and D. Dujovne, "Impact of Network Centrality on the Gateway Designation of Real-Time TSCH Networks", in **IEEE WFCS 2021**. **[Best Work-in-Progress Paper Award]**.

EXTENDED ABSTRACTS, POSTERS AND DEMO

[13] M. G. Gaitán, P. d'Orey, P. Santos, M. Ribeiro, L. Pinto, L. Almeida and J. Sousa, "Improving WiFi communication with surface nodes at near-shore on tidal waters", in **RTCM 2022**.

[14] D. Almeida, M. G. Gaitán, P. d'Orey, P. Santos, L. Pinto and L. Almeida, "Demonstrating RA-TDMAs+ for Robust Communication in WiFi Mesh Networks", in **IEEE RTSS 2021**.

[15] M. G. Gaitán, L. Almeida, A. Figueroa and D. Dujovne, "Network Centrality: An Insight for Gateway Designation in Real-Time Wireless Sensor Networks", in **DCE 2021**.

[16] M. G. Gaitán, L. Almeida, P. Santos and L. Pinto, "Improving Short to Medium Range Communication over Water Tides: Why Does Height Matter?", in **RTCM 2021**.

[17] M. G. Gaitán, P. Santos and L. Almeida, "Real-Time Communication Support for Overwater Wireless Multi-hop Networks", in **BSC Doctoral Symposium 2020**.

[18] M. G. Gaitán, P. Santos, L. Pinto and L. Almeida, "Wi-Fi-Based Network Systems Design Over Freshwater: Experimental Evaluation using COTS devices", in **DSIE 2020**.

[19] M. G. Gaitán, L. Pinto, P. Santos and L. Almeida, "An analysis of the Two-Ray model to Support Near-Surface Overwater Wireless Sensor Networks Design", in **DCE 2019**.

Other Publications (as Ph.D. student)

Journal Articles

[20] M. G. Gaitán and P. Yomsi, "Multiprocessor Scheduling Meets the Industrial Wireless: A Brief Review", in **U. Porto Journal of Engineering 2019**.

Conference Papers

[21] M. G. Gaitán, R. Sámano-Robles and J. R. Gonzalez, "Outage Probability of V2V Multiple-Antenna Rice Fading Links with Explicit Ground Reflection", in **IEEE GLOBECOM 2022**.

[22] M. G. Gaitán and R. Sámano-Robles, "Orthogonal Space-Time Block Coding for V2V LOS Links with Ground Reflections", in **MIKON 2022**.

[23] E. De La Fuente and M. G. Gaitán, "LibreDTE: Software Tools and Support for Electronic Invoicing in Chile", in **SCCC 2022**.

[24] R. Reddy, L. Almeida, M. G. Gaitán, P. Santos and E. Tovar, "Synchronous Framework Extended for Complex Intersections", in **EWGT 2021**.

[25] M. G. Gaitán and R. Sámano-Robles, "In-Tunnel Multi-Ray Analysis for LOS V2V Links with Multiple Antennas", in **IEEE WF-IoT 2021**.

[26] M. G. Gaitán and R. Sámano-Robles, "On the Optimum Number of Antennas for V2V LOS Links with Ground Reflection", in **IEEE LAMC 2021**.

[27] F. Lizana, R. Tello, M. G. Gaitán, D. Ruete and C. Gómez, "Building a Text Messaging-Based System to Support Low-Cost Automation in Household Agriculture", in **INGELECTRA 2020**.

[28] A. H. Farzamiyan, M. G. Gaitán and R. Sámano-Robles, "A Multi-ray Analysis of LOS V2V Links for Multiple Antennas with Ground Reflection", in **AEIT 2020**.

Work-in-Progress Papers

[29] R. Reddy, L. Almeida, M. G. Gaitán, H. Kurunathan, P. Santos and E. Tovar, "Work-in-progress: Worst-case response time of intersection management protocols", in **IEEE RTSS 2021**.

[30] M. G. Gaitán, P. Yomsi, P. Santos and L. Almeida, "Work-in-progress: Assessing supply/demand-bound based schedulability tests for wireless sensor-actuator networks", in **IEEE WFCS 2020**.

[31] M. G. Gaitán and P. Yomsi, "FF-DBF-WIN: On the forced-forward demand-bound function analysis for wireless industrial networks", in **ECRTS 2018**.

Extended Abstracts and Posters

[32] R. Reddy, L. Almeida, M. G. Gaitán, P. Santos and E. Tovar, "Sustainability analysis of complex multi-lane intelligent signalized intersections", in **DCE 2021**.

[33] R. Reddy, L. Almeida, M. G. Gaitán, P. Santos and E. Tovar, "Impact of intersection management on energy-efficiency when mixing electric and combustion vehicles", in **EWGT 2020**.

Contents

List of Figures

List of Tables

Abbreviations

AUV	Autonomous Underwater Vehicle
CC	Closeness Centrality
COTS	Commercial Off-The-Shelf
DC	Degree Centrality
EC	Eigenvector Centrality
EDF	Earliest Deadline First
IoT	Internet of Things
LoS	Line-of-Sight
LoRa	Long Range Radio
LPWAN	Low-Power Wide Area Network
MAC	Medium Access Control
MIMO	Multiple-Input Multiple-Output
MO	Minimal-Overlap
MOC	Minimal-Overlap Centrality
NJW	Ng-Jordan-Weiss
PDR	Packet Delivery Ratio
PHY	Physical layer
RA-TDMA	Reconfigurable and Adaptive TDMA
RF	Radio Frequency
RSSI	Received Signal Strength Indicator
RT-WSN	Real-Time WSN
S2S	Shore to Shore
S2V	Shore to Vessel
SN	Sequence Number
SNA	Social Network Analysis
SNR	Signal to Noise Ratio
SP	Shortest Path
TDMA	Time Division Multiple Access
TSCH	Time Slotted (or Time Synchronized) Channel Hopping
USV	Unmanned Surface Vehicle
WSN	Wireless Sensor Network

Chapter 1

Introduction

This dissertation addresses various aspects of communication and networking related to *real-time* wireless networked systems operating *over water* environments.

We envisage a tailored and comprehensive *cross-layer* framework consisting of novel design strategies able to cope with major issues in both real-time and overwater wireless communication. We adopt a *divide and conquer* approach to both conducting and organizing our investigations by dividing our research into two main action domains: *i*) *overwater*, which involves the physical layer aspects, and *ii*) *real-time*, entailing both data link and network layer matters.

We address research challenges in these two domains separately but with the shared perspective of enhancing both *real-time* and *overwater* wireless communication networks *by design*. We contribute to this vision by providing novel insights and methods, improving the state of the art.

The remainder of this chapter motivates our research directions, describes the major research challenges to address, and explicitly states our thesis and contributions.

1.1 Motivation

We are generally driven by the increasing adoption of *real-time* wireless networked systems in different *maritime* activities [35; 36; 37; 38], from scientific to industrial or commercial purposes, and in various water environments, including rivers [39], estuaries [40], coastal zones [41], harbors [42], among others. Several examples of relevant societal impact can be found both in academic and real-world applications. We argue the importance of such *real-time* networked systems in *overwater* scenarios is not under discussion but the sub-optimal performance of wireless facilities within these settings. We stress the need for further and specialized methods in this domain attempting of making better use of wireless technologies originally conceived mostly for terrestrial scenarios, and not necessarily for supporting *real-time* applications, i.e. with explicit timing constraints (e.g. packet deadlines). In this direction, we advocate for a research approach able to improve communication performance by *design*, particularly by proposing novel strategies which apply a *judicious* real-time overwater wireless network design, i.e. which take into account both the *real-time* and the *overwater* peculiarities of these network settings.

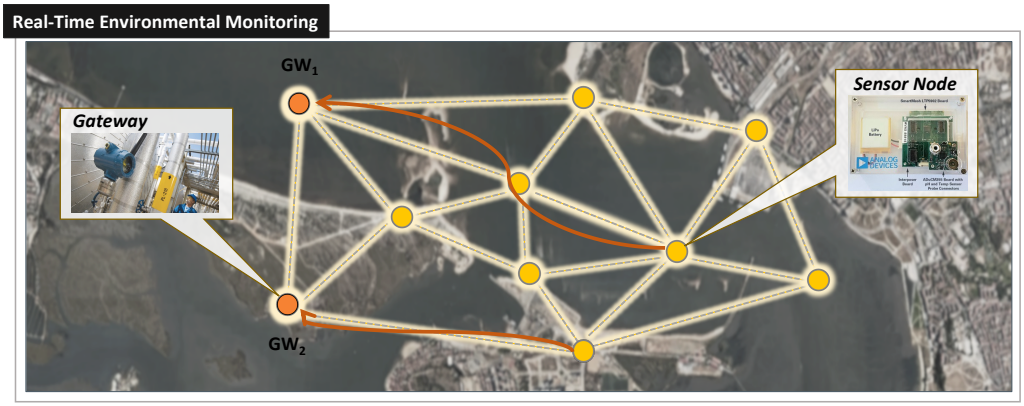

Figure 1.1: An illustrative example of an overwater WSN deployment to support a real-time environmental monitoring application in the Seixal Bay of the Tagus River Estuary, Portugal.

We consider two common real-world applications as valid use cases to motivate our research: *i*) *real-time* environmental monitoring with wireless sensor networks (WSNs) and *ii*) remotely-controlled robotic missions/operations with surface vessels. In the first case, we assume dynamic interconnections from few to many radio frequency (RF) links partially or fully deployed *over water* which connect stationary sensor nodes (e.g. buoys or floating platforms) supporting *real-time* monitoring scenarios, e.g. for flooding prevention, water quality assessment, among others. In the second case, we consider*marine* surface robotics missions/operations with at least one autonomous and/or remotely controlled vessel requiring to transmit *real-time* data, e.g. for vehicle maneuvering or supervision, to a ground (onshore) station, e.g., as commonly needed in activities such as seafloor mapping or search-and-rescue.

In the following, we provide additional motivational information to further illustrate the importance of these two use cases.

1.1.1 Environmental Monitoring

The protection of water environments is an important challenge for present and future societies around the world. Due to the relevance and timeliness of this issue, the United Nations (UNs) 2030 agenda for sustainable development advocates for access to safe water for all and the sustainable management of water resources in all its aspects [43]. Coastal zones, rivers, estuaries, wetlands, etc., are examples of fragile ecosystems threatened by varying factors, including pollution (e.g. microplastics), illegal dumping, water misuse, industrial activities, among others. These threats can have devastating consequences for the surrounding wildlife and local populations that make use of available water resources.

To properly protect these aquatic environments, resilient systems should be deployed in selected locations for *real-time monitoring* of key indicators (e.g. water quality); a task nowadays effectively carried out by static (e.g. [44]) and/or mobile (e.g. [45]) Internet of Things (IoT) devices. In particular, the use of low-power wide-area networks (LPWANs) technologies, such as LoRa (Long Range), are among the most popular, enabling low-cost, low-power and long-range

Figure 1.2: A set of illustrative examples of an AUV in real-world operation. It includes the so-called *Manta* gateway (GW) on the right and left pictures. The two middle image shows an AUV on the water (middle-top) and outside the water (middle-bottom) on a boat before a mission.

IoT-based monitoring applications [46]. While mostly deployed in terrestrial domains (e.g., urban or rural areas), its applicability in different types of marine and freshwater environments has been demonstrated successfully [47; 48; 49].

In order to better illustrate this use case, Figure 1.1 shows a referential picture for a real-world environmental monitoring application scenario motivated by the AQUAMON research project [50].

1.1.2 Marine Robotics

Marine robots such as autonomous underwater vehicles (AUVs) or unmanned surface vehicles (USVs) are nowadays key elements for several maritime activities. Examples of common applications include characterizing and modelling the oceans [51] (e.g. seafloor mapping [52]), understanding natural water phenomena (e.g. marine currents [53]), studying the impact of human activities (e.g. pollution), among others. AUV/USVs are also used for commercial activities (e.g. pipeline inspection [54]) or defense-related operations (e.g. surveillance). Usually, these vehicles perform pre-determined missions for collecting large amounts of sensing data (e.g. bathymetry) in a given area of interest resorting to a plethora of sensors (e.g. sonar, camera, echo sounder).

The collected data is transmitted often in *real-time* – through terrestrial or satellite infrastructure – to backend datacenters, e.g. for storage, further processing, or control. Cost constraints, operational restrictions and/or higher requirements on the timely delivery of data often require the communication exchange is performed resorting to ground stations (onshore) rather than satellite facilities. In the case of terrestrial systems, for the vessel-to-shore communication component, the majority of the AUVs/USVs use cellular [55; 56] or unlicensed frequency bands (e.g. WiFi, LoRa [57] or TV Whitespaces [58]).

In order to illustrate a typical real-world scenario, Figure 1.2 shows a set of referential pictures of an AUV being operated near the shore of Matosinhos, Portugal, for robotic scientific missions/operations performed within the context of the research project EU Marine Robots [59].

1.2 Research Challenges

In general, the research challenges for communication and networking that arise when dealing with real-time overwater wireless networked systems are multiple and non-trivial. We argue these challenges have typically *cross-layer* implications, i.e. issues in the operation at one of the layers of the communication stack may influence other layers, impacting overall system performance. As we mentioned before, we advocate for a layered approach to solve these issues, and as so we divide our research challenges into two domains: *overwater* and *real-time* communication.

On the *overwater* facet, we concentrate on physical layer (PHY) factors related to the overwater RF propagation in water environments. While multiple physical conditions in water surroundings can affect radio-propagation, we focus on those large-scale fading issues dominating link quality performance. We identify two major factors in this direction that still pose significant research questions from the perspective of link design: *i*) tides, and *ii*) intertidal zones[1] [60].

On the *real-time* flank, we focus on the upper layers' concerns related to the central aspect of real-time systems, i.e. the *schedulability* [61]. We study data-link and network layer factors playing a key role in real-time network performance with emphasis on their relationship with *network design*. In this regard, we recognize as an open and major research challenge the need for *judicious* criteria for designating a node as a gateway in order to facilitate real-time communication.

In the following, we provide further details on these specific challenges, both in terms of *real-time* and *overwater* action domains.

1.2.1 Overwater Communication Challenges

In general, the establishment of a reliable overwater link has been reported to be a difficult task due to the harsh conditions of water environments [37; 38]. Not only a number of environmental factors affecting the hardware devices have to be considered (such as humidity, heat, wind) [62] but also a different radio propagation behavior when compared to overland settings. While well-known RF propagation issues can also materialize in water environments (e.g. multi-path [63], diffraction [64], shadowing [65], scattering [66], etc.), this dissertation mostly focuses on those large-scale propagation issues still requiring further characterization and modeling, particularly, due to the interaction of RF waves with *tides* and *intertidal zones*.

Tides, particularly, can lead to changes in the antenna heights which cause varying interference patterns between direct and (water) reflected paths. This, in turn, may result in considerable signal variations at the receiver; a barely explored phenomenon also known as *tidal fading* [67]. Although prior studies have demonstrated tides can greatly impair link quality [67; 68; 69], conventional literature on *maritime communication* has largely focused on long-range communications; which may exhibit specific propagation conditions (e.g. evaporation ducts [70]) not necessarily applicable to short/medium range communications, which is our main target. Similarly, specific tide-driven circumstances such as the recurrent flooding and drying of the so-called *intertidal zones* have been generally ignored from a radio propagation perspective.

[1] Intertidal zones refer to areas repeatedly covered and uncovered by water as the tide rises and falls, respectively.

In this dissertation, we are greatly interested in the specific RF propagation behavior that arises when *tides* and *intertidal zones* influence the operation of short to medium-range overwater links at low antenna height settings. While this is a situation that can affect many types of existing IoT-driven overwater network deployments (e.g. [62; 41]), it has been commonly ignored in practice. This includes the case of AUVs/USVs operating at near-shore, which may also suffer communication impairments due to changes in the water level. In addition, these types of vessels use very low-height external antennas (i.e. comparable to the wavelength) which may cause additional or exacerbated propagation effects, often leading to non-conclusive modeling perspectives [71; 72].

While not in the scope of this dissertation, we certainly recognize the impact of further propagation phenomena, including those derived from different natural conditions, e.g. sea waves [73], or due to human influence, e.g. caused by objects in the surrounding [74], due to external interference [75], among others. All these effects may lead to widely fluctuating and unpredictable overwater communication links; a critical situation within the context of real-time communication.

1.2.2 Real-Time Communication Challenges

Prior to presenting the research challenges to be addressed in terms of real-time communication, we explicitly state two important assumptions in terms of global network operation. First, we assume reliable link connections and stationary network topologies are feasible. This implies *overwater* networks as the one presented in Fig. 1.1 have been already designed in a way that mitigates important physical-layer issues, e.g. tidal fading, being able to maintain the link quality above a certain threshold, and thus providing stationary network topologies. Second, we advocate for the use of globally synchronized time-triggered network protocols with centralized scheduling and routing, in order to facilitate real-time communication. Typical examples of such protocols are those resorting to the widespread time-synchronized channel-hopping (TSCH) medium access control (MAC) layer, a popular MAC layer protocol common to several standards for industrial monitoring. (e.g. WirelessHART [76], 6TiSCH [77], ISA-100.11a).

Under these assumptions, we mostly cover aspects of *real-time* communication related to data-link and network layers. In this regard, we endorse the use of *real-time* scheduling and routing schemes offering a strong mathematical framework for the analysis of the *traffic schedulability*, i.e. the ability of the network to satisfy specific timing constraints (e.g. packet deadlines). Without loss of generality, we support the use of the *earliest-deadline-first* (EDF) [78] real-time scheduler, and its associated literature on schedulability analysis for real-time WSNs. Within this framework, we focus on research challenges related to the improvement of real-time network performance *by design*, i.e. resorting to network design methods that facilitate real-time communication.

In concrete, this dissertation addresses research questions related to the existence of concurrent transmissions in wireless mesh networks, e.g. overwater WSNs, and their relationship with transmission conflicts, which influence the correct *real-time* network operation. More specifically, conflicts can translate into extra delays, which can lead to violations of timing requirements (i.e. deadline misses), which in turn may create serious consequences on the overall system performance. While the use of proper (e.g. predictable) *real-time* scheduling and routing methods has

been the classical approach to solve these issues, here we are interested in how a *judicious* wireless network design can help to improve network schedulability. Specifically, we consider the problem of finding which node(s) within an existing infrastructure can be adequate to play the role of gateway, from a real-time performance perspective. We refer to this problem as *gateway designation*.

While a similar problem can be applicable to scenarios with multiple AUVs/USVs operating in a swarm, e.g. for leader designation, we left this open challenge for future work. We finally emphasize this thesis addresses the *real-time* communication problem of gateway designation from a deterministic perspective, leaving eventual probabilistic approaches for the future. Other possible research challenges in real-time wireless networked systems which are also applicable to the overwater case will be covered later in this document, in the related work section.

1.3 Thesis Statement

This dissertation aims to verify the following:

> A *judicious* wireless network design which takes into account both *real-time* and *overwater* factors of wireless communication has the potential to significantly improve the performance of *real-time* wireless networked systems operating *over water* environments.

To check the validity of this statement, we present a set of novel design strategies able to cope with major communication issues both in terms of *real-time* and *overwater* communication. We cover various physical, data-link, and network layer factors with the end goal of improving the performance of real-time overwater wireless networked systems *by design*. We also consider validation experiments and simulations inspired by two use cases from real-world applications.

1.4 Contributions

In the following, we summarize our main contributions into two major parts, namely, *overwater communication* and *real-time communication*. In each part, we include a description of our major research findings, a list of contributions, and the list of associated publications.

1.4.1 Part I: Overwater Communication

The first part is mainly dedicated to the mitigation of the large-scale propagation fading issues associated with the impact of *tides* and *intertidal zones*. To this purpose, we first investigate overwater RF propagation from the perspective of channel modelling and characterization to then capitalize this understanding into novel design methods that effectively improve link quality (e.g. received power). Specifically, we propose a novel design method that uses a tidal-informed two-ray propagation model to provide both static (e.g. sensor nodes) and mobile nodes (e.g. autonomous

vessels) with better design options for antenna height and positioning. We also present a novel methodology for path loss prediction based on the non-trivial integration of the two-ray propagation model with precise location-dependent hydrodynamics (i.e. tidal model). A key aspect of this methodology is the ability to account for a reflective surface of varying altitude and permittivity as a function of the tide. This feature is shown to be crucial for an accurate path loss estimation over water environments with characteristic intertidal zones. Experimental measurements using commodity technologies (LoRa, WiFi) in different settings (estuaries, marinas) show major trends in the received power in agreement with our methods.

In a nutshell, we summarize our major *overwater communication* contributions as follows:

- ✓ A novel *tidal-informed* link design method for improved communication quality with static and mobile surface nodes based on both antenna height and positioning.
- ✓ A novel methodology for *overwater* path-loss prediction based on the non-trivial integration of the *two-ray* propagation model and precise location-dependent *hydrodynamics* modeling.

In the following, we list the publications containing the core scientific material of these contributions, as well as the preliminary and related empirical validation studies.

1) M. G. Gaitán, P. d'Orey, J. Cecilio, M. Rodrigues, P. Santos, L. Pinto, A. Oliveira, A. Casimiro and L. Almeida, "Modeling LoRa Communications in Estuaries for IoT Environmental Monitoring Systems", in **IEEE Sensors Journal 2022** [2].

2) P. d'Orey, M. G. Gaitán, P. Santos, M. Ribeiro, J. Sousa and L. Almeida, "Empirical Evaluation of Short-Range WiFi Vessel-to-Shore Overwater Communications", in ACM WINTECH'22 Workshop, co-located with **ACM MobiCom 2022** [10].

3) M. G. Gaitán, P. d'Orey, P. Santos, M. Ribeiro, L. Pinto, L. Almeida and J. Sousa, "Wireless Radio Link Design to Improve Near-Shore Communication with Surface Nodes on Tidal Waters", in **IEEE OCEANS 2021** [4].

4) M. G. Gaitán, P. Santos, L. Pinto and L. Almeida, "Optimal Antenna-Height Design for Improved Capacity on Over-Water Radio Links Affected by Tides", in **IEEE OCEANS 2020** [5].

5) M. G. Gaitán, P. Santos, L. Pinto and L. Almeida, "Experimental Evaluation of the Two-Ray Model for Near-Shore WiFi-Based Network Systems Design", in **IEEE VTC2020-Spring** [6].

6) M. G. Gaitán, L. Pinto, P. Santos and L. Almeida, "On the Two-Ray Model Analysis of Overwater Links with Tidal Variations", in **INForum 2019** [7].

We have also disseminated part of this material as posters and/or extended abstracts at DCE 2019 [19], DSIE 2020 [18], RTCM 2021 [16] and RTCM 2022 [13].

1.4.2 Part II: Real-Time Communication

The second part is devoted to enhancing network design with the aim of improving the *real-time* performance of upper layers methods of the network stack, namely *real-time scheduling* and *routing*. To this purpose, we advocate for the idea of *judicious* gateway designation for enhanced traffic schedulability at system's design time. Concretely, we introduce the concept of *network centrality* from social network analysis (SNA) as an effective heuristic for gateway designation that facilitates real-time communication. We also generalize this idea to multiple gateways with the aid of the unsupervised learning method of *spectral clustering*. More importantly, we propose a novel metric termed *minimal overlap* centrality which conveniently exploits the relationship between path node-overlaps and gateway designation for improved network schedulability. In a similar fashion, we propose a novel scheme termed minimal-overlap shortest-path routing based on a new greedy heuristic for path-overlap minimization. This strategy increases traffic schedulability regardless of the gateway designation criterion, being complementary to our prior methods.

In a nutshell, we summarize our major *real-time communication* contributions as follows:

- ✓ A new metric termed *minimal overlap centrality* that exploits the relationship between path-node overlaps and gateway designation for improved traffic schedulability.
- ✓ A novel *routing* scheme based on a new greedy heuristic for *minimizing overlaps* that improves schedulability regardless of the gateway designation criterion.

In the following, we list the core publications containing the main scientific material of these contributions, including preliminary and related empirical validation studies.

1) M. G. Gaitán, L. Almeida, P. d'Orey, P. Santos and T. Watteyne, "Minimal-Overlap Centrality for Multi-Gateway Designation in Real-Time TSCH Networks", in **ACM Transactions on Embedded Computing Systems 2023** (Under Review). [1]

2) M. G. Gaitán, D. Dujovne, J. Zuñiga, A. Figueroa and L. Almeida, "Multi-Gateway Designation for Real-Time TSCH Networks using Spectral Clustering and Centrality", in **IEEE Embedded Systems Letters 2022**. [3]

3) M. G. Gaitán, P. d'Orey, P. Santos and L. Almeida, "Minimal-Overlap Centrality-Driven Gateway Designation for Real-Time TSCH Networks", in RAGE 2022 Workshop, co-located with **DAC 2022**. **[Best Paper Award]**. [8]

4) M. G. Gaitán, L. Almeida, T. Watteyne, P. d'Orey, P. Santos and D. Dujovne, "Joint Scheduling, Routing and Gateway Designation in Real-Time TSCH Networks", in JRWRTC 2022 Workshop, co-located with **RTNS 2022** [9]

5) M. G. Gaitán, L. Almeida, A. Figueroa and D. Dujovne, "Impact of Network Centrality on the Gateway Designation of Real-Time TSCH Networks", in **IEEE WFCS 2021**. **[Best Work-in-Progress Paper Award]**. [12]

6) M. G. Gaitán, L. Almeida, P. Santos and P. Yomsi, "EDF Scheduling and Minimal-Overlap Shortest-Path Routing for Real-Time TSCH Networks", in NG-RES 2021 Workshop, co-located with **HiPEAC 2021**. [11]

We have also disseminated part of this material as extended abstracts at RTSS@Work 2021 [14], DCE 2021 [15] and BSC-DS 2020 [17].

1.5 Thesis Organization

The remainder of this thesis is organized as follows. Chapter 2 elaborates an overall discussion on the essential background and related work, essential for the better understanding of this thesis. Chapters 3, 4 and 5 constitute PART I, and are dedicate to overwater communication. Chapter 3 presents common channel modeling and characterization studies, key for the novel link design methods and methodology elaborated in Chapters 4 and 5, respectively. Chapters 6, 7 and 8 constitute PART II and are devoted to real-time communication. Chapter 6 firstly introduces the idea of centrality-driven gateway designation, which is core for the minimal-overlap centrality approach in Chapter 7. Chapter 8 presents our minimal-overlap shortest-path routing. Finally, Chapter 9 concludes the thesis and provides future work directions.

Chapter 2

Background & Related Work

This chapter covers general information on wireless communication and networking which are essential for a better understanding of this thesis. We start by providing an overview of the relevant physical, data-link, and network-layer aspects of real-time and overwater wireless networked systems to then provide specific background and related work on each of the core parts of this dissertation, i.e. *overwater communication* and *real-time communication*. We conclude with an integrated summary of these two parts by giving emphasis on those aspects which are more relevant within the scope of our research in real-time overwater wireless network design.

2.1 Real-Time Overwater Communication

We refer to *real-time overwater communication* to the complex process of exchanging data messages among a transmitter and a receiver when both real-time and overwater conditions hold. We use the term *real-time* as in the common literature of *real-time systems* [61] to refer to communication systems whose objective is to meet individual timing requirements of each (communication) task, e.g. expressed as a packet deadline. We use the term *overwater* literally, i.e. assuming wireless communication occurs above water, e.g., as in the case of an overwater RF link crossing a river, lake, or coastal zone. Both these *real-time* and *overwater* conditions impose unique performance challenges involving all layers of the wireless communication stack. We focus here on those specific features at each layer that are more relevant within the scope of this dissertation:

i) RF propagation at the **physical** level,

ii) medium access control and real-time scheduling at **data link**, and

iii) routing and topology tracking at the **network** level.

2.1.1 Physical Layer

By definition, the physical layer deals with aspects of (wireless) communication directly related to the transmission medium, thus, being closely influenced by the environment and surrounding

conditions. This translates into the consideration of different physical features and elements depending on the wireless technology being used (e.g. RF band, antenna polarization, etc.) which may also vary based on the target application (e.g. modulation, bandwidth, etc.).

Here, we do not restrict our research to a specific communication technology, yet we focus on **RF signal propagation**, which is transversal. Still, we perform studies assuming three common PHY technologies in IoT-driven communication, namely, IEEE 802.15.4, LoRa, and WiFi, due to their relevance for our target use cases. The two first technologies are typical in environmental monitoring, while the latter one is often employed, e.g., for shore-to-vessel communication with AUVs/USVs, as well as for sensor networks requiring higher bandwidth. All these technologies present basic technical factors with a direct influence on signal propagation, namely the wavelength (or equivalently, the RF band), antenna polarization, and directivity. In this sense, our research deals with communication operating in commercial RF bands (e.g. 868 MHz for LoRa, and 2.4 GHz for WiFi) which use vertically polarized antennas and assume omnidirectional radiation patterns. While we also include some preliminary analysis for horizontal polarization in Chapter 3, our core research focuses on vertical polarization only.

2.1.1.1 RF Propagation

Radio signals traveling through the wireless medium may suffer from several propagation effects, e.g. path loss, shadowing, diffraction, reflection, refraction, scattering, and absorption, among others. These effects can be caused either by natural environmental phenomena, e.g. weather changes, or, e.g. by static and/or moving objects in the surroundings. Formally, the influence of such effects in signal propagation is described mathematically through *channel models*. These models aim to predict the link quality, e.g. in terms of received signal strength, under specific propagation conditions. While different taxonomies may exist based on the type of attenuation (or fading) experienced, radio propagation models are broadly classified into two categories:

i) **large scale**, which captures average fading effects occurring typically in the order of many wavelengths, e.g. due to motion or terrain variability over a large area,

ii) and **small scale**, representing localized average fading effects in the order of a few wavelengths or less, which occur spatially near the receiver side.

The large-scale fading effects are typically associated with *slow* dynamics, occurring in the long term w.r.t to the signal temporality. Conversely, small-scale fading effects are often associated with *fast* or instantaneous fluctuations, e.g. in terms of the received signal strength. Common models for large-scale fading include the classical free-space and the two-ray path loss models [79; 80]. The former is the most fundamental method used to predict the impact of distance on the average path loss attenuation, while the second adds to the previous one the effect of a dominant surface signal reflection (e.g. from ground or water). These two models are deterministic since offering an exact formulation for the attenuation or signal strength output. Other models are stochastic, e.g. the Okumura-Hata model, providing statistical distribution for the average signal

strength in particular operation conditions (e.g. urban or rural areas). Small-scale fading models can also be deterministic or stochastic. Hybrid models made of deterministic and stochastic fading components are another alternative for both large and small-scale fading models.

This dissertation considers only deterministic modeling approaches while giving special attention to large-scale fading due to path loss. More specifically, as we will further detail later, our research is built upon the two-ray propagation model, due to its commonly good adequacy to predict the impact of surface reflections on the overwater RF channel [37].

2.1.2 Data Link Layer

In short, the data link layer is responsible for the seamless handling of data messages from the physical to the network layer, and vice versa. The overall process is divided into two main sub-layers better known as the logical link control (LLC) and the medium access control (MAC). The former supports the establishment of a logical connection (e.g. half or full duplex) with the upper layers, often offering additional services such as error control and flow control. Conversely, the latter allows coordinating the seamless access to the transmission medium, abstracting its physical complexities to the upper layers. Both these sub-layers have an influence on the real-time performance of communication and are thus relevant for the purpose of this dissertation.

Concretely, we advocate here for the use of standard wireless radio interfaces (e.g. WiFi, LoRa, etc.) using *half-duplex* commercial hardware, while resorting to a time-division multiple-access (TDMA) MAC framework for improved predictability. Time synchronization is thus a fundamental aspect to consider, not only to enable a precise TDMA-based MAC operation but also to deal with real-time scheduling policies for packet transmissions. In this regard, we adopt an EDF (Earliest-Deadline-First) global scheduler due to its well-known real-time performance benefits when compared to fixed priority schedulers, e.g. in terms of competitive acceptance ratios and low computational cost [81; 82]. In the following, we provide more details and illustrative examples of the operation with different TDMA-based mechanisms.

2.1.2.1 TDMA: Time Division Multiple Access

In a TDMA network, different nodes are allowed to transmit data over a shared medium at different time instances called *slots*, thus providing temporal isolation opportunities to each node. Concurrent conflict-free transmission/reception operations within the same time slot are still possible, e.g. at different geographical areas (spatial isolation) or by using different RF channels. Wireless standards such as 6TiSCH [77] or WirelessHART [76] naturally adopt this latter approach by means of TSCH, a multi-channel TDMA MAC working on top of the widely used IEEE-802.15.4 PHY. Other common PHY technologies, e.g. LoRa or WiFi, use random-based medium access mechanisms which require protocol adaptations to enforce a TDMA-based behavior. While this aspect is outside of the scope of this dissertation, we remark such a kind of adaptation is feasible.

In the case of WiFi, we advocate for the use of RA-TDMA, a family of *reconfigurable and adaptive* (RA) TDMA protocols providing a robust overlay MAC on top of the CSMA/CA MAC

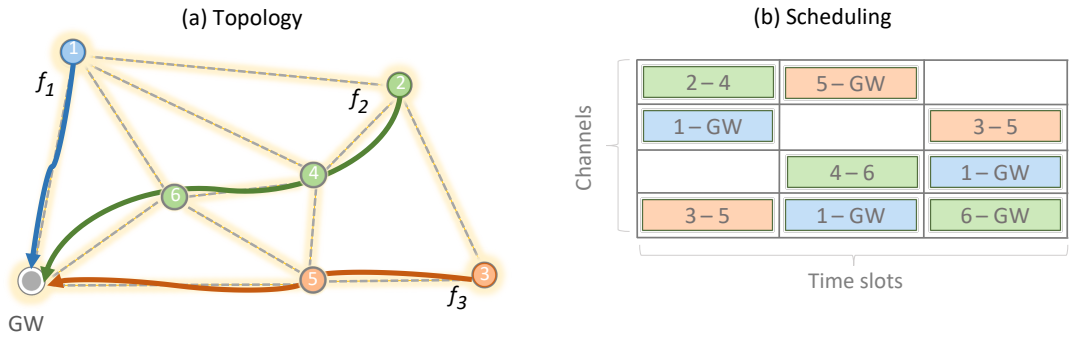

Figure 2.1: A toy example of TSCH wireless network topology (a) including (b) a scheduling diagram of the transmissions associated with it. The network shows three flows in different colors, starting from the respective source node and directed to the gateway through arbitrary paths.

of WiFi. In the case of LoRa, we do not endorse any particular adaptation, yet we refer the reader to some recent efforts in the literature (see e.g. [83; 84]). More importantly, we emphasize that enforcing a TDMA-like operation over WiFi, LoRa, or any other not deterministic PHY, responds to the need for a more predictable timing behavior in the scope of real-time communication.

In the following, we provide illustrative examples for both: *i*) the underlying multi-channel TDMA operation of TSCH along time and over a set of available channels, and *ii*) the RA-TDMA operation over WiFi which uses a single RF channel, yet using a larger number of time slots.

Illustrative Example: TSCH. Figure 2.1 (a) shows an arbitrary graph characterizing a wireless TSCH network topology. The network consists of 7 nodes including 6 field nodes and 1 gateway (GW). Among the field nodes, 3 nodes represent sensors generating data flows directed to the gateway, denoted as f_1, f_2, and f_3. Each flows consist of recurrent single-packet messages generated at each source that repeat periodically, and then are relayed through pre-defined multi-hop paths. Fig. 2.1 (b) shows an arbitrary message scheduling for this topology configuration when using only 4 of the maximum 16 available (i.e. non-blacklisted) channels in TSCH.

In Fig. 2.1 (b) it can be observed how the first of these flows, f_1, repeats at each time slot using different channels (see the light-blue box with recurrent transmissions from node 1 to the gateway, i.e. [1-GW]). The other two flows, f_2 and f_3, only repeat after the corresponding flow's first message has been delivered. Note Fig. 2.1 (b) is only an arbitrary section of the continuous operation of the network, thus a larger schedule portion will show a diagram that repeats such transmissions using a pseudo-random channel assignment. Note this process although pseudo-random do to not influence the timing predictability properties of TSCH [85].

In a nutshell, with this example, we aim to illustrate how a simple configuration can work from the temporal point of view of scheduling in a small-scale mesh network. A larger wireless network configuration involving more flows with overlapping paths is visually similar but not trivial to set, especially if dealing with priority-driven and deadline-constrained flows. Later in this thesis, we provide in-depth discussions of this challenge from the perspective of network design for real-time communication, particularly when resorting to the EDF real-time scheduling policy.

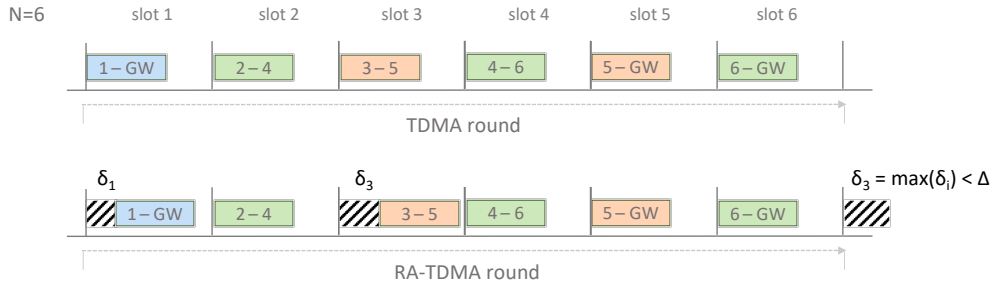

Figure 2.2: The frame configuration for the topology and flows in Fig. 2.1(a) when using a TDMA with global synchronization (top) and the RA-TDMA round which uses a clockless synchronization (bottom). The figure highlight differences in terms of delay compensation at the next round.

Illustrative Example: RA-TDMA. Fig. 2.2 presents a scheduling example for RA-TDMA working on the previous network topology and flows setting. On top, Fig. 2.2 shows an ideal case for RA-TDMA with no delays (i.e. deviations from the expected transmission time at each slot) which reduces RA-TDMA to a classical TDMA scheme with global synchronization. This is alike to the TSCH MAC using only one RF channel. On the bottom, Fig. 2.2 shows a particular situation when both *slot 1* and *slot 3* suffer delays at each slot. This is a toy example of the RA-TDMA relative synchronization. It illustrates how the protocol adaptation works by using the maximum of these delays to then postpone the start of the next transmission round (only if greater than a maximum delay factor, Δ). Particularly, in this case, the delay at the *slot 3* (δ_3) is greater than the delay at the *slot 1* (δ_1), while the other slots do not present deviations from the expected transmission times. Thus, δ_3 is used to delay the next TDMA round.

Note that in both cases transmissions are set at the beginning of the slot, maximizing the separation between them to minimize contention (due to the underlying CSMA/CA). This means each slot is used only partially by the node's transmission, letting the unused part for uncontrolled traffic. Moreover, consider that at each slot, all node's data is piggybacked into a single packet. Note also that RA-TDMA operates with a predefined value for the TDMA round period, which is the same for all transmitting nodes. This period, denoted as T_{up}, set both the temporal resolution and responsiveness of global communication [86]. RA-TDMA divides T_{up} equally into N consecutive time slots, each of them assigned to each of the N transmitting nodes in the network. In this example, the gateway is set to receive messages only, thus the TDMA round is set to $N = 6$ slots. Accordingly, the duration of each time slot can be computed as $t_{slot} = \frac{T_{up}}{N}$.

Different variants of RA-TDMA are available in the literature, including adaptations for vehicular platooning applications [87] and multi-hop relay streaming over aerial drones [88]. These schemes although offering appealing features for our target applications are no part of the current work. The main intention of including RA-TDMA at this point is to show roughly how an overlay TDMA protocol can enforce deterministic behavior over WiFi. That being said, we make clear our research efforts on the real-time communication part only focus on TSCH networks, yet assuming the ideas can be extended to RA-TDMA in the future. In the simplest case, this can be done straightforwardly by considering RA-TDMA operates under a global synchronization scheme.

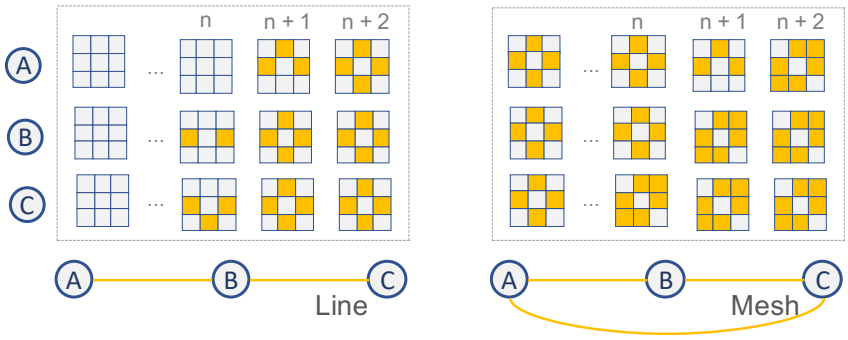

Figure 2.3: A toy example of the RA-TDMAs+ topology tracking for a mesh with 3 nodes [14]. The figure shows the evolution of the adjacency matrix connectivity by highlighting in yellow the pair of nodes (row-column pair) connected by a link at different time instants. It also contrasts the case of a line topology and a mesh topology from a given starting point (i.e. topology).

2.1.3 Network Layer

The main responsibility of the network layer is to enable the interconnection between different network entities. The *routing*, i.e. the mechanism allowing to determine the best paths for the data to travel - within and outside the network - is a key aspect of the network layer. Specifically, we consider networks that when scale become *mesh networks*, where data flows travel using *multi-hop paths*. This implies the knowledge of the network topology (i.e. beyond direct neighbors of each node) is relevant for routing mechanisms, e.g. to planning efficient routes in advance.

Particularly, since in this dissertation we aim to improve real-time communication *by design*, we focus on the class of routing known as *source routing* which allows providing (or designing) the full path at the source node beforehand. Moreover, since we are also dealing with wireless networks which may change the topology due to (stationary) link dynamics, we also assume this topology is maintained, e.g. by means of a *topology tracking* algorithm [89; 14; 90].

2.1.3.1 Mesh Topology Tracking

Even in static networks, the topology can change e.g. due to link quality variations. If the network topology is stable, changes can be seen as *slow*, e.g. when compared with the periodicity of packet transmissions or the instantaneous fluctuations of the signal. Still, these changes can influence the length of the routing paths, and in turn impact, e.g. real-time communication performance. Keeping track of these changes is thus essential not only for *routing*, but also for other *network design* strategies resorting to spectral properties of the network (i.e. topological).

Here, we do not advocate for a specific topology tracking algorithm, yet we emphasize on the importance of such a method for our research direction. Concretely, we rely on approaches encoding network connectivity as an *adjacency matrix* since mathematically convenient for both the routing and network design methods proposed later in this thesis.

As an example, we illustrate in Fig. 2.3, the temporal evolution of the topology tracking algorithm associated to RA-TDMA (as described in [14]). The output matrix is shown graphically in

the figure by colouring in yellow the cells in which the row-column pair indicates an active link, i.e. equivalent to a logical true value. In the case of RA-TDMA, this matrix allows to determine the length of the TDMA round, and in turn, the order and number of the slots and transmissions.

For brevity reasons, we do not provide further details on the operation of this method, nor for other methods, e.g. applicable to TSCH or LoRa. We yet further emphasize the general relevance of this service to realize our vision of real-time over-water mesh networks.

2.2 Part I: Overwater Communication

2.2.1 Preliminaries

We adopt the two-ray propagation model as the primary prediction method for modeling large-scale fading dynamics in overwater RF links affected by tides. While we recognize the existence of other alternatives, we advocate for the use of two-ray due to its simplicity and foundational basis to describe the dominant impact of (water) surface reflections on average path loss performance. We also deem as important in this model the explicit consideration of the antenna height parameter as relevant for modeling the water level variation due to tides. We further argue that additional propagation phenomena, e.g. small-scale fading, can be added later, on top of the two-ray-based modeling efforts conducted in this thesis. That being said, we focus in this chapter on providing specific background for LOS overwater links in shore-to-shore (S2S) and shore-to-vessel (S2V) communication scenarios. We thus revisit the two-ray model fundamentals when taking into account both these cases and the impact of tides.

In the following, we include a number of expressions that represent the common modeling framework for Chapters 3, 4, and 5. Alternate expressions (e.g. in terms of path loss) are presented in each chapter, when applicable. Comments on the challenges for the two-ray model when applied to intertidal zones are also included below, for completeness.

2.2.2 The Two-Ray Model

The two-ray propagation model [79; 80] assumes the average path loss trend of a LOS link affected by multipath fading is dominated by a single surface reflection. This implies the received signal

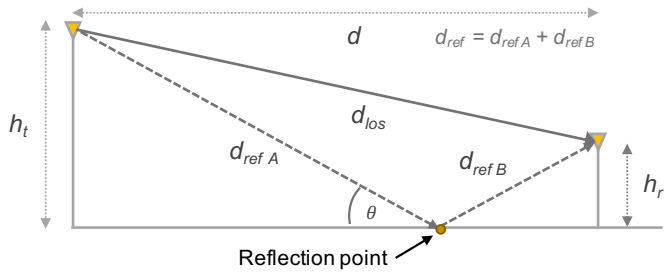

Figure 2.4: The classical two-ray model showing (1) the direct line-of-sight (LoS) path, and (2) the ray reflected on the surface. It also highlights the notion of reflection point.

strength can be computed as the vectorial summation of only two copies of the same transmitted signal that arrive simultaneously at the receiver following two different paths. The first ray follows a direct LOS path between the transmitter and the receiver, and the second one, an indirect path reflected by the surface (Fig. 2.4). The length of the reflected ray ($d_{ref} = d_{refA} + d_{refB}$) is longer than the length of the direct path (d_{los}), and thus a phase shift $\Delta_\phi = 2\pi(d_{los} - d_{ref})/\lambda$ exists between the two copies of the received signal, where $\lambda = c/f$ is the wavelength, c the speed of light and f the operating frequency.

Formally, the two-ray model can be expressed in terms of the average received power P_r [79] as in Eq. 2.1, where P_t is the transmit power and G_t and G_r are the transmitter and receiver antenna gains, respectively.

$$P_r = P_t G_t G_r \left[\frac{\lambda}{4\pi d}\right]^2 \left| \frac{1}{d_{los}} + \Gamma \frac{e^{-j\Delta_\phi}}{d_{ref}} \right|^2 \tag{2.1}$$

The parameter Γ is the Fresnel reflection coefficient given by Eq. 2.2.

$$\Gamma = \frac{\sin(\theta) - Z}{\sin(\theta) + Z} \tag{2.2}$$

The parameter Z is given by Eq. 2.3, where ε_r is the relative permittivity or dielectric constant of the reflective medium (e.g. ground or water) and θ is the angle of incidence of the ray reflected from the surface.

$$Z = \begin{cases} \sqrt{\varepsilon_r - \cos^2\theta}/\varepsilon_r & \text{for vertical polarization} \\ \sqrt{\varepsilon_r - \cos^2\theta} & \text{for horizontal polarization} \end{cases} \tag{2.3}$$

From simple geometry, the angle θ can be computed using Eq. 2.4, where d is the horizontal link distance, and h_t and h_r denote the respective transmitter and receiver antenna heights.

$$\theta = \arctan\left(\frac{h_t + h_r}{d}\right) \tag{2.4}$$

Similarly, the path lengths d_{los} and d_{ref} can be calculated with Eqs. 2.5 and 2.6.

$$d_{los} = \sqrt{d^2 + (h_t - h_r)^2} \tag{2.5}$$

$$d_{ref} = \sqrt{d^2 + (h_t + h_r)^2} \tag{2.6}$$

2.2.2.1 Two-ray Model Over Tidal Waters

From the two-ray model perspective, the rise and fall of water levels will impact the link geometry whenever at least one of the (relative) antenna heights to the surface is modified by the impact of tides. This can be interpreted as the influence of a water level variation Δ_h that shifts either h_t, h_r, or both, depending on whether it is an S2S or an S2V link scenario, as shown in Fig. 2.5(a) and Fig. 2.5(b), respectively. This, in turn, implies the angle of incidence and the lengths of the

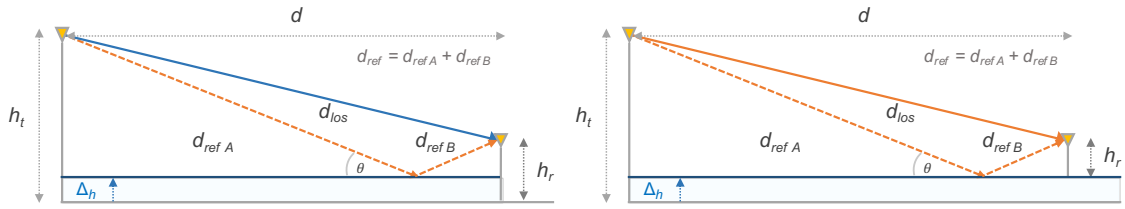

(a) **Shore-to-Shore (S2S)** (b) **Shore-to-Vessel (S2V)**

Figure 2.5: Two-ray model geometry for the (a) shore-to-shore and (b) shore-to-vessel link scenarios when influenced by a water level variation of Δ_k. Both pictures highlight in blue the corresponding direct and/or indirect rays being influenced by the water level shift.

two-ray paths, i.e., θ, d_{los} and d_{ref}, can also vary as a consequence of tides (Δ_h), but differently for each scenario, as follows.

Shore-to-Shore (S2S). In this case, both transmitter and receiver nodes are assumed as static onshore. This presumes the $\pm|\Delta_h|$ variations on the water level (along the link path) shift both height terminals simultaneously, and by the same shift amount. This implies Δ_h induces variations on the values of θ and d_{ref}, but not on d_{los}, which remains unchanged due to the shifts getting canceled after incorporating them into the expression of d_{los} (see Table 2.1).

Shore-to-Vessel (S2V). In this case, only one of the nodes is onshore while the other is on water (e.g., a vessel or buoy). This implies Δ_h only influences the relative height of the onshore antenna h_t, but not h_r that remains constant w.r.t the water surface[1]. This, in turn, induces variations on all the geometrical parameters of the link, i.e., θ, d_{los} and d_{ref}, in contrast with the S2S case.

2.2.2.2 Reflection Point over Tidal Waters

The reflection point is a fundamental concept in the two-ray model geometry being defined as the distance w.r.t. the receiver side at which the second ray touches the reflective surface (see Fig. 2.4). This concept is often left aside from conventional discussions on two-ray propagation modeling since typically invariant, given the common assumption of having a flat and static (ground) reflecting surface. Formally, it can be computed with Eq. 2.7, where d is the link distance, and h_t and h_r are respectively the Tx and Rx antenna heights.

$$RP = d\left(1 - \frac{h_t}{h_t + h_r}\right) \tag{2.7}$$

For the case of RF links over tidal waters, Eq. 2.7 can be trivially extended by considering either h_t, h_r, or both, being affected by a water-level variation Δ_h depending on whether it is an S2S or S2V link scenario, as summarized in Table 2.1.

[1]Note that the Tx-Rx convention defining the Tx onshore and the Rx on water (or vice-versa) is arbitrary, and thus, it doesn't impact the geometry.

Table 2.1: Two-ray model geometry when incorporating Δ_h.

Variable	Shore-to-Shore (S2S)	Shore-to-Vessel (S2V)
h_t	$h_t + \Delta_h$	$h_t + \Delta_h$
h_r	$h_r + \Delta_h$	h_r
θ	$\arctan\left(\frac{(h_t+\Delta_h)\,(h_r+\Delta_h)}{d}\right)$	$\arctan\left(\frac{(h_t+\Delta_h)\,h_r}{d}\right)$
d_{los}	$\sqrt{d^2+(h_t-h_r)^2}$	$\sqrt{d^2+(h_t-h_r+\Delta_h)^2}$
d_{ref}	$\sqrt{d^2+(h_t+h_r+2\Delta_h)^2}$	$\sqrt{d^2+(h_t+h_r+\Delta_h)^2}$
RP	$d\left(1-\frac{h_t+\Delta_h}{h_t+h_r+2\Delta_h}\right)$	$d\left(1-\frac{h_t+\Delta_h}{h_t+h_r+\Delta_h}\right)$

2.2.2.3 Reflection Point falling within the Intertidal Zone

When the RF links are deployed over tidal environments, the reflection point may fall within the intertidal zone. This implies a dual condition for the reflection point, which is the possibility of falling on 1) water or 2) soil as a function of the tide. While the former case is equivalent to the one summarized in Table 2.1, the latter imposes a static definition that may not necessarily fall on flat terrain, nor on a surface of the same altitude as the average water level in the estuary. This not only influences the geometry, but also the dielectric properties of the composite medium (e.g. permittivity), which do not present a constant behavior throughout the day [91; 92; 93], but vary depending on the floods and ebbs. The overall situation entails extra considerations on the two-ray channel modeling, which have not been addressed by conventional approaches.

2.2.3 Related Work

The relevant state-of-the-art works have been classified into three categories: *i*) tidal fading, *ii*) intertidal zones and *iii*) RF propagation over mixed/water land paths. While the literature on RF propagation for maritime communication is much broader (see e.g. the review papers in [37; 38]), we restricted the interest of this section to those efforts matching more closely the distinguishing aspects of our research direction, i.e. the impact of tides and the intertidal zone in RF signal propagation. Likewise, despite not considering literature beyond the maritime domain, we recognize the existence of further research proposing related procedures or methodologies in specific environments (e.g., mountains [94; 95]) that exploit local conditions (e.g. terrain profile) for improved path-loss estimation.

2.2.3.1 Tidal Fading

Wireless RF propagation in water environments is known to be affected by multiple factors [37; 38] including the natural oscillations of the water surface. Specifically, tides and waves are among the most common phenomena heavily affecting RF propagation due to the changes in the water level. While prior literature has recognized and addressed this situation (e.g.,[68; 69; 96; 97; 73; 55; 48]) several gaps from the perspective of channel modeling and characterization are still open.

Tides, particularly, can lead to a severe but barely explored condition known as *tidal fading* [68], i.e. path loss changes induced by the varying (relative) antenna heights of the nodes w.r.t. the surface resulting from the recurrent influence of floods and ebbs. Despite some aspects of this phenomenon having been effectively described by the two-ray model (e.g. [67; 98]), further investigations on diverse environmental settings (e.g., estuaries), using emerging communication technologies (e.g., LoRa) and/or incorporating precise tidal modeling methods, are still scarce.

Traditionally, research reporting and/or mitigating tidal fading have typically focused on kilometric RF links [68; 69; 67; 98; 96; 99], often using antennas installed at several meters above surface. This is in contrast with the current trend in IoT-driven application scenarios (e.g., water-quality monitoring, flooding prevention, etc.), which often require (shorter) links at near-shore with antennas relatively close to the surface [100; 101]. These different implementation settings imply tides can induce changes in the water level that are in the order of magnitude of the antenna height, possibly intensifying tidal fading and other propagation effects. Although being addressed by a few works in the literature [40; 100], this issue has been largely ignored in practice and thus represents one of the main targets of our research.

2.2.3.2 Intertidal Zones

Tidal environments such as estuaries and their surrounding wetlands offer distinctive water dynamics (e.g., due to shallow water tides or intertidal zones) that deserve dedicated RF propagation studies. Specifically, the *intertidal zone*, i.e. the area within the (estuarine) shoreline that is submerged by water during the high tide and then becomes unveiled during the low tide [60], may pose difficult challenges to channel modeling and characterization. Though a few works have already demonstrated its impact on different aspects of wireless communications (e.g., link quality estimation [102], energy consumption [103], or time-synchronization [104]), these prior works considered communicating nodes deployed at the ground level, which become covered by water during the high tide, in contrast to our research. These works offer little insight into the path loss dynamics occurring *above* the intertidal zone, which is our major concern.

2.2.3.3 RF Propagation over Mixed Water/Land Paths

The case of intertidal zones entails a challenging and unusual condition for channel modeling which is to have a dynamic water/land portion along the link path continuously changing according to the tide. This situation, as far as we know, has been addressed only partially by a few works modeling RF signal propagation over the so-called mixed water/land paths [105; 106; 107; 108]. While these works show ideas resembling our geometrical analysis of the direct and reflected ray using different reflection coefficients depending on where the reflection occurs, they did not consider important challenges such as tidal fading or intertidal zones. The work in [107] assumes that the river level can take different values along the day, thus having an effect on the radio modeling. Still, their analysis focused on a kilometric link using antennas of up to 200 m high, in contrast to our research. By comparison, our work is more general and challenging since targeting

path loss modeling over dynamic mixed water/land paths that change their physical properties during the day depending on the tide, e.g., from a relatively flat (water) surface with varying level to a possibly rough (soil) surface of varying moisture and specific terrain profile. Without loss of generality, our research could be straightforwardly applied to different types of tide-induced environments for which tides and bathymetry are known.

2.3 Part II: Real-Time Communication

2.3.1 Preliminaries

We adopt a multi-channel TDMA framework to support real-time wireless communication in (overwater) wireless mesh networks. The model is most suitable for TSCH since directly mapped to account for its salient features such as multiple channels and time-slotted globally synchronized operation. The framework is also applicable to any other multi-channel (or single-channel) TDMA framework with the natural adaptation in terms of the size of the time slot, number of channels, among other details. That being said, the framework can be applied, e.g. to the RA-TDMA WiFi-based overlay introduced before, by considering a stationary operation with specific time slots and one channel. While we do not support any particular protocol adaptation for LoRa mesh networks, we recognize the existence of many ongoing efforts in this direction (see e.g, [40]). We only stress the need for a framework enabling time-triggered communication with global synchronization.

On top of this framework, we consider single packet transmissions at each slot and centralized network management. In particular, the cornerstone network functions such as scheduling and routing are assumed to be globally handled. In terms of scheduling, we advocate for the use of EDF, due to its superior performance when compared with other classical priority-driven real-time methods. In terms of routing, we assume standard shortest-path operation (e.g. based on Dijkstra) as still common in many practical and academic studies. A tailored routing scheme is part of the contribution of this thesis in Chapter 8.

In terms of gateway designation, we do not consider any specific approach since finding suitable methods for it is part of the research challenges to be addressed in this thesis. We only assume the existence of one or multiple gateways. Moreover, although throughout the dissertation we consistently use the term gateway to refer to nodes enabling seamless communication with external entities (e.g. a host application), the problem to be addressed assumes gateways also play the role of sinks (or even EDGE-computing nodes), therefore are also used to centrally (and timely) gather data transmissions from source nodes, e.g. for further processing or storage. We finally emphasize the gateway designation is supposed to be a process orthogonal to the modeling framework and thus can be treated and discussed separately.

The network, flow, and performance models described in the following represent a common framework for the research presented in Chapters 6, 7, and 8, on real-time communication.

2.3.2 Real-Time Network, Flow and Performance Models

2.3.2.1 Network Model

The wireless sensor network is abstracted as an undirected graph $G = (V, E)$ where V is the set of vertices or nodes and E is the set of edges or links between those nodes. The order of the graph G is denoted as $N = |V|$, of which a set of $N - k$ nodes act as field nodes (e.g. sensors) while the rest of k nodes are designated as gateways. All nodes can perform the sensing, relaying or gateway functions and are connected wirelessly forming a wireless mesh network (see Fig. 1.1). We also assume full knowledge of the network topology (i.e. the graph G) in the form of an adjacency matrix representing binary connectivity with lossless links. Topology tracking can be assumed as a native in-built centralized service that can be further implemented, e.g., as in [14].

Multiple access is governed using a TSCH-like protocol which uses fixed-size TDMA slots combined with multi-channel hopping. TSCH allows concurrent transmissions over up to $m = 16$ different radio-frequency channels with global synchronization. A time slot interval, here $t_s = 10$ ms, allows the transmission of a single packet and receiving the corresponding acknowledgment.

2.3.2.2 Flow Model

We consider a subset of $n \leq N - k$ field nodes as sensor nodes (sources), thus required to transmit periodically their sensing data toward any of the k designated gateways (destinations). These messages need to reach their corresponding gateways before specific timing constraints, i.e. deadlines. We denote as $F = \{f_1, f_2, \ldots, f_n\}$ the set n of *real-time flows* potentially transmitting an infinite number of deadline-constrained messages, periodically. Each of the n flows is characterized by a 4-parameter tuple (C_i, D_i, T_i, ϕ_i), where C_i represents the transmission time between the source node s_i and any of the k gateway destinations. T_i is the transmission period, D_i is the (relative) deadline, and ϕ_i is the multi-hop routing path. The γ^{th} transmission of each periodic flow f_i is released at time $r_{i,\gamma}$ such that $T_i = r_{i,\gamma+1} - r_{i,\gamma}$. Then, according to the EDF scheduling policy, each of these flow instances $f_{i,\gamma}$ is constrained to reach the gateway before its absolute deadline $[d_{i,\gamma} = r_{i,\gamma} + D_i]$.

2.3.2.3 Performance Model

We consider the schedulability assessment framework in [30] to evaluate the real-time performance of our TSCH-like network under global EDF. The performance evaluation method is a state-of-the-art supply/demand-based schedulability test leveraging the concept of *forced-forward demand-bound function* (FF-DBF) [109] from multiprocessor scheduling theory. Essentially, this method evaluates if the *supply-bound function* (SBF), here the minimal transmission capacity offered by an RT-WSN with m channels, is equal or larger than the upper-bound of the FF-DBF network demand when adapted to WSNs (FF-DBF-WSN) [31].

Formally, Eq. (2.8) presents the traffic schedulability test for RT-WSNs, where $\text{sbf}(\ell)$ is such that satisfies the conditions in (2.9), and the FF-DBF-WSN is defined in Eq. (2.10).

$$\text{FF-DBF-WSN}(\ell) \leq \text{sbf}(\ell),\ \forall \ell \geq 0. \tag{2.8}$$

$$\text{sbf}(0) = 0 \wedge \text{sbf}(\ell + h) - \text{sbf}(\ell) \leq m \times h, \forall \ell, h \geq 0. \tag{2.9}$$

$$\text{FF-DBF-WSN}(\ell) = \overbrace{\frac{1}{m}\sum_{i=1}^{n} \text{FF-DBF}(f_i, \ell)}^{\text{CHANNEL CONTENTION}} + \overbrace{\sum_{i,j=1}^{n} \left(\Delta_{i,j} \cdot \max\left\{ \left\lceil \frac{\ell}{T_i} \right\rceil, \left\lceil \frac{\ell}{T_j} \right\rceil \right\} \right)}^{\text{TRANSMISSION CONFLICTS}} \tag{2.10}$$

Note that the expression for FF-DBF-WSN is composed by two terms, namely, *i*) channel contention and *ii*) transmission conflicts. The former - in the left parcel of (2.10) - represents the mutual exclusive condition for allocating concurrent transmissions on multiple channels, equivalent to the FF-DBF expression for multiprocessors scheduling [109]. The latter – in the right parcel of (2.10) – models the delay contribution due to multiple flows encountering at a common half-duplex node. Eq. (2.11) defines $\Delta_{i,j}$ as a delay factor representing the node-path overlapping between any pair of flows f_i and $f_j \in F$ (with $i \neq j$), as in [110].

$$\Delta_{i,j} = \sum_{\alpha=1}^{\delta(ij)} Len_{\alpha}(ij) - \sum_{\beta=1}^{\delta'(ij)} (Len_{\beta}(ij) - 3) \tag{2.11}$$

where $\delta(ij)$ is the total number of overlaps between flows f_i and f_j of which $\delta'(ij)$ are the ones larger than 3. The length of the α^{th} and β^{th} path overlaps between f_i and f_j are termed $Len_{\alpha}(ij)$ and $Len_{\beta}(ij)$, respectively, with $\alpha \in [1, \delta(ij)]$ and $\beta \in [1, \delta'(ij)]$. Note that this expression considers the fact that after 3 hops slots can be reused, not causing further transmission conflicts.

2.3.3 Related Work

2.3.3.1 Single-Gateway Designation

Prior work has addressed the problem of how to properly designate a node for the role of gateway, i.e. among the existing nodes in the infrastructure, to choose the one which is more suitable according to a given key performance indicator. These works have often targeted specific metrics such as energy efficiency [111], timeliness [112], etc., or composite trade-offs [113], e.g. with the goal of reducing load and interference[114]. Moreover, a great part of related work has considered optimization-based problems [115], yet often relying on positions or distance-based inputs to find a suitable solution. This, however, is typically deemed as a different problem called gateway *placement*. Conversely, in our research, we capitalize on the concept of *network centrality* from graph mining to propose a (position-agnostic) centrality-driven gateway designation method for real-time WSNs with improved performance in terms of *schedulability*. The concept of network centrality has been widely applied in previous research on wireless networks to solve several problems, namely, for information dissemination in Delay-Tolerant Networks (DTN) [116] or for reducing traffic congestion in Information-Centric Networking (ICN) [117] to improve, for instance,

caching and content delivery. Centrality has also been applied in wireless networks for network modeling or protocol design, e.g. for routing [118], topology control [119], security [120], among others. Nevertheless, the notion of centrality for gateway designation has been considered in few works only (e.g. [112]). Specifically, Xing et al. [112] proposed a method for gateway designation for improving information timeliness, although close to our research, without explicitly targeting *real-time* performance guarantees, e.g. worst-case end-to-end delays or schedulability.

2.3.3.2 Multi-gateway designation.

Previous works in the literature have demonstrated that using multiple sinks or gateways increases parallelization of flows and improves traffic timeliness in WSNs (e.g. [121; 122]). Similarly, several studies (e.g. [123][124]) in the field have focused on the problem of selecting a subset of nodes as gateways for a WSN. Chen et al. [123], for example, have shown that the minimum gateway designation problem with latency and reliability guarantees in a TSCH network is NP-hard. The authors proposed a method to address this problem that jointly considers RPL routing and DeTAS [125] scheduling, but they didn't target schedulability. Dobslaw et al. [124] explicitly addressed *schedulability* as a QoS constraint by proposing a complete cross-layer configuration for industrial WSN that considers, among others, the possibility of adding multiple sinks. This work - as many others in related literature - relied on actual node positions for finding an appropriate gateway or sink designation/placement, in this case, based on the popular k-means clustering. This approach, however, is not applicable when physical positions are unknown, and when the only information available is the logical network topology; as in our case. Other studies have addressed alike problems (e.g. [126; 127]), either from the perspective of clustering and/or from the viewpoint of multi-sink placement, targeting common delay or reliability issues; yet, often ignoring the cornerstone aspect of real-time performance, i.e. *schedulability*, and/or assuming a match among physical and logical topologies. In contrast, our research tackles these downsides by relying on topological information only - in the form of an adjacency matrix - to designate multiple gateways in real-time WSNs while still resorting to the concept of *network centrality*.

2.3.3.3 Real-Time Routing

Theoretical and empirical studies for modeling and assessing the real-time performance of multi-channel TDMA networks have been discussed in recent literature, e.g., [128; 129; 130; 131], usually having as the main focus priority-based packet scheduling algorithms. The span of analytical works includes the design of methods based on response-time analysis [128], supply/demand-based tests [110], network calculus [132], etc., often deriving theoretical/empirical bounds attempting to guarantee worst-case real-time network performance. Both fixed-priority (e.g. RM) and dynamic-priority schedulers (e.g. EDF) have been covered, often assuming a standard behaviour for the rest of network features, e.g., routing. While for routing there are many works in the literature of TSCH-like globally synchronized networks [133], only a few of them fit into the class of *real-time wireless routing* [134], i.e., tailored routing methods aiming to enhance and/or

guarantee the real-time performance of wireless networks. Particularly, Wu et al. [134] made a step ahead in this direction by proposing a *conflict-aware real-time routing* for WirelessHART networks under a fixed-priority policy, but they did not address dynamic-priority schedulers. Conversely, we advocate for the use of EDF, in conjunction with our *minimal-overlap* real-time routing scheme. While by reducing *overlaps* we also diminish worst-case conflict delays, as in [134], our approach does not generate the routes one by one until they become schedulable, as in [134]. Instead, we offer a set of optimized routes which, overall, reduces overlaps to improve schedulability. Note also that we support the use of this routing method jointly with a centrality-driven gateway designation method to further improve real-time performance; as no other work in the literature.

2.4 Summary & Concluding Remarks

This chapter has provided essential background for the remaining of this dissertation. We have included general definitions to contextualize our research directions, as well as specific theoretical frameworks common to each of the two main parts of this thesis: overwater and real-time.

In terms of the general background, we have also clarified the scope of this thesis in terms of physical, data-link and network layer fundamentals which are most relevant for our research.

- At the physical layer, we provided notions on overwater RF propagation and limited our dissertation to the large-scale fading effect of path loss.
- At the data-link level, we support a predictable network operation by means of a globally time-synchronized framework, e.g. using a single- or multi-channel TDMA MAC. We also support the use of the EDF real-time policy for scheduling all transmissions.
- At the network layer, we have assumed a standard (source) routing operation, e.g. using shortest paths. We are also constrained by the full knowledge of logical network connectivity, e.g. implemented by means of a topology tracking or maintenance algorithm.

We have also provided specific background in overwater propagation where we established the two-ray as the fundamental tool to be used to model the impact of tides on overwater links. In this direction, we revisited the classical expressions of the two-ray model both shore-to-shore and shore-to-vessel scenarios. These expressions represent a common framework for the channel modeling and characterization efforts in Chapter 3, as well as for the proposal of the design methods and methodology in Chapter 4 and Chapter 5, respectively.

Similarly, we have also discussed specific background on real-time communication. In these terms, we defined common modeling basis for the network, flows and performance evaluation, using a real-time systems perspective. This common framework is used later in our synthetic simulation studies for gateway designation in Chapter 6 and Chapter 7, and for our real-time routing proposal in Chapter 8. Note we have not discussed *centrality* here since included then in the specific chapters where the idea of centrality-driven gateway designation is introduced.

Finally, we have also discussed a selection of relevant works in the literature for each of the core parts of the thesis, i.e. overwater and real-time communication, respectively. The first part included three categories of closely related work on overwater communication, particularly covering research on tidal fading, intertidal zones, and RF propagation over mixed water/land paths. We focused on these categories since they represent our main research targets in overwater communication. The second part reviewed literature on real-time communication focusing on the topics of single gateway designation, multi-gateway designation and real-time routing. Overall, offering essential basis to better understand and contextualize the work in this thesis.

Part I: Overwater Communication

Chapter 3

Modeling & Characterization for Overwater Links affected by Tides

In this chapter, we investigate overwater RF propagation from the perspective of channel modeling and characterization. We focus on large-scale fading dynamics due to the impact of *tides*, and more specifically, on how a modeling approach based on the two-ray propagation model can be useful to characterize this effect. We consider links of short to medium range distance (of up to 1 km) with antennas at a few meters above the surface, particularly, when different antenna heights and/or type of antenna polarization are employed. Analytical results for this configuration show the performance of overwater links may be better with lower antennas than higher antennas as well as with one polarization or the other, intuitively, during part of the tidal cycle. Experimental results from shore-to-shore overwater links operating in the 2.4 GHz RF band show considerable consistency between measurements and model estimates, leading us to conclude the two-ray model may bring benefits when applied to network design over tidal waters; our end goal.

Most material included in this chapter is derived from the following scientific publications:

- M. G. Gaitán, L. Pinto, P. Santos and L. Almeida, "On the Two-Ray Model Analysis of Overwater Links with Tidal Variations", in INForum 2019 [7].
- M. G. Gaitán, P. Santos, L. Pinto and L. Almeida, "Experimental evaluation of the two-ray model for near-shore WiFi-based network systems design", in IEEE VTC2020-Spring [6].

3.1 Problem Overview

We leverage the common understanding in RF propagation which deems the two-ray model as one of the effective tools to predict large-scale fading dynamics over water scenarios [37]. While most of existing research has focused on long-range communication, we conjecture the geometrical and physical principles of the two-ray model can also be applied to short/medium range settings, even when using antennas close (or very close) to the surface. In this direction, we aim to understand

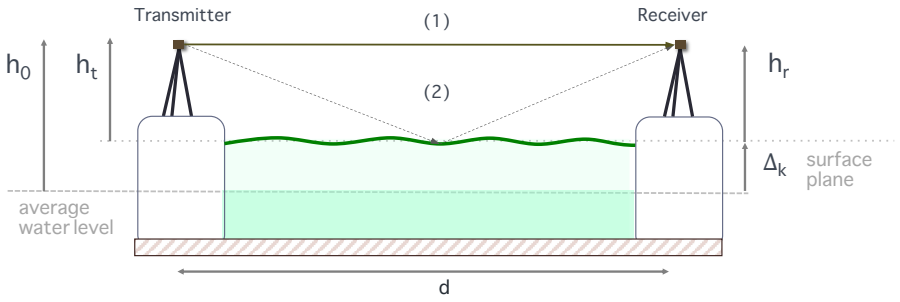

Figure 3.1: A shore-to-shore overwater link showing parameters according to the two-ray model.

and verify how water level shifts in the order of the antenna heights (e.g. due to tides) can influence link quality, given the limited distance/height setting of operations.

In the following, we resort to an illustrative example for a shore-to-shore overwater link to better describe the channel modeling and characterization factors we are taking into account.

Illustrative example. Fig. 3.2 shows results for the two-ray model assuming a shore-to-shore scenario as the one presented in Fig. 3.1. We consider the case when both transmitter and receiver antennas are at the same height (i.e. $h_t = h_r = h_0$) w.r.t. an average water level, and we analyze this setting for link distances within the range of 10m to 1000m. We do not explicitly consider the water level variation Δ (in Fig. 3.1) influencing the surface reference, yet we analyze the case when using two different antenna heights, i.e. 2m and 3m. This setting is somehow equivalent to the situation of having a shore-to-shore link with equal antenna heights, either 2m or 3m, but when being influenced by an upward or downward water level shift of $\Delta = 1$m, respectively.

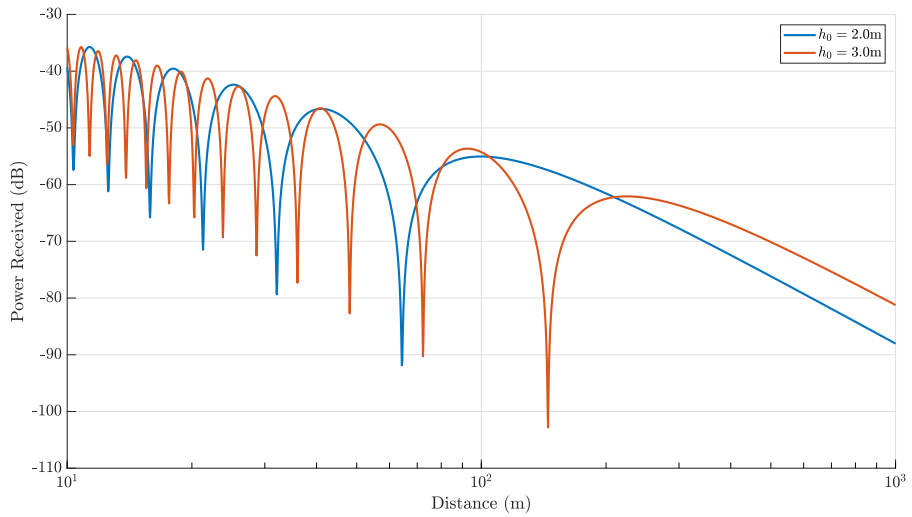

Figure 3.2: Two-ray model showing that received power is affected by both the link distance and the antenna height (h_0) relative to the reflective surface.

In the following, we provide some observations related to this particular setting, with a focus on the shift/impact of antenna heights, e.g. due to tides.

- *i*) **The shift of deep fades**. It can be seen that a small variation in antenna heights (i.e. 1m) can be translated into a shift in the position of deep fades or nulls on the x-axis. A similar effect occurs with the maximum signal strength (peaks) which also shifts on the x-axis due to the same reason. This suggests tides may produce alike dynamics but on a temporal basis.

- *iii*) **Break point distance**. After the last null of each curve, we can see a change of trend/slope in path losses; after a point called *break point distance* or d_{break}. We observe that a shorter antenna height shows a shorter break point distance. We recall that after d_{break} path loss decay is more accentuated, thus worse (on average) than if being in the nulls region.

- *ii*) **The density of nulls**. The number of nulls along the link path is visually greater for the higher than for the lower height. This suggests a more steady and better signal behavior (on average) for the lower antenna heights; at least until the break point distance. This is opposed to the common design principle of having antennas at the largest feasible height.

- *iii*) **Complementary behavior**. At some distances, one antenna configuration may present a null while the other is at a peak or at a higher signal strength level. This, of course, enables complementary (or spatial diversity) opportunities for improving signal quality.

Discussion. While the above observations are certainly somehow part of prior propagation studies, wireless link practitioners often do not take into account all of them together, especially when deploying RF links over tidal waters. The shift of nulls, e.g., although graphically trivial, does not necessarily offer trivial dynamics from the temporal viewpoint. Similarly, the d_{break} although more commonly considered as a link design parameter, it is often assumed to be static, an assumption that does not hold true when links are influenced by a shift in antenna heights, e.g. due to tides.

The density or number of nulls, although relevant for the overall stability of link quality is not always explicitly considered by prior research. Since most efforts focus on long-range communication, links often operate beyond the nulls region (i.e. after d_{break}), and thus this factor is typically ignored. However, as we could see in the illustrative example. a lower antenna height looks to be less prone to suffer nulls or deep fades if evaluated over a full span of distance or height values. This can be important, e.g., when accounting for the average attenuation experienced over a full tidal cycle, or equivalently, over a complete span of distances along the link path.

While spatial diversity has been traditionally used to counteract such a kind of issues, this technique is often engineered to be effective at a given worst-case instant (e.g. between two extreme antenna heights) but not necessarily along a full gamut of distance/height values.

In the following, we present analytical and empirical results related to the impact of shifts in antenna heights on shore-to-shore overwater RF links. The material, although yet initial, offers crucial modeling and characterization insights for the contributions in the next chapters.

Organization. The rest of this chapter is organized as follows. Section 3.2 presents analytical results based on the two-ray model for shore-to-shore overwater links affected by tides. Section 3.3 offers an experimental evaluation of the two-ray model over a given set of link distances and two antenna heights. Section 3.4 provides concluding remarks.

3.2 Analytical Results: Antenna Height & Polarization

In this section, we aim to assess the impact of antenna height and polarization on the path loss performance of overwater links during a full tidal cycle. We perform this assessment from the perspective of the two-ray propagation model with output in terms of received power given the more practical usage of this measure. We target links of short and medium-range distances with antennas at a few meters above surface. We consider this link configuration due to its particularly challenging conditions when in presence of tides. We note that, in general, shorter link distances are more prone to the occurrence deep fades or nulls than longer distances, while low antenna heights, in the order of magnitude of the tides, may intensify this effect.

3.2.1 Simulation Setup

We consider shore-to-shore RF links as those in Fig. 3.1 using either vertically or horizontally polarized antennas. We assume these links operate in the 2.4 GHz RF band (e.g., common for WiFi, TSCH or LoRa) over a reflective medium with relative permittivity set to $\varepsilon_r = 81$ (typical value for sea/fresh water) [80]). We also consider two link distances, $d = 100$m and $d = 200$m, and two nominal antenna heights, $h_0 = 2$m and $h_0 = 3$m, for both transmitter and receiver, i.e. $h_0 = h_t = h_r$. Nominal heights are measured w.r.t. an average water level, then influenced by tides.

We assume the water surface fluctuates due to tides $\Delta = 1.25$m above and below the average water level, following a cosine function along a full tide cycle. As result, the relative antennas heights to the water surface can be represented mathematically as follows:

$$h(t) = h_0 + \Delta\cos(2\pi t/100), \forall t \in [0, 100] \tag{3.1}$$

For clarity, note that this setup offers parametric inputs only then used by simply writing and then running the two-ray model equation with tides in MATLAB.

3.2.2 Simulation Results

Fig. 3.3 and Fig. 3.4 show the results for the power received in dB for both vertical (top) and horizontal (middle) polarization when using antenna heights fixed to $h_0 = 2$m (blue) and $h_0 = 3$m (red), with link distance of $d = 100$ and $d = 200$, respectively. Both figures also show the amplitude of the (instantaneous) relative antenna heights (bottom) with respect to the water surface as a function of the progress on the tidal cycle.

These results reveal vertical polarization (top) manifests significant dips in the received power for both antenna heights as a consequence of variations in the water level; a phenomenon also

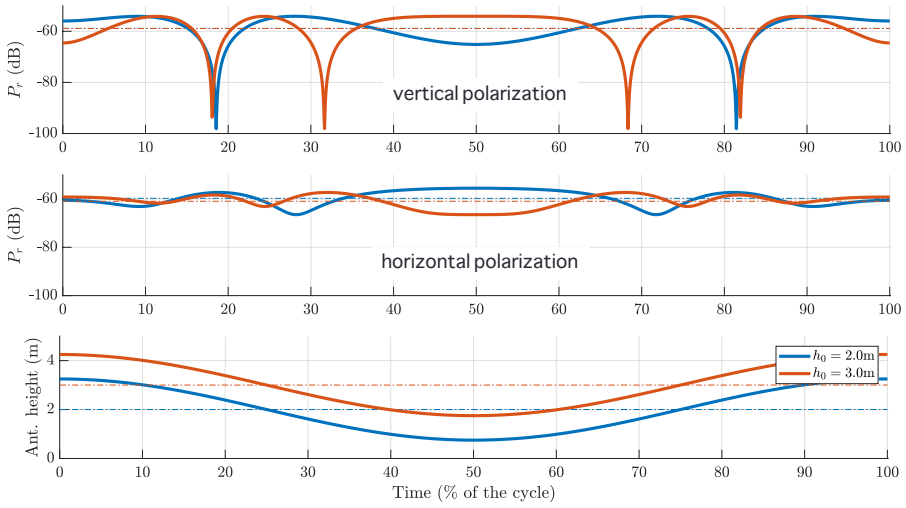

Figure 3.3: Power received at $d = 100m$ for vertical (top) and horizontal (middle) polarization, and relative antenna height to the surface $h(t)$ (bottom) along a tidal cycle.

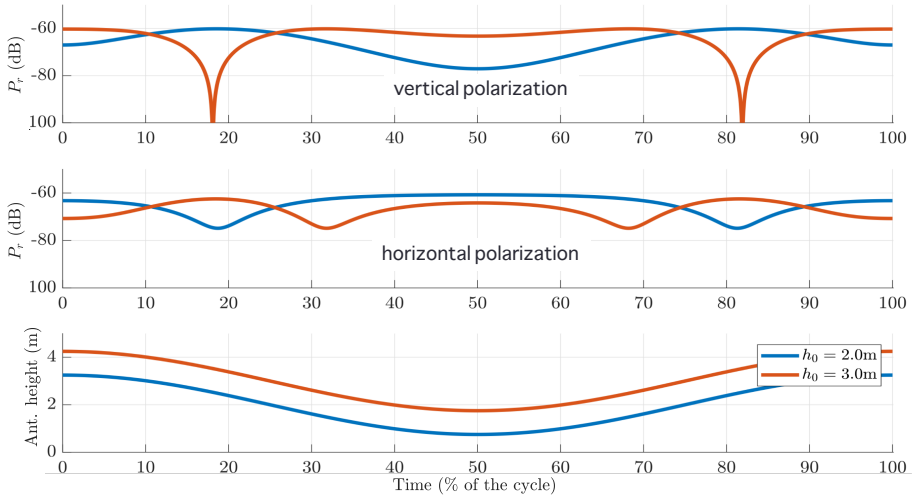

Figure 3.4: Power received at $d = 200m$ for vertical (top) and horizontal (middle) polarization, and relative antenna height to the surface $h(t)$ (bottom) along a tidal cycle.

known as *tidal fading* [67]. Interestingly, the number of the dips (and thus the percentage of the time the dips degrade the received power) is higher for the case of antennas being placed higher. This is consistent with previous observations in terms of the density of deep fades. Concretely, Fig. 3.3 shows only two dips for the case of $h_0 = 2$m and four dips for the case of $h_0 = 3$m. Similarly, Fig. 3.4 shows one dip for $h_0 = 3$m but only slight degradation due to tides for $h_0 = 2$m, which suggest this latter configuration falls after the region where so-called nulls or deep fades occur, i.e. d_{break}. Moreover, in both cases, Fig. 3.3 and Fig. 3.4 show long and continuous time-spans of at least 20% to 40% of each respective tidal cycle with good signal reception.

Notably, in the horizontal polarization case, i.e., Fig. 3.3 (middle) and Fig. 3.4 (middle), the

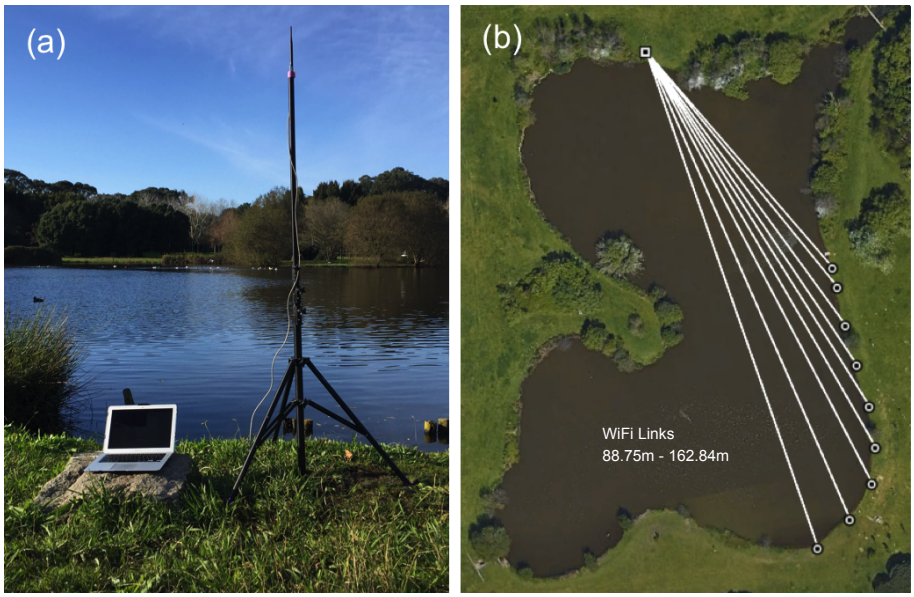

Figure 3.5: The experimental setup showing: (a) a representative node deployment at the actual location, and (b) the set of links and nodes positions evaluated.

signal strength is quite similar and stable during the full cycle for both antenna configurations, as well as for both link distances. Particularly, showing no significant dips as a consequence of the vectorial cancellation between reflected and direct rays. Also, in both cases, the average power received for horizontal polarization is generally higher than the observed for the vertical scenario.

Note that although these results may suggest less susceptibility to signal degradation when using horizontally polarized antennas, this theoretical condition may not be easy to verify in practice. This is because horizontal polarization is typically set up by placing dipole antennas horizontally, which puts extra consideration on the directionality required for the antenna alignment. Unfortunately, such a factor may represent a considerable drawback for a real-world overwater network deployment, reason why we don't further explore it in this dissertation.

3.3 Experimental Results: Shore-to-Shore Overwater Links

In this section, we present signal strength measurements from an experimental campaign at the shore of a freshwater body to verify if the two-ray model can predict the major trends of the path loss experienced by a 2.4 GHz overwater wireless link. These experimental results complement the analytical study by providing practical insights within the distance/height range of interest.

3.3.1 Testbed Setup

We deployed a temporary testbed at the shore of a small freshwater lake situated at the Porto City Park, in Porto, Portugal, to collect packet-based RSSI measurements using different links. We used two WiFi-based nodes using COTS devices to set up each link. Each node consisted of a

USB dongle wireless card installed at the top of a tripod and connected to a laptop through a cable extension, as shown in Fig. 3.5 (a). One node acted as a transmitter and was kept at a specific position on one side of the shore. The other node acted as a receiver and was placed at other 9 different positions on the other side of the shore; as shown in Fig. 3.5 (b). Both nodes were always kept at a constant distance of $\sim$ 1m from their respective shore.

The receiver positions were chosen in order to generate a set of links within a range akin to the one in the analytical study of the previous section. The positions were saved in a KML (Keyhole Markup Language) file from which the distances were obtained using the Google Earth tool. The resulting distances were 88.75m, 94.33m, 105.2m, 117.28m, 130.11m, 141.9m, 151.17m 158.11m and 162.84m. Concerning the heights, they were measured w.r.t. the water surface using a conventional measuring tape. Specifically, we consider two different antenna heights, 1.45m and 2.45m, for the transmitter and receiver, respectively. Note the lake at which the measurements were performed is not affected by tides. Thus, the water level was kept constant over the duration of the experiments. Moreover, the water was calm (i.e. without significant undulation), while not being greatly affected by other environmental phenomena, e.g., wind, fog, or evaporation.

As radio hardware, we used two USB dongle Amiko WLN-880 coupled to a standard short monopole (rubber ducky) antenna, vertically[1] positioned. The commercial antennas used had omnidirectional radiation patterns with a nominal gain of 5 dBi in the 2.4 GHz RF bands. We set all transmission to Channel 1 (2412 MHz) using default IEEE 802.11b (WiFi) configurations, namely: beacon frames sent periodically every $\sim$ 100ms, and at a fixed transmission power of 20dBm. Finally, we collected data during $\sim$ 3min at each height/distance combination.

3.3.2 Measurements Results

Figure 3.6 presents the RSSI measurements collected utilizing the configurations above described together with the corresponding values predicted by according to the two-ray model (in dBm).

These results reveal two particular features related to our prior analytical studies. First, the RSSI obtained with the lower antenna height (1.45m) was on average higher than the one obtained with larger antenna height (2.45m), for distances up to 150 m. After that, the relationship is inverted. Second, we observed a substantial deviation (of about 8 dB) in the received power when the antenna is at 2.45m, approximately within the 90m and 130m range. These results are consistent with the rough trends predicted by the two-ray model, which indicate: *i*) an inversion of the antenna height that experiences the highest RSSI for the same distance (at 130m); and *ii*) a considerable null in received power for the 2.45m antenna height (between 80-120m).

While the measured and estimated patterns are graphically similar, there is some numerical mismatch both in the received power and the distances at which the mentioned phenomena occur. We argue this stems mainly from two reasons. First, the measurement methodology may have suffered some relevant limitations, e.g. regarding the accurate measurement of distances, heights,

[1]Note that despite the promising theoretical results for the horizontal antenna polarization in the previous section, we only considered vertical polarization here for practical reasons.

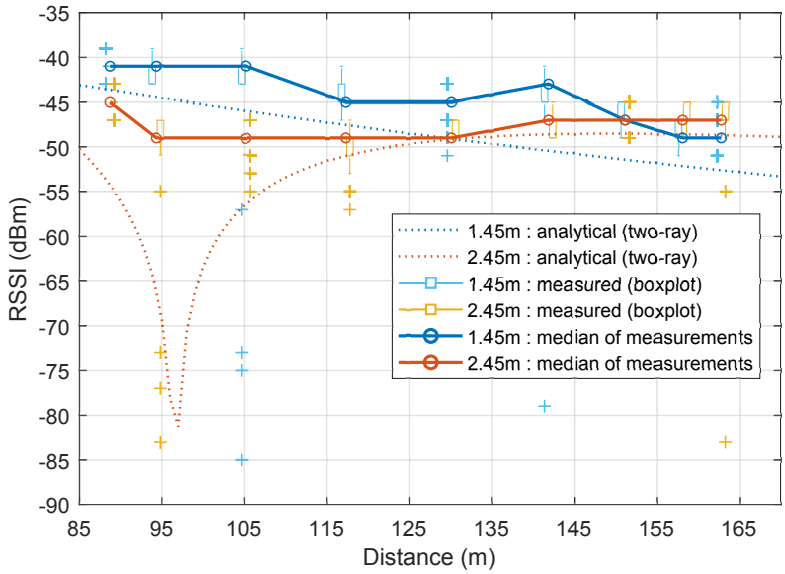

Figure 3.6: Two-ray model RSSI estimates for two antenna heights (dotted lines) and field measurements at selected distances (per distance, two side-by-side boxplots [one per height], slightly offset to true distance and color-faded for readability; outliers shown as crosses); medians of measurements are connected (solid line).

and cable attenuation. A thorough revision of the methodology is necessary for future experimental campaigns to minimize such sources of error. Nevertheless, this was beyond the exploratory nature of the current measurements. Second, although the two-ray model is able to capture the impact of one of the main path loss components in near-surface communications (the reflected ray), this is not the only propagation effect taking place. Other phenomena, such as additionally reflected rays due to multipath, scattering, diffraction, among others, can also contribute to variations in the measured received power, and may explain, e.g. why the signal loss obtained for the 2.45m height around 95m was not of the magnitude predicted by the model.

3.4 Summary & Concluding Remarks

In this chapter, we have presented initial modeling and characterization studies for shore-to-shore overwater links affected by tides. We have provided analytical results for two antenna heights and polarization showing revealing dynamics due to the impact of shifts on the antenna heights. Then, since we advocate for the use of the two-ray propagation model to predict those dynamics, we have also provided empirical measurements in this direction. Overall, the experimental results showed reasonable agreement with the model in terms of path loss trends, yet also showed a mismatch due to additional propagation phenomena. We argue these initial results are a useful input to further improve the modeling of large-scale dynamics in overwater RF links affected by tides, showing evidence of the applicability of the two-ray model in limited distance/height configurations. In the

next two chapters, we capitalize on some of these results by providing novel link design methods to effectively improve link quality (e.g. received power) in both shore-to-shore and shore-to-vessel communication scenarios; our end goal.

As future work, that is not necessarily related to the direction of the next two chapters, we see two concrete opportunities. First, to further dig into the potential horizontal polarization benefits from an experimental point of view, i.e. looking for opportunities in which this typically less practical configuration (when using a monopole) may have applicability. Similarly, further explore the potential benefits of horizontal polarization as part of polarization diversity configuration, both, theoretically and empirically. Second, to perform a more complete sensitivity analysis of different parameters (e.g. distance, heights, tidal range) influencing path loss in the two-ray model, while looking into details such as number (and depth) of the nulls, break point distance, and the number of horizontal shifts incurred. Also, by considering related concepts such as the Fresnel Zone.

Finally, an additional opportunity related to diversity and the impact of different antenna heights is to formally extend these notions to the domain of multiple-input and multiple-output (MIMO) systems. While a similar modeling direction was taken in [28] for vehicle-to-vehicle communication channels, maritime communication and sea-level dynamics not only related to tides offer clear challenges and opportunities for MIMO systems, especially from the perspective of diversity on counteracting fading, and/or self-interference patterns. We argue this is a promising modeling research line too which may improve the understanding of the vessel-to-shore overwater channel, e.g. by complementing empirical related studies such as [72].

Chapter 4

Tidal-Informed 2-Ray-Model-Based Link Design and Positioning

In this chapter, we address the detrimental impact of tides and surface reflections on RF links of short to medium-range distances for both *shore-to-shore* (S2S) and *shore-to-vessel* (S2V) communication. We propose novel link-design strategies aiming at improving path loss performance during the whole tidal cycle and/or at a specific point of the tide. Particularly, our approach capitalizes on the geometrical basis of the two-ray model to contribute with tailored antenna heights and positioning-based methods for stationary (e.g. buoys) and/or mobile (e.g. AUVs) communication nodes. Experimental results with WiFi technology operating in the 2.4 GHz RF band clearly validate our link quality model. Analytical results with varying parameter configurations evidence the importance of our research directions. Notably, in experiments with a mobile AUV operating at the surface, our approach showed to outperform the common practice of placing onshore antennas at the largest possible height and/or surface nodes at a short but arbitrary distance.

Most material included in this chapter is derived from the following scientific publications:

- M. G. Gaitán, P. Santos, L. Pinto and L. Almeida, "Optimal Antenna-Height Design for Improved Capacity on Over-Water Radio Links Affected by Tides", in IEEE OCEANS 2020 [5].
- M. G. Gaitán, P. d'Orey, P. Santos, M. Ribeiro, L. Pinto, L. Almeida and J. Sousa, "Wireless Radio Link Design to Improve Near-Shore Communication with Surface Nodes on Tidal Waters", in IEEE OCEANS 2021 [4].

4.1 Problem Overview

Wireless RF links deployed over water environments (e.g., rivers, lakes, or harbors) are known to be affected by the conductive properties of the water surface, strengthening signal reflections and increasing interference effects [37; 38]. Additionally, recurrent natural phenomena such as tides (or waves) cause shifts in the water level that, in turn, intensify self-interference patterns and/or cause additional propagation impairments, e.g. *tidal fading*. In particular, this latter effect

– resulting from the impact of tides on the link quality – becomes noticeable when at least one of the communication terminals does not keep a fixed height w.r.t. the water level. While prior methods have been proposed to counteract this detrimental issue [67; 98], conventional studies have mostly focused on long-range communication, typically exhibiting propagation conditions different than those for short/medium-range communication scenarios; our main target.

In this chapter, we go beyond conventional studies by proposing methods to mitigate tidal fading in both S2S and S2V scenarios showing few or all the following characteristics:

1. **Short/medium range distances**. Long-range communication links (e.g. > 1km) often fall after the so-called *break point* distance, i.e. the distance point at which (according to the 2-ray model) RF propagation offers a monotonically decreasing trend. The short/medium range region instead, offers a challenging non-linear behavior leading to *deep fades* (or nulls) which can be shifted or further aggravated by the influence of tides.

2. **Low antenna-heights** (Onshore). Typically, remotely-controlled marine robotics (S2V) and IoT environmental monitoring systems (S2S or S2V) rely on onshore stations that use antennas at a low height (e.g. 1m to 5m). This implies water level variations due to tides (e.g. 0.5m or 1.5m) can be in the order of magnitude of the antenna heights, which may lead to big shifts on the propagation conditions experienced between high tide and low tide.

3. **Very low antenna-heights** (On vessel). Small vessels such as AUVs or USVs often include external antennas of very low height (e.g. 17.5cm for an AUV [135]) with lengths comparable to the signal wavelength (e.g. 12.5cm for WiFi@2.4 GHz). Despite being often ignored, tides represent an extra challenge for this cm-level situation that may exacerbate existing propagation effects and/or lead to still unexplored propagation conditions.

In order to take into account these specific observations, we propose here a set of novel tidal-informed and two-ray-based link design strategies to improve communication in S2S and S2V scenarios, considering stationary (e.g. buoys) and/or mobile (e.g. ASVs) communication nodes.

Organization. The remainder of this Chapter is organized as follows. Section 4.2 formulates our antenna-height design problem for stationary nodes that minimizes tidal fading when taking into account the whole tidal cycle. Section 4.3 presents a method for short-term positioning of mobile nodes in order to minimize path losses at a specific point of the tide. Section 4.4 offer extensive analytical results for the problem/solution in Section 4.2, while Section 4.5 present experimental results related to Section 4.3. Section 4.6 provide concluding remarks.

4.2 Tidal-Informed Path Loss Minimization for Stationary Nodes

In this section, we consider the problem of *minimizing* the average path loss performance of over-water RF communication links consisting of stationary (and static) nodes when taking into account the impact of the whole tidal cycle. We target both S2S and S2V communication scenarios in which common physical parameters such as link distance and antenna heights can be known

and/or controlled beforehand. We also assume knowledge of the tidal pattern or alternatively of the *tidal range*, defined as the difference between high tide and low tide magnitudes.

In both S2S and S2V scenarios, we rely on the validity of the well-known two-ray propagation model to describe the average large-scale fading dynamics of links deployed over tidal waters. In particular, for the purposes of problem formulation, we consider the following simplified version of the two-ray model in its average path loss form (in dB):

$$L_{2ray} = -10\log_{10}\left(\frac{\lambda^2}{(4\pi d)^2}\left[2\sin\left(\frac{2\pi h_t h_r}{\lambda d}\right)\right]^2\right) \tag{4.1}$$

where $\lambda = c/f$ is the signal wavelength (with c the speed of light and f the operating frequency), d is the link distance, and h_t and h_r are the respective transmitter[1] and receiver antenna heights measured with respect to the water surface.

In the following, we formulate an antenna height design problem for minimizing average path losses experienced by an S2S and an S2V link over the span of a tidal range. We consider both S2S and S2V scenarios separately, due to their different response to the impact of tides (see Fig.2.5). We emphasize that although both S2S and S2V scenarios are assumed in line-of-sight (LoS), only the S2S link never modifies its direct (LoS) path w.r.t. shifts in the water level. The S2V scenario, instead, always suffer instantaneous variations on both direct and reflected paths due to tides.

4.2.1 Shore-to-Shore: Onshore Antenna-Height Design

Consider an S2S communication link as the one presented in Figure 2.5(a) where the Tx and Rx antennas are static, installed at specific heights, namely h_t and h_r, respectively, measured w.r.t. to an average water level. Also, consider both Tx and Rx are separated by a horizontal (x-axis) link distance termed d. Then, assume a tidal pattern causing (discrete) variations on the average water level which influence both transmitter and receiver antenna-to-surface heights in $\pm|\Delta_k|$ meters.

By resorting to Eq. 4.1, we can trivially incorporate the Δ_k into the two-ray model as follows:

$$L_{2ray} = -10\log_{10}\left(\frac{\lambda^2}{(4\pi d)^2}\left[2\sin\left(\frac{2\pi(h_t+\boldsymbol{\Delta_k})(h_r+\boldsymbol{\Delta_k})}{\lambda d}\right)\right]^2\right) \tag{4.2}$$

where h_t and h_r are now *nominal* antenna heights measured with respect to an average water level.

Then, we formulate the problem of finding the optimal (single) onshore antenna height $h = h_t = h_r$[2] that minimizes the average path losses experienced over all possible Δ_k values within a

[1] Note that when we consider the transmitter on one specific shore or the other, e.g., for the S2S scenario, or the transmitter on shore and the receiver at the surface node (or vice-versa), for the S2V scenario, is just an example. The two-ray model is symmetrical and the roles of the nodes can be switched without any impact on the analysis.

[2] While we have considered the case of having both Tx and Rx antennas with the same nominal height, the problem can be trivially adapted to the case in which one of the antenna heights is given while the other needs to be optimized.

given tidal range as follows:

$$\begin{aligned} \underset{\boldsymbol{h}}{\text{minimize}} \quad & \frac{1}{N}\sum_{k=1}^{N} L_{2ray}(d,\boldsymbol{h},\Delta_k) \\ \text{subject to} \quad & \Delta_k \in [\Delta_L,\Delta_H],\ \forall k \in [1,N], \\ & h \in [h^{min},h^{max}] \end{aligned} \tag{4.3}$$

where $N \in \mathbb{N}$ is the number of steps of the discretized tidal range where the optimization expression is evaluated; Δ_k is the (signed) value of the k^{th} step, valid within the respective low tide (Δ_L) and high tide (Δ_H) maximum deviations (w.r.t. h); and $[h^{min},h^{max}]$ is the h feasibility region.

4.2.1.1 Onshore Antenna-Height Design with Two Antennas

We extend the previous method to incorporate a second[3] Rx antenna by assuming the first one is already positioned at the optimal antenna height h, hereinafter, h_1. We then choose the second antenna (h_2) as the one providing the largest improvement w.r.t. the path loss attenuation obtained using only h_1. To this purpose, we assume our antenna system is always capable of selecting as receiver the antenna (between the two) with the best signal signal quality. This reasoning implies the original objective function in (4.3) can now be modified to select as the second receiver antenna (height) the one experiencing the *minimum* path loss attenuation at each Δ_k step.

We formally express the described method for two antennas as follows:

$$\begin{aligned} \underset{\boldsymbol{h_2}}{\text{minimize}} \quad & \frac{1}{N}\sum_{k=1}^{N} \min[L_{2ray}^{h_1}(d,h_1,\Delta_k), L_{2ray}^{h_2}(d,\boldsymbol{h_2},\Delta_k)] \\ \text{subject to} \quad & \Delta_k \in [\Delta_L,\Delta_H],\ \forall k \in [1,N], \\ & h_2 \in [h_2^{min},h_2^{max}] \end{aligned} \tag{4.4}$$

where $L_{2ray}^{h_1}$ and $L_{2ray}^{h_2}$ denote the corresponding path loss attenuation (in dB) for h_1 and h_2 when using Eq. 4.2 influenced by a specific water level variation Δ_k .

4.2.2 Shore-to-Vessel: Onshore Antenna-Height Design

Consider now a stationary node at the surface as the one Fig. 2.5(b) (e.g., a buoy or floating mooring node) that needs to communicate with an onshore station (e.g. a gateway or base station), either continuously or over a long period w.r.t. the tidal cycle, and thus it is affected by fading due to tides. Further, assume these nodes are separated by a Tx-Rx separation d.

In order to mitigate tidal fading, we make use of the method in (4.3) adapted to the S2V scenario. The adaptation is rather simple since only requires modifying the two-ray model expression

[3] A general expression that incorporates n diversity antennas can be found in [5]. We do not include here this expression for brevity reasons. The case of $n \geq 3$ although useful for the overall system reliability (e.g., under unpredictable connectivity) might not be of further help when mitigating tidal fading, thus we do not further explore it here.

in Eq. 4.2 as follows:

$$L_{2ray} = -10\log_{10}\left(\frac{\lambda^2}{(4\pi d)^2}\left[2\sin\left(\frac{2\pi(h_t+\boldsymbol{\Delta_k})h_r}{\lambda d}\right)\right]^2\right) \tag{4.5}$$

where h_t is now the onshore antenna height and h_r the constant antenna height of the surface node.

Then, by using Eq. 4.5 into (4.3) we obtain the same method in (4.3) but now applicable for the S2V link scenario. Equivalently, the method provides an onshore antenna height $h = h_t$ that minimizes average path loss in an S2V link scenario over a given tidal range, with h_r given. Without major modifications[4] we could also assume h_t as given and h_r to be determined.

4.3 2-Ray-Based Positioning for Mobile Nodes

Consider now a mobile surface node, e.g. either a USV or an AUV at the surface, that executes a mission in a given area and, at some point in time, needs to communicate intensively, in a short time interval, with an onshore base station, be it for data offloading or for acquiring new mission information. The problem consists of determining a convenient distance to shore d_{conv} that will lead to sustained high received signal strength in a broad region so that the node can be driven to that distance and initiate communication reliably. Clearly, if the time span between the start and end of the mission is long enough to experience changes in the water level, the output d_{conv} will also take into account that fact, so the proposed positioning is assumed as aware of the tide.

By leveraging the validity of the two-ray model to describe RF overwater propagation in these conditions, we argue that a suitable region can be determined numerically as in Eq. 4.6, from the local maximum after the last null (or deep fade) predicted by the two-ray model.

$$d_{conv} = max(d) : \frac{\partial P_r(d)}{\partial d} = 0 \tag{4.6}$$

where P_r is the average power received of the link according to the two-ray model (with tides), which for the sake of completeness we formally present as follows:

$$P_r = \frac{\lambda^2}{(4\pi d)^2}\left[2\sin\left(\frac{2\pi(h_t+\Delta_k)\,h_r}{\lambda d}\right)\right]^2 P_t G_t G_r \tag{4.7}$$

where P_t is the Tx power, and G_t and G_r the respective Tx and Rx antenna gains.

We then claim that a good region for communication with high quality would be between d_{conv} and $2 * d_{conv}$ which although further away from the last null generally exhibits marginal attenuation w.rt. the maximum power at d_{conv}; as was observed empirically.

[4] Another trivial modification is to switch the variable to be solved to d, i.e. to find a convenient position when h_t and h_r are given. This adaptation can be found in [4], but it is not included here for brevity reasons.

4.4 Analytical Results: Stationary Nodes

This section provides analytical simulations with varying parameters for both S2S and S2V cases.

- In S2S scenarios, we assess the performance of our methods (4.3) and (4.4) against classical techniques, namely the *i*) largest feasible height, for the single-antenna case, and *ii*) a classic space-diversity criterion, for the dual-antenna case. For this latter benchmark, we use the criterion in [136] that recommends the use of a second antenna height (at least) at d_{sep}[5] meters apart from the first one, here assumed to be placed at the highest feasible position.
- In S2V scenarios, we asses method (4.3) for antenna-height design but when using the S2V version of the two-ray model in Eq. 4.5. In particular, we explore the impact of distance and antenna heights on the path loss performance when compared against the use of the tallest and worst (not the shortest) feasible heights.

4.4.1 Shore-to-Shore: Results

Consider links of distance d operating at $f = 2.4$ GHz that use both Tx and Rx antennas at the same nominal antenna height, i.e. $h_t = h_r = h$. Also, assume an arbitrary tidal pattern with a range equal to $|\Delta_L| + |\Delta_H|$ which influences the antenna-to-surface heights by step-wise water level variations of Δ_k, with Δ_k sufficiently small for the purpose at hand. Finally, consider a feasibility range of $h \in [h^{min}, h^{max}]$ with heights tall enough to avoid water reaching the antennas.

Fig. 4.1 present average path loss curves as a function of the antenna height for the methods (4.3) and (4.4) in blue and orange, respectively. These plots allow comparing our methods against the chosen benchmarks. The largest feasible height is visible by inspecting the x-axis, while the classical technique is marked with an arrow in all plots. The black-dotted curve is an alternate solution that considers one antenna at the top and the other placed using method (4.4).

1) Impact of link distance Fig. 4.1 (top) presents the average path loss when tidal deviations are between [−1,+1]m and when using two different link distances: $d = 100$m (top-left) and $d = 200$m (top-right). These results show that our method outperforms classical techniques on the two distances analyzed. The single-antenna solution achieves lower overall attenuation using a considerably lower antenna height, i.e., $h_1 = 2.29$m ($\ll 4m$) on both Tx-Rx separations. This much lower antenna-height solution also shows an improvement of $\sim$ 2dB and $\sim$ 5dB, for first and second link distances, respectively. Similarly, our dual-antenna method outperforms the classical space-diversity technique, both in terms of antenna height and path loss. The alternate antenna-height method although sub-optimal (but simpler) also outperforms the classical technique in terms of average path loss, albeit using a taller second antenna (3.64m vs. 3.22m).

2) Impact of tidal range. Fig. 4.1 (middle) presents results akin to the prior case with $d =$ 100m (top-left) but when the tidal range is reduced to [−0.5,+0.5]m (middle-left) and increased to [−1.5,+1.5]m (middle-right). The case of smaller tidal deviations (typically deemed as a better

[5] $d_{sep} \simeq \alpha \frac{\lambda \cdot d}{h_1}$, where α is $\simeq 0.25$, λ is the wavelength, d is the link distance, and h_1 is the height of the first antenna.

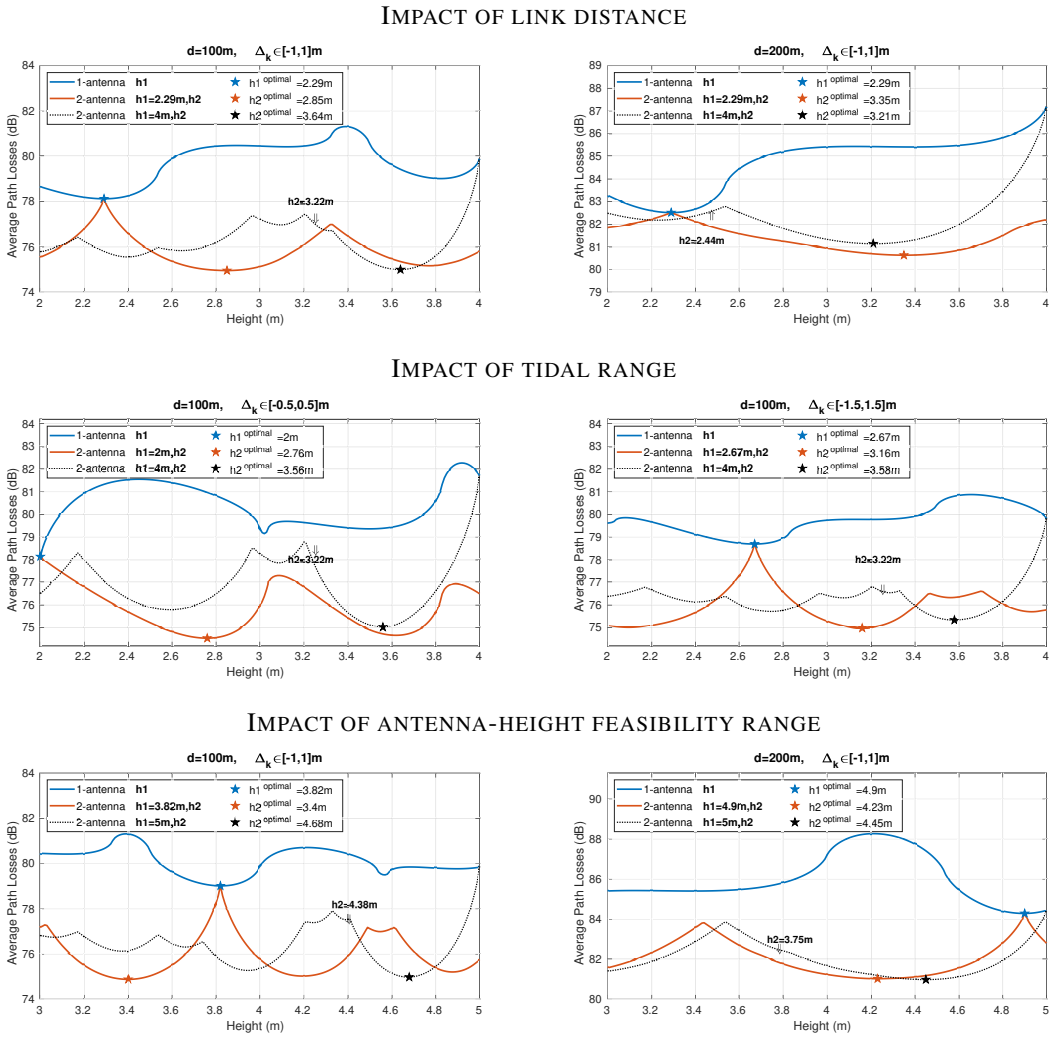

Figure 4.1: Average path losses over a tidal range as a function of the antenna height when using: (blue) 1 antenna; (orange) 2 antennas, one of them at the optimal single-case height; and (black-dotted) 2 antennas, one of them placed at the top, and the other by means of our method. In all cases, the star marks the antenna heights at which reception experiences minimal attenuation. The arrow indicates the second antenna height (and path loss) for the classical space diversity when using one antenna at the top, and the other vertically separated according to the criterion in [34].

condition) shows that for the single-antenna method the minimum attenuation is obtained at $h_1 =$ 2m, instead of $h_1 = 2.29$m, which is a better result in terms of antenna-height but of comparable attenuation. Interestingly, the results also reveal that by keeping the previous antenna height, i.e., $h = 2.29$m for the smaller range, we obtain a worse path loss performance (in about 5dB); thus not representing a better (tidal) scenario. The dual-antenna comparison against the classical approach shows our method (4.4) is superior both in terms of attenuation (in $\sim$ 2-3dB) and antenna heights. However, a key observation when interpreting this is the fact that the classical criterion (d_{sep}) in [136] does not incorporate tidal range as a parameter, thus making h_2 (classical) independent of it.

3) Impact of antenna-height feasibility range. Fig. 4.1 (bottom) shows results with a configuration alike to the one presented in Fig. 4.1 (top), i.e. with two link distances, but when antenna heights are constrained in the range [3,5]m. These results show that our methods are still superior than benchmarks for $d = 100$m, both in terms of height and path loss, but the improvement is marginal on the longer link ($d = 200m$) (see Fig. 4.1(bottom-right)). In addition, when comparing these results with the prior case (feasibility region within $[2,4]$m) (see top left and right), both the new second diversity antennas (h_2) of the classical technique show to be larger.

4.4.2 Shore-to-Vessel: Results

To assess the performance of S2V methods for stationary surface nodes we consider a set of analytical simulations covering a wide space of configurations of interest. Particularly, we explore link distance in the range $d \in [10, 1000]$ m and onshore antenna heights in the feasibility range of $h \in [3, 6]$ m. We assume the use of communication devices operating in the 2.4 GHz and 5 GHz frequency bands and a set of Rx antenna heights $h_r = \{0.3, 0.6, 1.2\}$ m characterizing different surface nodes, from floating mooring nodes to buoys of different sizes. Finally, we consider a relatively small tidal range $[-0.5, 0.5]$ m, which we step through with a step-size $\Delta_k = 0.1$ m.

Fig. 4.2 shows the average path loss as a function of the link distance d obtained by our antenna-height design method (solid blue line). For benchmarking, we also plot the path loss achieved when the onshore antenna is placed at the largest feasible height (dashed yellow line). We contrast both approaches against the worst-case scenario (dotted red line), i.e., the antenna height within the h feasibility range that maximizes average attenuation for each link distance.

As expected, given our optimal design method, our results are always better (or equal) than using the onshore antenna at the top of the feasibility range. Fixing the antenna at the top leads to strong variations in average attenuation in the near-shore region of the link, varying between the

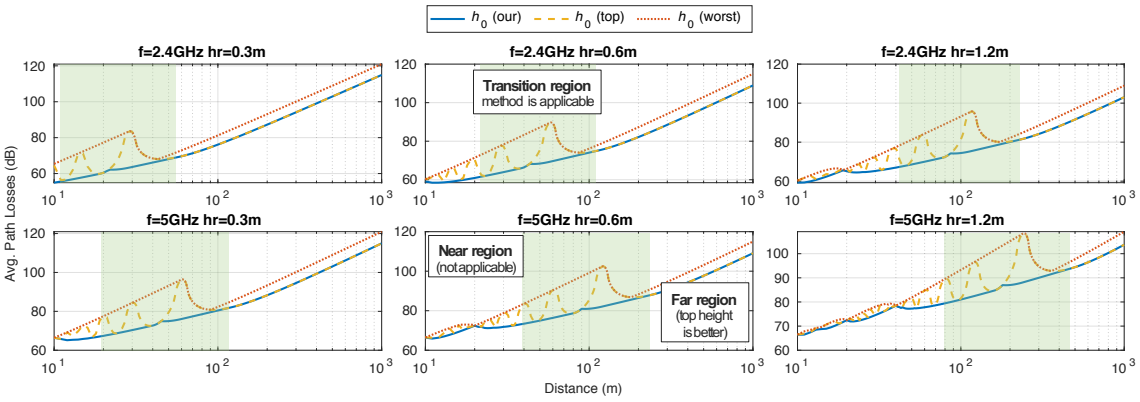

Figure 4.2: Link average path loss experienced over a given tidal range as a function of the link distance when using: our antenna-height design method (solid blue), the largest possible antenna height (dashed yellow), or the worst antenna-height (dotted red) for two frequency bands: 2.4 GHz (top row) and 5 GHz (bottom row); and three different heights of surface nodes: 0.3m (left column), 0.6m (middle column) and 1.2m (right column).

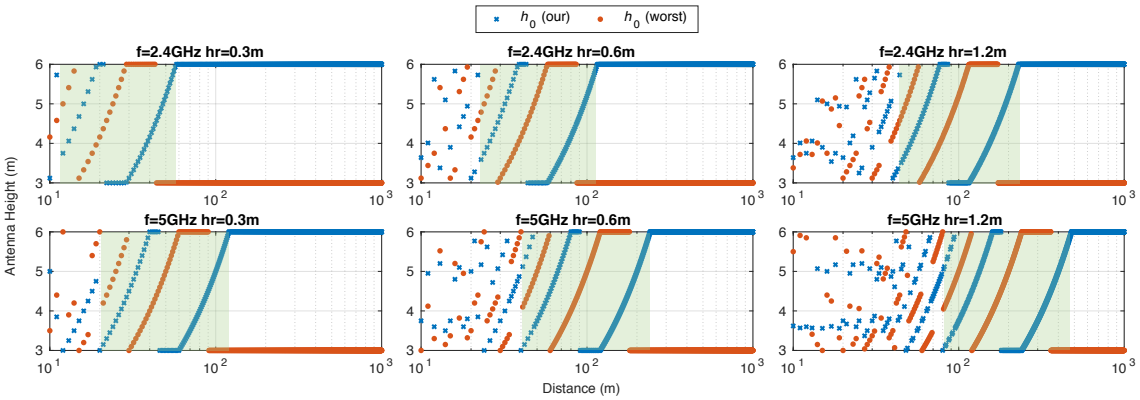

Figure 4.3: Onshore antenna height as a function of the link distance provided by our antenna-height design method (blue crosses), together with the worst performing height (red circles) within the feasibility range, for two frequency bands: 2.4 GHz (top row) and 5 GHz (bottom row); and three different heights of nodes: 0.3m (left column), 0.6m (middle column) and 1.2m (right column).

worst-case and the best-case for close link distances. Similar behavior also occurs with any fixed antenna height. This shows the importance of the careful choice of a specific antenna height for each target distance, particularly in the near-shore region. The results also show that the near-shore region expands significantly with the antenna height of the surface node, from 0.3m to 1.2m, and with the frequency band used, from 2.4 GHz to 5 GHz.

Fig. 4.3 shows the direct output of our antenna-height method, i.e., h as a function of the link distance d. The antenna height design method (blue crosses) is compared against the worst-case height (red circles) as defined before. These plots are very revealing, showing three clear zones in the link distance for each scenario:

- **Far region**. On the right in each plot, corresponding to the 2-ray model tail, without nulls and a steady behavior. For such distances, the specific height of the onshore antenna makes little difference and the attenuation increases logarithmically with link distance. Moreover, the best height is the top of the range, confirming why this approach is common in practice.

- **Transition region**. In the center of each plot, where the difference between the worst-case and best-case is maximal and a fixed antenna height creates strong variations in attenuation within small changes of the link distance. It corresponds to the area around the last null or few nulls in the two-ray model. This is where our method is more useful allowing good control of the average attenuation.

- **Near region**. On the left of each plot, where the best and worst average attenuation are rather close together. This is the region in the two-ray model where many nulls appear in close sequence, with high instability of the link. In this case, the onshore antenna heights that produce the best and worst-case attenuation vary almost erratically but have little impact on the attenuation. Our method is not effective in this region.

4.5 Experimental Results: Mobile Node

4.5.1 Experimental Setup

We set up an AUV-to-shore communication link in the 2.4 GHz frequency band using a real-world testbed. The measurement campaign was conducted in the Port of Leixões, Matosinhos, Portugal in July 2021. The node onshore was placed in close proximity ($\sim$1 m apart) on a concrete pier of the harbor at (41.185273, -8.704882). The AUV was set to operate autonomously following a predetermined trajectory, while exchanging data with the gateway (GW) through a WiFi link, acting as an Access Point (AP). Particularly, packet-based measurements of RSSI from a Light Autonomous Underwater Vehicle (LAUV) *Xplore-4* were collected using the standard interface provided by the manufacturer [135]. The testbed setup at the actual location, including the portable gateway, the AUV, and the remote operator are shown in Fig. 4.4(a).

The AUV performed 15 equivalent round-trip missions starting from the quay and moving away from this structure until reaching up to approximately 100 m. For safety reasons, the AUV was controlled manually close to the quay (up to $\sim$30 m). The distances were obtained based on the AUV positions acquired using a high-precision GPS device. All the time, the AUV was configured to operate at a low speed ($\sim$ 1m/s) as a surface vehicle, thus it was never completely submerged when on mission. The height of the AUV's external antenna was kept constant at $\sim$17 cm above the water surface. The gateway antenna height was $\sim 4.4-4.7$ m measured with respect to the water surface. The difference of $\sim$ 30 cm is due to the water level that changed over the duration of the experiment, between the first and the last AUV missions. All the heights were obtained using a conventional measuring tape, to the best of our abilities.

4.5.2 Experimental Results

Figure 4.4(b)(top) shows the aggregated RSSI measurements collected at the AUV when using the setup above described. Figure 4.4(b)(bottom) presents the corresponding theoretical output of the two-ray model when using the simplified version of the power received expression (in dBm). Note that most 2-ray model parameters were selected according to the testbed setup, except for the product of the Tx power and the antenna gains, which was arbitrarily set to $P_t \cdot G_t \cdot G_r = 10$ dBm. This value simply offsets the output of the model vertically, not affecting path losses nor the shape of the function, particularly in terms of the position of its minima and maxima.

We further explored the influence of the 30 cm change in the tide level that occurred during the experiment's time span. Fig. 4.5 shows the model output for the [0 20]m range and the two extreme values of antenna height. We can see a $\sim$ 1m shift in the null position to the right when increasing antenna height. Fig. 4.6 shows the RSSI measurements obtained in the first two trips, at the beginning of the experiment when the antenna height was $\sim$ 4.4m (top), and those obtained in the last two trips, at the end of the experiment when the antenna height was $\sim$ 4.7m (bottom). A similar shift to the right is observed, despite the high variability of the RSSI signal.

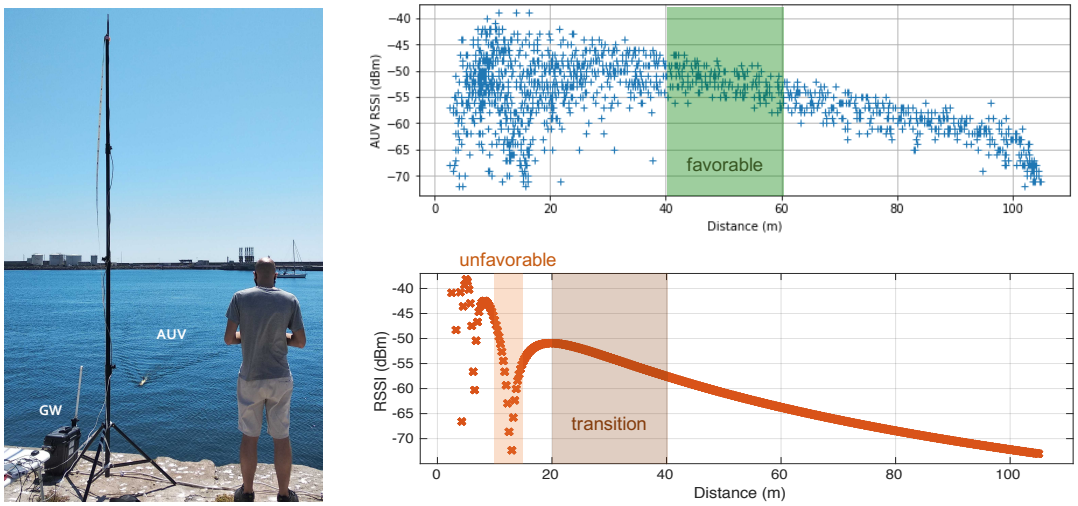

(a) Testbed setup. (b) RSSI measurements (top) and two-ray model (bottom).

Figure 4.4: Shore-to-AUV measurements for a Wi-Fi link in line-of-sight (LOS) showing: (a) the testbed setup at the actual location, (b)(top) the RSSI measurements from the AUV over distance, and (b)(bottom) the two-ray propagation model prediction.

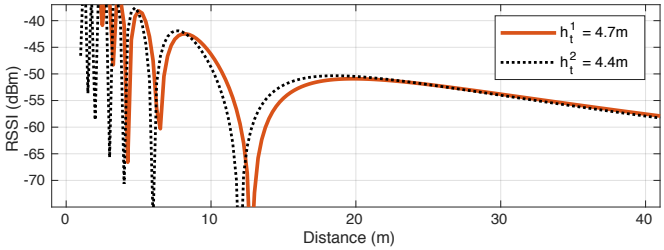

Figure 4.5: Received Signal Strength (RSS) as a function of the distance to shore in the near-shore region, for two moments in the tide, leading to two slightly different antenna heights.

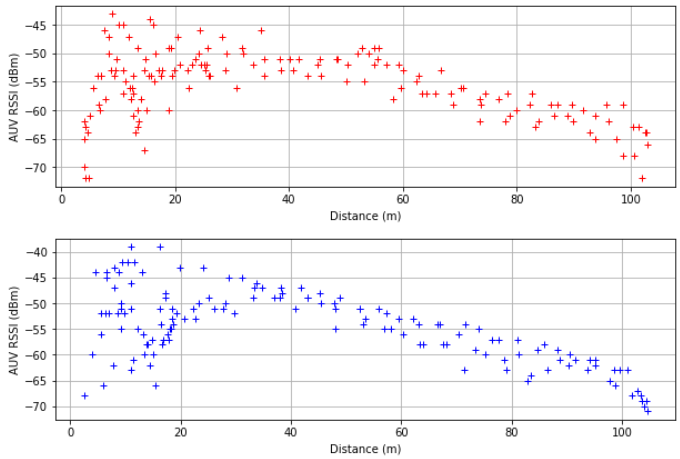

Figure 4.6: RSSI measurements in the beginning of the campaign (top) and at the end of the campaign (bottom), with a tide difference of $\sim$ 30 cm.

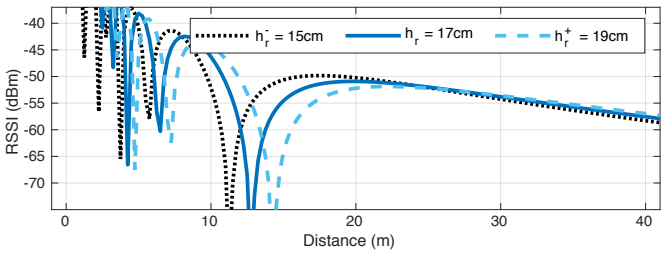

Figure 4.7: Received Signal Strength (RSS) as a function of the distance to shore in the near-shore region, for small deviations in the antenna height for low antennas on the surface node.

The theoretical results obtained with the two-ray model show a good agreement in terms of the path loss dynamics experienced by the AUV measurements, particularly predicting the significant drop in the RSSI (null) at $\sim$ 15m. The actual measurements seem to indicate a slight shift of the null to the right, from the estimated 12-13m to closer to $\sim$ 15m. This can be caused by a slight increase in the actual antenna height on the AUV side while it is traveling (e.g., caused by roll oscillations or salinity affecting the AUV floating line), as predicted in Fig. 4.7.

Another slight difference is the speed of decay of measured RSSI as a function of the Tx-Rx distance which is not as steep as estimated by the model. This has a direct impact on the approach suggested for solving problems such as those of antenna-height design or positioning for stationary nodes. In fact, the actual measurements in the range between d_{conv} and $2 * d_{conv}$ still show some signal strength instability ([20,40] m in Fig. 4.1). Conversely, the range between $2 * d_{conv}$ and $3 * d_{conv}$ ([40,60] m) shows better stability. This area is represented by the solid green semi-circle in Fig. 4.8, while the area suggested by the model appears in brown.

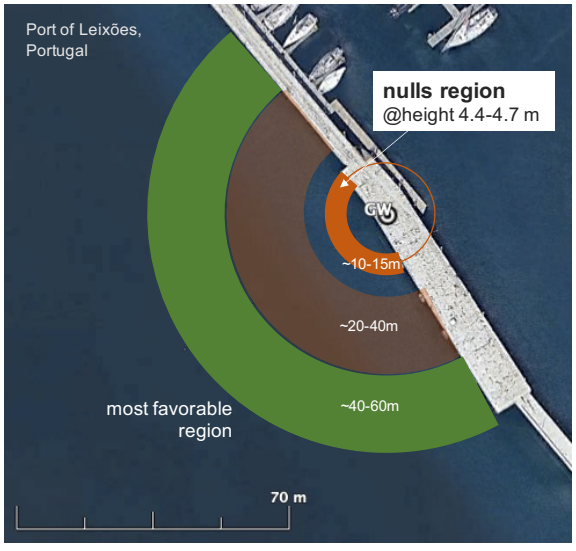

Figure 4.8: Top view of the quay in the harbor showing favorable (solid green), transition (brown) and unfavorable (red) regions for the shore-to-AUV WiFi link.

4.6 Summary & Concluding Remarks

This chapter has described novel antenna-height-based and positioning methods for improved communication over water environments affected by *tidal fading*, considering S2S and S2V link scenarios. The methods target the improvement of average path loss performance during the whole tidal cycle and/or at a specific point of the tide

On one hand, the antenna-height design methods for stationary nodes offer valuable insight to deal with the intricate path loss dynamics resulting from the applicability of the two-ray model in tide-affected water environments. Analytical results clearly show their benefits in terms of reduced path loss performance and size of infrastructure (i.e. shorter antenna heights) while further confirming that placing the antenna at the largest feasible height does not necessarily represent a reasonable criterion. The classical space-diversity technique for placing a second antenna also shows its limited capability to decrease path loss, as it is not informed by the tidal range.

On the other hand, our RSSI measurements with WiFi technology from an AUV-to-Shore campaign show outstanding conformity with the theoretical trends predicted by the two-ray model, further confirming its suitability to describe the large-scale fading on the S2V LOS channel. These results allow us to refine our convenient distance (d_{conv}) method for positioning of surface nodes by avoiding unstable regions of received power, e.g. which can dips of more than 20 dB w.r.t. an approach not informed by two-ray model.

To conclude, we argue that both the analytical and experimental results here included, represent consistent evidence of the relevance of tidal-informed and two-ray-based methods when dealing with LOS communication in tidal environments. While a thorough revision of other relevant factors/parameters (e.g. radiation patterns, sea waves, occlusions, etc.) is certainly needed to improve the accuracy and efficacy of the related models and methods, we believe this chapter offers pioneering findings toward more judicious design on both S2S and S2V link scenarios.

Chapter 5

Path Loss Prediction Methodology for Intertidal Zones

In this chapter, we investigate large-scale fading dynamics of Long Range (LoRa) Line-of-Sight (LoS) links deployed over an estuary with characteristic intertidal zones, considering both *shore-to-shore* and *shore-to-vessel* communications. We propose a novel methodology for path loss prediction which captures *i*) spatial, *ii*) temporal, and *iii*) physical features of the RF signal interaction with the environmental dynamics, integrating those features into the two-ray propagation model. In this direction, we resort to precise hydrodynamic modeling of the estuary location, including the specific terrain profile (*bathymetry*) at the reflection point. This latter aspect is key to accounting for a reflecting surface of varying altitude and permittivity as a function of the tide. Experimental measurements using LoRa communication devices operating in the 868 MHz band show major trends in the received power in agreement with the methodology's predictions.

Most material included in this chapter is derived from the following scientific publication:

- M. G. Gaitán, P. d'Orey, J. Cecilio, M. Rodrigues, P. Santos, L. Pinto, A. Oliveira, A. Casimiro and L. Almeida, "Modeling LoRa communications in estuaries for IoT environmental monitoring systems", in IEEE Sensors Journal 2022 [2].

5.1 Problem Overview

Tidal environments such as estuaries and their surrounding wetlands offer distinctive water dynamics (e.g., due to shallow water tides or intertidal zones) that deserve dedicated RF propagation studies. Specifically, the *intertidal zone*, i.e. the area within the (estuarine) shoreline that is submerged by water during the high tide and then becomes unveiled during the low tide [60], may pose difficult challenges to channel modeling and characterization. Though a few research works have already demonstrated the impact of intertidal zones on different aspects of wireless communications (e.g., link quality estimation [102], energy consumption [103], or time-synchronization [104]), existing literature have typically considered communicating nodes deployed at the ground level,

which become covered by water during the high tide. Nevertheless, this situation offers little insight into the path loss dynamics occurring *above* the intertidal zone, our major concern.

In this chapter, we take a step forward on the existing research by simultaneously addressing the following shortcomings related to path loss modeling in these specific settings:

1. **Spatial variability**. Tidal data is typically available for a subset of key spots only, e.g. where tidal gauges are installed (e.g. ports, harbors). However, water level estimations can differ significantly even between two close locations due to local dynamics, especially in shallow and border waters such as coastal zones or estuaries.

2. **Low temporal resolution**. Tidal data publicly available often provide only estimates on the so-called *High Water* and *Low Water* levels, usually 4 samples per day. Although this resolution might be useful for some activities (e.g. fishing, sailing), they are insufficient to accurately describe complex tidal dynamics at specific locations (e.g. estuaries, marinas).

3. **Varying reflecting surface**. In a realistic scenario, links deployed above an intertidal zone offer a land surface that is covered (and uncovered) with water on a recurring basis. This implies signal reflections do not always occur on water, but on a surface of varying altitude and water content, which may change from water to wet/dry soil throughout the day.

To solve the listed shortcomings, we present next a novel methodology that includes specific elements for increasing the 1) spatial and 2) temporal resolution of tidal data, as well as to account for 3) a reflective surface of varying altitude and permittivity as a function of the tide. The end goal is to integrate these tidal-informed features into the well-known two-ray model for improved path loss prediction in RF links deployed over an intertidal zone.

Organization. The remaining of this Chapter is organized as follows. Section 5.2 formally presents our novel methodology for path loss prediction over intertidal zones. Section 5.3 described the experimental setup and measurements used to validate our approach. Section 5.4 presents an illustrative example of the usage of the methodology and discusses the results presented in the previous section. Section 5.2 summarized and conclude the chapter.

5.2 Methodology

In brief, our methodology considers *i*) the precise and location-dependent hydrodynamic modeling of the water environment and *ii*) the physical and geometrical basis of the two-ray model as the two key components that when combined improve path loss estimation. Specifically, the proposed approach captures *i*) spatial (height, distance), *ii*) temporal (over-time tidal dynamics) and *iii*) physical (terrain profile, permittivity) features of the RF signal interaction with the environment and seamlessly integrates them into the two-ray propagation model.

The proposed methodology including its major building blocks is presented in Fig. 5.1. Each of these components is generally described as follows:

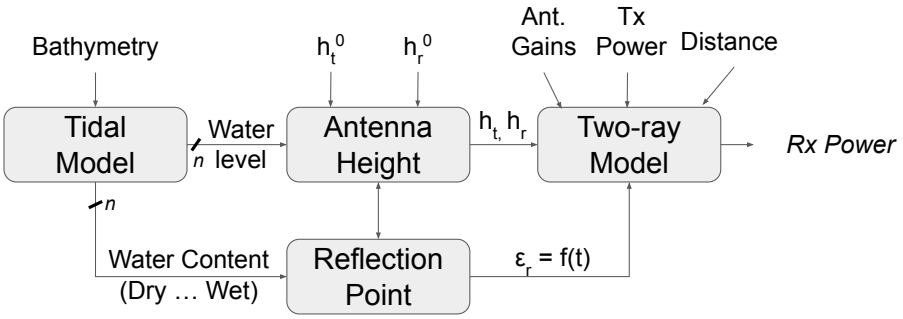

Figure 5.1: The proposed methodology for path loss prediction and its major building blocks.

- **Tidal model**. This component resorts mainly to bathymetry and further environmental input data to provide a tidal model of high precision (see I/O parameters summarized in Table 5.1). The quality of the input data is thus foundational for the precision of the tidal model. In our methodology, the tidal model allows us to obtain precise hydrodynamic outputs to be used in the following components of this methodology, namely, i) the water level[1] or the terrain profile/altitude of the soil surface, and ii) its associated water content.

- **Antenna height.** This building block has two primary inputs: *i*) the water level estimate, and *ii*) the nominal heights of the Rx and Tx antennas w.r.t. the water level measured at the high tide (here denoted as h_r^0 and h_t^0, respectively). These inputs are used to compute the (relative) antenna heights (w.r.t. the reflecting surface) to be used then by the two-ray model, here h_r and h_t. As shown in Fig. 5.1, the antenna height component also represents a recursive input for the computation of the reflection point.

- **Reflection point.** The reflection point component resorts to the water content input to estimate whether the dominant signal reflections will happen on water or on dry/wet soil. This, in turn, enables the recursive computation of the relative antenna heights, as well as the location-specific relative permittivity (ε_r) of the reflective medium; which are the two main tide-driven inputs to be used then by the two-ray propagation model.

- **Two-ray model**. This component applies the physical/geometrical basis of the two-ray model as the last step. Essentially, it combines both static (e.g. Tx power, antenna gains, distance) and varying (e.g. permittivity and relative heights) parameters to determine the primary output of this methodology, i.e. the received power. This output is in practice equivalent to the propagation concept of average path loss, here modeled as a function of a tide-shifted reflection point of time-varying tidal/terrain data and permittivity (see further I/O parameters of the two-ray model summarized in Table 5.1).

[1]The water level also provides the water content as a value of -99 means that the sampling point is dry.

Table 5.1: Main methodology input & output parameters for the Hydrodynamic (baroclinic mode) and Two-ray models. Note that for the hydrodynamic model, the number of input/output parameters is reduced when simulating for barotropic applications (*: optional field).

Model	Type	Data
Hydrodynamic	Input	**bathymetry**, atmospheric data (atmospheric pressure, humidity, wind, air temperature*, downwards/longwave shortwave radiation*), river boundary conditions (flow, salinity*, water temperature*), ocean boundary conditions (tides, salinity, water temperature)
	Output	**water level**, velocity, salinity*, water temperature*
Two-ray	Input	varying **antenna heights** (h_t, h_r) and varying **permittivity** (ε_r), static parameters (e.g. tx power, distance)
	Output	Rx Power

5.3 Experimental Measurements

We conducted experimental campaigns targeting two different types of link settings: *i*) *shore-to-shore* (S2S) and *ii*) *shore-to-vessel* (S2V). Each link considered two types of nodes: a gateway and one or two terminals. All nodes were kept static during the experiments given the intention of characterizing the long-term impact of the tidal environment on stationary nodes. The measurements were carried out at the Bay of Seixal of the Estuary of the Tagus River, Portugal, on October 26, 2019, (08:20 AM to 19:02 PM) and November 23, 2019 (06:32 AM to 16:07 PM), also referred to here as Day 1 and Day 2, respectively. The Seixal Bay has a maximum width of approximately 750 m and is surrounded by a promenade for recreational, commercial, and industrial activities.

5.3.1 Testbed Setup

The gateway and receivers were predominantly in LoS conditions, although a low number of surrounding static and mobile objects (e.g. boats) were present during the measurements. All experiments considered a link consisting of one gateway and at least one terminal node. In the S2V link, two different terminal nodes were used, Node A and B. In the S2S case, Node A only. In both scenarios, links were deployed across the intertidal zone.

In terms of hardware, we used commercially available LoRa radios, namely a Raspberry Pi Dragino hosting an SX1276 chipset. Each radio was coupled to a vertically positioned omnidirectional antenna operating in the 868 MHz RF band. The antennas had nominal gains of 1.5 dBi and 1 dBi for the gateway and terminals, respectively. All radios were configured using the same parameters: *i*) Tx power of 14 dBm, *ii*) spreading factor (SF)[2] of 12, iii) coding rate of $4/5$, and iv) bandwidth of 500 kHz. The SF was set to maximum for improved range, despite the lower data rate, higher channel usage (i.e. higher time-on-air), and increased energy consumption.

The gateway was placed onshore at a fixed height of 3.2 m from the ground. The relative height of the gateway w.r.t. the water surface varied along the day according to the tide. A minimum

[2]SF is defined as the ratio between chip rate and the symbol rate.

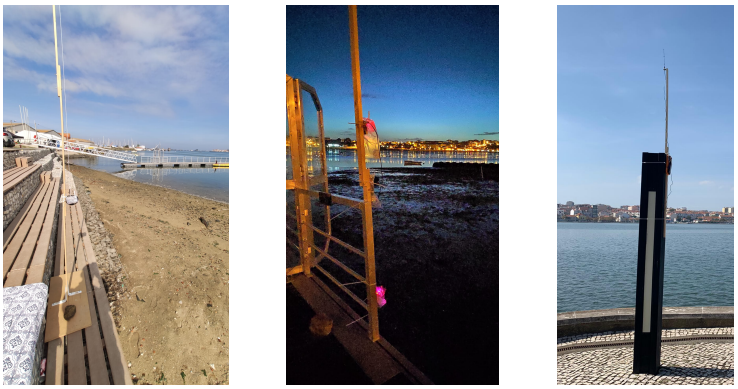

(a) Node (Day 1) (b) Nodes (Day 2) (c) Gateway

Figure 5.2: Measurement setup and installation locations for the end nodes (a)(b) and gateway (c) for the campaigns conducted on Oct. 26 and Nov. 23, 2019.

height to the water of 4 m was measured during the high tide period. In both link scenarios the gateway was kept at the same position (see Fig. 5.2(c)). Conversely, terminals were installed in two different structures: 1) a portable mast pole, for the S2S scenario, and 2) a floating platform, for the S2V equivalent scenario. The mast pole and the floating platform structures are shown in Fig. 5.2(a) and Fig. 5.2(b), respectively, and described in more detail next:

- **Shore-to-Shore (S2S)** (Mast pole). Node A was installed on a temporary wood pole at a nominal height of 1.5 m w.r.t. the water surface, measured during the high tide. The effective height varied throughout the whole tidal cycle as a function of the water level.
- **Shore-to-Vessel (S2V)** (Floating platform). Node A and Node B were installed on an existing metal structure. Their nominal heights were 0.5 m (Node A) and 1.5 m (Node B), measured during the high tide w.r.t. the water surface. The platform floated after a given tide-level threshold and sat on the land/mud otherwise. The effective heights were thus constant when the platform was floating, but varied according to the tide the rest of the time.

The link distance was estimated using the median of the GPS coordinates. The resulting distance was approximately 740 m and 750 m for the S2S and S2V link scenarios, respectively.

5.3.1.1 Measurement Protocol

Link quality measurements were performed using a request-reply protocol implemented in both terminals. The protocol considered a measurement phase of 5 min interleaved with a stand-by phase of 10 min duration, for improved energy efficiency. During the measurement phase, terminal radios transmitted packets with an average size of 85 Bytes every ~ 2 s with requests being triggered by the gateway. The gateway stored the messages received by itself and by the end nodes appended as part of the end node's reply message. Three types of timestamped metrics were stored in logs for further processing: packet RSSI, SNR, and packet sequence number (SN).

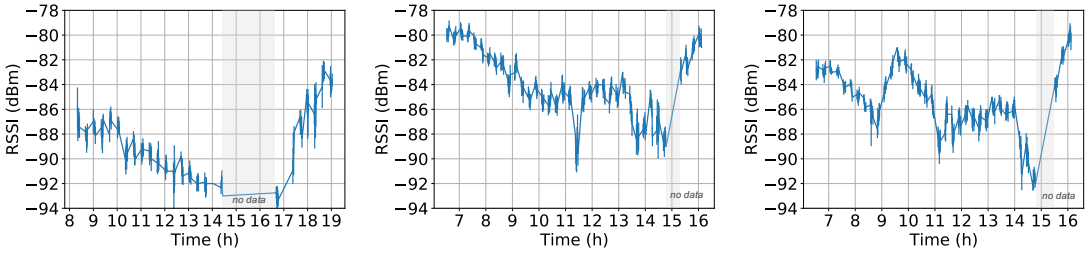

(a) **S2S:** Day 1 (Node A) (b) **S2V:** Day 2 (Node A) (c) **S2V:** Day 1 (Node B)

Figure 5.3: Received Signal Strength Indicator (RSSI) for shore-to-shore (S2S) and shore-to-vessel (S2V) link scenarios as a function of time. RSSI data has been aggregated into 1-minute bins presenting the mean and standard deviation for each bin.

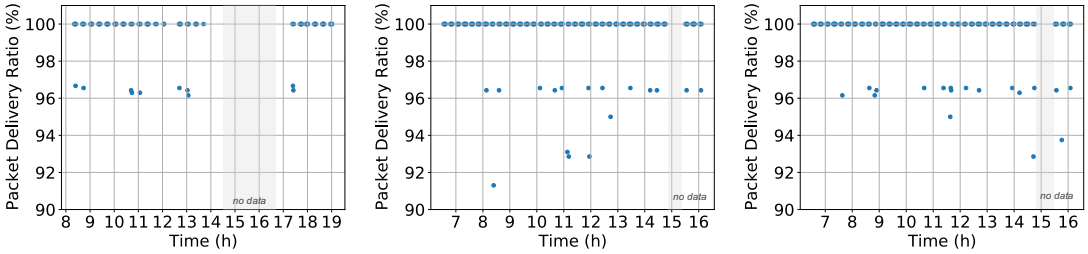

(a) **S2S:** Day 1 (Node A) (b) **S2V:** Day 2 (Node A) (c) **S2V:** Day 2 (Node B)

Figure 5.4: Packet Delivery Ratio (PDR) for shore-to-shore (S2S) and shore-to-vessel (S2V) link scenarios as function of time. Data has been aggregated into 1 min. bins considering at least 15 transmitted packets.

The SNs were used to identify gaps in packet transmission allowing us to determine the Packet Delivery Ratio (PDR) during a given time interval. In all cases, we only considered the data between the gateway and the end nodes, assuming a strong degree of link reciprocity [137].

5.3.2 Measurement Results

5.3.2.1 RSSI

Fig. 5.3 presents the variation of RSSI as a function of time for both measurement days (Oct. 26 and Nov. 23, 2019), link types (S2S and S2V) and for all nodes (i.e. Nodes A and B). The results show a clear impact of the tides on the measured signal power with variations exceeding 10 dB during the measurement span. In broad terms, RSSI decreases/increases as the water level raises/falls, which can be explained by the changes in the effective antenna height to the water surface, which – for the considered Tx-Rx separation – leads to an increase in the signal attenuation as shown in previous studies [40].

As detailed previously, for the S2V case, Node A (Fig. 5.3b) and Node B (Fig. 5.3c) were installed at the same location but at different heights (0.5 m and 1.5 m, respectively). Comparing the RSSI measurements of both nodes the signal strength is, in general, larger for the upper node (i.e. Node A) as expected, although this does not hold true for short periods of time. Note these nodes are installed in a floating platform that is *static* during low tide and that *floats* during the

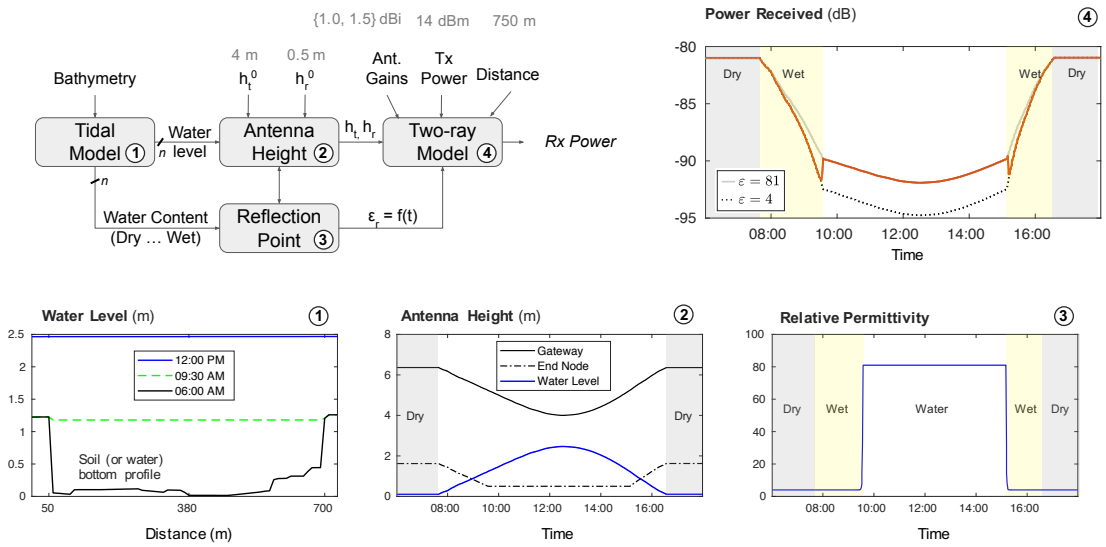

Figure 5.5: Illustrative example of the proposed methodology for modelling the received signal strength of Node A ($h_r = 0.5$ m) for the S2V measurement campaign of Day 2. The figure includes the intermediate outputs from the tidal model, antenna height and reflection point stages, as well as the final output.

high tide, which renders different propagation conditions. As for the S2S case, Node A (Fig. 5.3a) exhibits an increase/decrease relationship which is in agreement with the tidal influence, and thus with the effective antenna-to-surface heights of the nodes.

5.3.2.2 PDR

Fig. 5.4 presents the PDR as a function of time for both measurement days, link types, and nodes. As expected, the PDR is fairly constant at around 100% with occasional packet losses despite the wide variations in RSSI. As empirically verified, – not included here for brevity reasons – the effective sensitivity of the receiver is around -94 dBm. For the S2S link (Fig. 5.4a), this implies packets that have been sent slightly after the 14 h and before 17 h were not received due to the RSSI being below the receiver sensitivity. Similarly, no packets are received for a shorter period of time around 15 h by Node A (Fig. 5.4b) and Node B (Fig. 5.4c) for the S2V link. Previous studies [100; 47; 48; 40] also shown that LoRa's effective communication range is severely compromised when using antennas close to the surface (water or ground), due to reduced Fresnel zone.

5.4 Evaluation of the Methodology

5.4.1 Illustrative Example

In order to illustrate the application of the methodology in a real-world case study, we analyze here the measurements collected on Nov. 23, 2019, for Node A (S2V link) as this case provides the

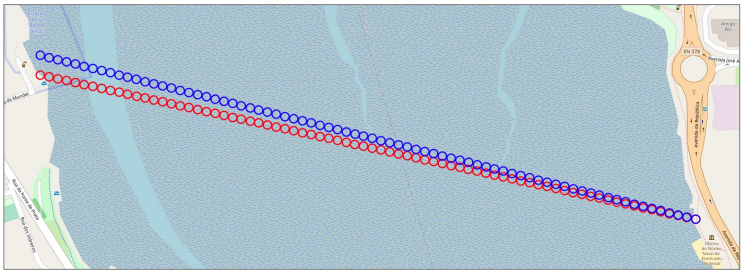

Figure 5.6: Tidal model sampling points for the two experiments days represented in red for Oct. 26, 2019 (*S2S link*), and in blue for Nov. 23, 2019 (*S2V link*). The gateway was placed on the right side of the river bank, while the receivers were placed in structures on the left bank of the river.

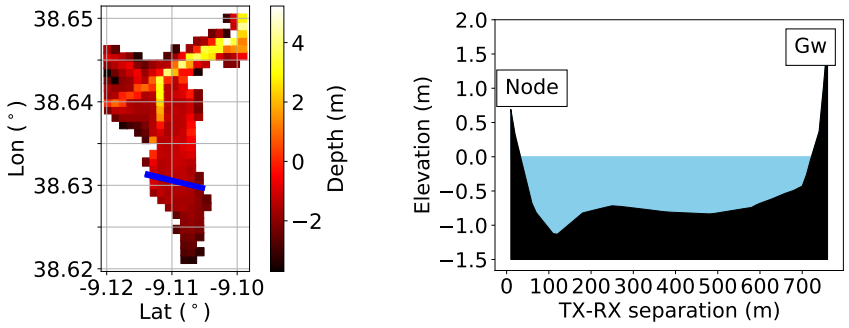

(a) Bathymetry Data (b) Bathymetric Cross-section

Figure 5.7: Bathymetry data for the Seixal Bay and the bathymetric cross-section of the simulation mesh for Nov. 23, 2019. The cross-section for the other measurement day (Oct. 26) is very similar.

most representative and complete scenario among our experiments. In the following, we will break down the output of the different building blocks presented in the processing pipeline in Fig. 5.5.

5.4.1.1 Tidal Model ①

The first step of the processing pipeline consists of determining the specific i) *water level* and ii) *water content* associated with the output of the tidal model component of the methodology. To this aim, we resort to high-resolution tidal data obtained from hydrodynamic modeling which has been previously calibrated and validated using field data from the specific location (i.e., Seixal Bay). Table 5.1 provides the simulation outputs provided by the tidal model within this context.

For the sake of brevity, we do not describe here further technical and theoretical foundations behind this model. We yet rely on the model's ability to represent the main spatial and temporal patterns of circulation and water quality in the particular test site, as shown by prior studies [138; 139]. In concrete, we obtain the tidal data associated with the link from a specific set of sampling points along a cross-section of the simulated geographical area, as illustrated in Fig. 5.6. The cross-section follows the aerial path of the specific link under evaluation and uses 76 sampling points resulting from a spatial resolution of about 10 m, as the link distance was about 750 m. In terms of the temporal resolution, we used a time step of 60 s, along a 24 h period. The bathymetric

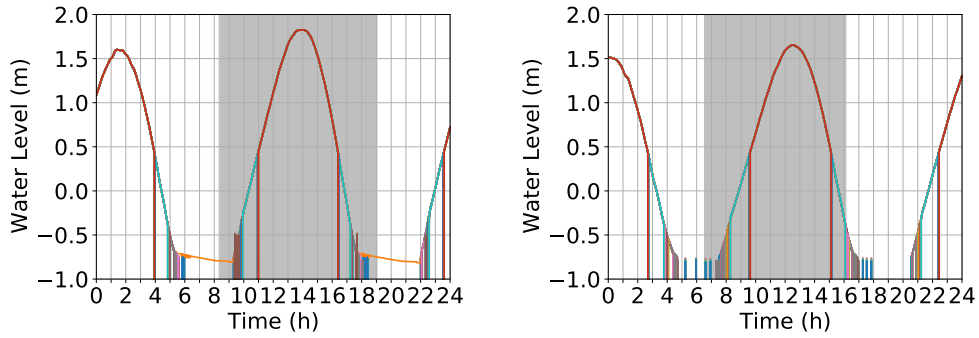

(a) **S2S link:** Day 1.

(b) **S2V link:** Day 2.

Figure 5.8: Water level variation w.r.t. the average level (0 m) for each sampling point throughout the two measurement days, namely Oct. 26 and Nov. 23, 2019 (different colors per curve; curves overlap). Most of the 76 sampling points are dry during the two low tide periods. The period during which the experiments were carried out is highlighted in grey.

data of the Seixal Bay in Fig. 5.7 alongside the given interpolation of the bathymetry mesh across the communication link path is also presented here, for completeness.

The resulting *water level* output from the tidal sampling points is shown jointly with different colors in Fig. 5.8. These results show that most points differ from others only during the low tide period while reporting the same level of water during high tide. The mismatches that occur during the low tide occur mainly due to terrain profile differences. The water level is given w.r.t. the average sea level of the measurement site, i.e. 2.26 m above the hydrographic zero of Portugal. The output of the model also shows that drying[3] occurs in this region during the morning and afternoon periods for the vast majority of sampling points. This implies that solely the river banks and the deeper navigation canal of the estuary can be considered covered by water all the time.

Back to our illustrative pipeline, Fig. 5.5 (bottom-left) shows the water level along the link path for three specific times (6:00 AM, 09:30 AM, 12:00 PM). These snapshots complement the full-cycle water level variations reported in Fig. 5.8b by offering a different perspective of the sampling points, particularly, when plotted at three specific instants: *i*) low tide (6:00 AM), *ii*) high tide (12:00 PM) periods, and *iii*) the moment slightly before the water reaches the platform (9:30 AM). This latter instant is relevant since reports the status when the (vessel-like-)platform starts to float. Note that at the low tide the curve reports the lowest water level of the basin area or equivalently the model's *soil bottom* as a result of truncating those *water content* values denoting a dry soil (-99) to the minimum water level (or altitude) of the sampling point. The resulting bottom profile follows thus a similar trend to the bathymetric cross-section in Fig. 5.7.

5.4.1.2 Antenna Height ②

The subsequent step in the pipeline is to compute the actual Tx/Rx antenna heights that are going to be used then by the two-ray model. To this purpose, this component resorts to the water level

[3]The tidal model attributes a -99 m water level to a given sampling point whenever drying occurs. This value is not depicted in Fig. 5.8 for visual clarity.

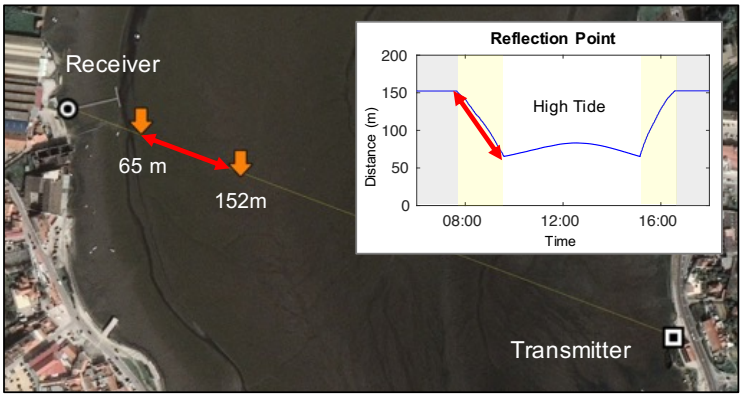

Figure 5.9: **Background**. Aerial view of the link path area for the campaign on Nov. 26, 2019, including Tx and Rx locations. The arrow marks (in orange) highlight the maximum and minimum bounds on the reflection point, 65 m and 152 m, respectively, for Node A ($h_r = 0.5$ m), due to tide influence. **Box**. Temporal evolution of the reflection point highlighting the distance span incurred.

estimates provided by the output from the previous step, the tidal model. The antenna-height outputs are calibrated using empirical antenna height measurements (h_t^0 and h_r^0) performed during the high tide period. As expected, the antenna heights shown in Fig. 5.5 (bottom-middle), varied with the tidal cycle as a function of the tide, decreasing from approximately 6 m to 4 m during the high tide period. Note the height of the receiver node was constant at 0.5 m with respect to the water surface while the platform was floating (i.e., between 9:34 and 15:08). After the platform sat on the mud, the antenna height increased until approximately 2 m during the ebb period as a consequence of the currents leading the water mass outside the Bay. Note the Tx and the Rx antenna heights solely vary *simultaneously* during the short transition period between low tide to high tide (7:37 - 9:34) and vice-versa (15:08 - 16:35). In Fig. 5.5 (bottom-right), these periods correspond to the *wet* areas, in which the reflecting surface transitions from dry soil to water.

5.4.1.3 Reflection Point ③

In this step, the relative permittivity (ε_r) of the reflecting medium is determined as a function of an estimated time-varying reflection point. The reflection point has also a bidirectional relationship with the resulting Tx and Rx antenna heights from the second step (h_t and h_r, respectively) which denote relative height measurements w.r.t. the soil or water level at the reflection point. The relative permittivity is then computed using data from the specific location at the reflection point, namely using antenna heights from step two and water content from step one.

Fig. 5.9 shows an aerial view of the spatial span incurred by the reflection point along the link path for the Nov. 23, 2019, measurement campaign. It also marks the maximum and minimum distance bounds (w.r.t. the receiver) resulting from the respective low tide and high tide peaks on the water level. Note that the reflection point is geometrically-defined, thus computed differently depending on whether it is an S2S or an S2V link scenario, as described in Chapter3.

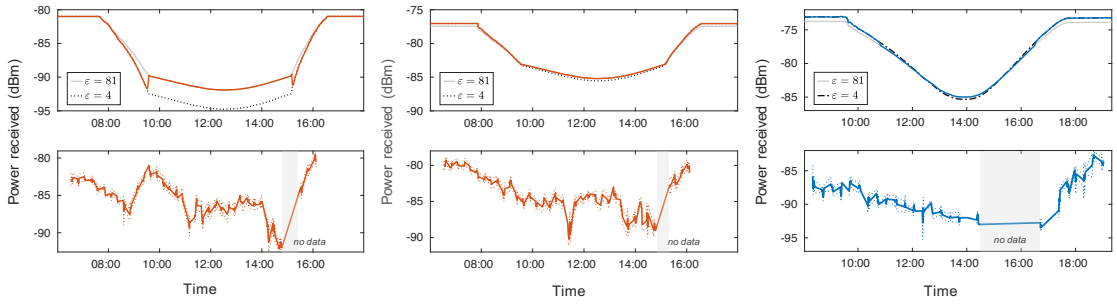

(a) **S2V:** h_r=0.5 m (b) **S2V:** h_r=1.5 m (c) **S2S:** h_r=1.5 m

Figure 5.10: Average power received and corresponding experimental measurements for both the shore-to-vessel (S2V) (a)(b) and shore-to-shore (S2S) (c) link scenarios.

After determining the point at which the secondary ray reflects, the methodology computes whether the reflection occurs on the water mass or on the bottom terrain of the intertidal zone. This latter case implies the terrain might have a varying water content as water evaporates/infiltrates when the tide is decreasing/increasing, respectively. In order to take into account this fact, we assume the relative permittivity to be constant whenever the reflection occurs on the ground ($\varepsilon_r = 4$) or on water ($\varepsilon_r = 81$) but presents a varying behavior within the transition area between these two states. Particularly, for improved accuracy, we assume this transition shows an exponential increase in the value of permittivity with increasing distance from the soil surface, as explained in [91]. The resulting permittivity curve is depicted in Fig 5.5. (bottom-right).

5.4.1.4 Two-ray model ④

The final step consists of determining the average received power using the two-ray model considering the time-series data computed in the previous steps and other conventional (static) inputs for path loss modeling, namely the Tx-Rx distance, Tx power, and antenna gains. The final output of the methodology is, essentially, the result obtained by the two-ray propagation model when using precise inputs on the relative antenna heights and permittivity at the time-varying reflection point.

The resulting model output in Fig 5.5 (top-right) shows a clear relationship between received power and antenna height variations which suggests lower antenna heights led to increased signal attenuation. Another particular observation is in the transition period behavior, which suggests that, in this case, the passage from ground to water reflections leads to an increase in the received signal power due to the higher permittivity of the water medium.

5.4.2 Methodology Validation

We now analyze the validity of the methodology with all the measurements. Fig. 5.10 reports the average received power obtained using our proposed methodology and the corresponding empirical measurements for the two experimental campaigns, S2S and S2V. Fig. 5.10a and Fig. 5.10b show the results for the S2V links of Day 2, when the receiver antennas are at $h_r = 0.5$ m and

$h_r = 1.5$ m, respectively, measured w.r.t. the water surface during high tide. Fig. 5.10c shows the results for the Day 1, S2S case, i.e. with $h_r = 1.5$ m.

In general, the impact of water level (and corresponding relative antenna heights) on the power received is noticeable in all the evaluated cases, showing increasing/decreasing trends in agreement with the methodological predictions. Particularly, the extreme and central parts of the curves show consistent behavior with the dual condition of the intertidal zone, generally, with higher power received during low tide periods, and thus with more attenuation during the high tide.

The influence of the relative permittivity is substantial in the case illustrated in Fig. 5.10a, where a rapid shift in the received power is predicted by the methodology between the $\varepsilon = 4$ and $\varepsilon = 81$ permittivity curves, in the central area of the figure. A similar trend but with a larger difference (~ 5 dB) is exhibited by the experimental measurements. The exponential change of permittivity in the methodological predictions (see Fig. 5.5) leading to an abrupt shift up/down on the predicted power received is also similar, but with a less abrupt empirical transition. Fig. 5.10b, although corresponding to the same measurement campaign (S2V), shows marginal differences in this effect. Similarly, the results reported for the S2S case in Fig. 5.10c are also negligible.

Further phenomena not explained by our methodology are visible, for example, in Fig. 5.10a and Fig. 5.10b, between 11:00 AM and 12:00 PM, and 13:00 PM and 15:00 PM, respectively. A period without data is reported in Fig. 5.10c, between around 14:00 PM, and slightly after 15:00 PM. Despite these limitations, we argue that trends in the path loss predictions are, in general, in good agreement with the empirical results. Note that we use the two-ray model for *path loss* prediction only, thus leaving other propagation effects beyond the scope of this methodology. To reduce the mismatches between the measured and estimated power, it would be convenient to account also for additional factors (e.g., scattering, diffraction) instead. Although not significant for the comparatively shorter links (750 m) that are the target of this study, tropospheric effects [140][141] could also be included in an extended methodology that considers substantially larger links (i.e. several kilometers) typically common in other maritime communication activities.

5.5 Summary & Concluding Remarks

This chapter has described a novel methodology for improved path loss prediction in water environments with characteristic intertidal zones. The proposed methodology conceives an original approach to address a number of important shortcomings in existing research, namely, *i*) low spatial variability, *ii*) low temporal resolution, and *iii*) and varying reflective surfaces. The approach can generally be described as the seamless integration between the well-known two-ray propagation model and the precise modeling of the tides at the specific location.

In our validation experiments, we showed that this non-trivial combination of models offers an improved estimation of the link quality able to predict RSSI trends magnitude differences ($\sim$5-10 dB) that would have not been possible without a tide-informed framework. A naive path loss estimation (e.g., with the common free-space path loss model) will not consider antenna heights at all, producing a single (distance-based only) RSSI output model for the whole measurement

span and thus missing the impact of tides. Likewise, an approach based on the two-ray model with tides that do not keep track of the temporal reflection point evolution will not consider the changes between dry, wet, or water permittivity, nor the possible terrain profile differences. As observed, this can lead to significant RSSI differences both in modeling and experiments, in this case of up to 10 dB, which further justifies the importance of our research direction.

In future work, we plan to validate the proposed methodology in various types of surroundings (e.g. harbors, marinas), as well as using different RF communication bands (e.g. 2.4 GHz and 5 GHz). We also intend to include additional propagation effects (e.g. scattering, multipath) and environmental phenomena (e.g. sea waves) into the current modeling framework to further increase the accuracy of link estimation. Additional measurements will also be conducted on consecutive days to characterize possible day-to-day variations of the received signal power, as well as to quantitatively assess the quality of our prediction. The end goal is to provide RF practitioners with a network design tool specifically proposed for the deployment of IoT-based environmental monitoring systems operating over different kinds of water environments.

Part II: Real-Time Communication

Chapter 6

Centrality-Driven Gateway Designation for Real-Time WSNs

In this chapter, we introduce *network centrality* as a criterion to designate one or multiple gateways in real-time WSNs (e.g. TSCH-based). The end goal is to improve network schedulability by design, particularly, by means of a *judicious* designation of the gateway node. We explore common centrality metrics from social network analysis (i.e. degree, betweenness, closeness, and eigenvector) under varying configurations and show that assigning the gateway role based on any of these metrics is, in general, an effective and promising approach that facilitates WSN real-time communication. We generalize the idea to multiple gateways with the aid of the unsupervised learning method of *spectral clustering*. This latter approach shows to produce WSN designs that greatly reduce the worst-case network demand. Notably, in a situation with 5 gateways, 99% schedulability can be achieved with 3.5 times more real-time flows than in a random benchmark.

The chapter herein mostly include scientific material from the following publications:

- M. G. Gaitán, L. Almeida, A. Figueroa and D. Dujovne, "Impact of Network Centrality on the Gateway Designation of Real-Time TSCH Networks", in IEEE WFCS 2021. **[Best Work-in-Progress Paper Award]** [12].
- M. G. Gaitán, D. Dujovne, J. Zuñiga, A. Figueroa and L. Almeida, "Multi-Gateway Designation for Real-Time TSCH Networks using Spectral Clustering and Centrality", in IEEE Embedded Systems Letters 2022 [3].

6.1 Problem Overview

The ability of WSNs to guarantee a timely delivery of deadline-constrained data flows is a subject of foremost importance for several applications[1]. Theoretical and empirical studies have covered various upper-layer concerns in extenso, from scheduling to routing, and often with a special focus on the real-time performance assessment using formal guarantees, e.g. *schedulability*. The

[1] Consider, for example, a real-time overwater WSN supporting our environmental monitoring use case in Fig. 1.1.

relatively vast amount of work on this field has considered both specific and random topological settings, yet often assuming an *arbitrary* designation of the gateway node. Nevertheless, this rather common assumption has a non-negligible impact on the WSN traffic schedulability. More importantly, the problem of how to properly designate a node as gateway in WSNs has not been fully addressed from a real-time systems perspective.

In this chapter, we attempt to solve the challenge of how we can improve WSN traffic schedulability by judiciously designating a specific node as gateway. We assume full knowledge of the network topology and we target both single- and multi-gateway designation problems while simultaneously dealing the following limitations of existing research:

- **Arbitrary gateway designation**. Performance studies for WSNs often rely on synthetic datasets based on *random* generation. While this generally allows exploring a broad design space, a *random* choice of the gateway node is certainly not valid as a design method. Obviously, neither is in practical studies. Proper gateway designation methods are needed for *real-time* WSNs in order to facilitate end-to-end data messages to be delivered timely.

- **Position-dependent gateway designation**. Real-world settings often rely on position-based rules for deploying sink nodes (e.g. based on the nominal range of access points). While this may have some practical validity when logical and physical topologies matches, this is not always the case, e.g. due to links breaking caused by tidal fading. Moreover, physical positions can be unknown, and logical topology could be the only information available.

In the following, we tackle the above factors by proposing both single- and multi-gateway designation methods based on classical centrality metrics from network science (e.g. eigenvector, betweenness). We highlight this approach pioneers the use of *judicious* and position-agnostic criteria for designating nodes as gateways in order to facilitate real-time communication in WSNs.

Organization. The remainder of this chapter is organized as follows. Section 6.2 presents both single- and multi-gateway designation methods. Section 6.3 offers an evaluation of both methods in terms of real-time performance under varying configurations. Section 6.4 provides concluding remarks.

6.2 Multi-Gateway Centrality-Driven Designation

This section formally presents both our single- and multi-gateway centrality-driven gateway designation methods. To this purpose, we first present the common modeling framework for both designation problems, including network, flow and performance models. Then, we also present formal definitions for each of the centrality metrics included in this study. Finally, we introduce spectral clustering and describe how the extension to multiple-gateway is performed.

6.2.1 System Model: Network, Flow and Performance Models

We consider a globally synchronized wireless mesh network resorting to a TSCH-based MAC layer which enables a predictable network operation. The network consists of sensor nodes, relays, and one or multiple gateways. Sensor nodes transmit periodic deadline-constrained data messages toward the gateway(s) in multi-hop and convergecast fashion. The network relies on global management using standard real-time scheduling and routing schemes. In this sense, we assume here all transmissions are scheduled according to a global EDF policy and using shortest-path routing.

1) Network model. The WSN is abstracted as a graph $G = (V, E)$ with a set of vertices (nodes) V and set of edges (links) E. The order of the graph is $N = |V|$, with $N - k$ nodes acting as sensors and the rest of k nodes as gateways. All nodes are enabled to perform sensing, relaying or gateway functions. We also assume knowledge of network topology in the form of an adjacency matrix A, assumed to be transparently maintained using a built-in topology tracking service.

2) Real-time flow model. $F = \{f_1, f_2, \ldots, f_n\}$ denotes the set of $n \leq N - k$ real-time flows transmitting periodic data messages toward any of the k gateways. Each flow uses a 4-parameter representation $f_i = (C_i, D_i, T_i, \phi_i)$, where C_i is the effective transmission time between source and destination, T_i the transmission period, D_i the (relative) deadline, and ϕ_i the routing path. The term $f_{i,\gamma}$ represents the γ^{th} transmission of flow f_i released at time $r_{i,\gamma}$ such that $T_i = r_{i,\gamma+1} - r_{i,\gamma}$. $f_{i,\gamma}$ is constrained to reach its respective gateway before its absolute deadline $[d_{i,\gamma} = r_{i,\gamma} + D_i]$.

3) Performance model. To assess WSN traffic schedulability under EDF scheduling, we resort to the supply/demand-bound based framework in Chapter 2, without further adaptation.

6.2.2 Centrality-Driven Single-Gateway Designation

Given the models presented above, we address the challenge of how to *judiciously* designate a node as gateway for enhanced traffic schedulability. We conjecture that since centrality is a quantitative measure of how important is a node in relation to others in a given network, it has potential to become a good candidate for gateway designation. Specifically, we select four of the most common centrality metrics in social network analysis, namely, eigenvector, closeness, betweenness, and degree, and we evaluate their real-time performance. We selected these metrics since they are deemed as almost optimally correlated for the purposes of benchmarking [142].

In the following, we formally define these metrics. Note that since we are first addressing the case of single gateway designation, we are consider the prior modeling framework when $k = 1$.

6.2.2.1 Eigenvector Centrality (EC)

This metric quantifies how *influential* a specific node is w.r.t. others in a given network. This means a node with has a high EC score is connected to many other nodes which themselves also are highly scoring nodes. The score is determined from the analysis of the principal eigenvector extracted from the adjacency matrix representing the network topology. Formally, the EC for a

given node $v_q \in V$ can be expressed by Eq. 6.1:

$$EC(v_q) = \frac{1}{\lambda_{max}(A)} \cdot \sum_{j=1}^{N} a_{j,q} \cdot x_j \tag{6.1}$$

where $\lambda_{max}(A)$ is the largest eigenvalue of the adjacency matrix $A = [a_{j,q}]_N$, $a_{j,q}$ is the matrix element at row j and column q, x_j is the jth value of the eigenvector x of graph G, and N is number of nodes in the network.

6.2.2.2 Closeness Centrality (CC)

This metric quantifies the level of *proximity* a specific node has w.r.t. the rest of nodes in the network. For a given node $v_q \in V$, CC is defined as the inverse of the sum of the geodesic distances from v_q to all the other nodes. Formally, the CC metric is presented in Eq. 6.2 as follows:

$$CC(v_q) = \frac{1}{\sum_{p \neq q} distance(v_p, v_q)} \tag{6.2}$$

where $distance(v_p, v_q)$ is the shortest path distance between the nodes v_p and v_q, with $p \neq q$, $\forall\, v_p \in V$. Note that, for simplicity, here we only consider hop-count-based shortest path distances.

6.2.2.3 Betweenness Centrality (BC)

This metric quantifies how many shortest-path routes pass through a specific node in the network. For a given node $v_q \in V$, the metric can be computed as the fraction between the number of shortest paths of any pair v_r and v_s ($\forall\, v_r, v_s \in V \wedge\ r \neq s \neq q$) passing through node v_q, and the total number of shortest paths in the network. Eq. 6.3 formally presents the BC metric:

$$BC(v_q) = \sum_{q \neq r} \frac{sp_{r,s}(v_q)}{sp_{r,s}} \tag{6.3}$$

where $sp_{r,s}$ is the number of shortest paths between any pair of nodes v_r and v_s, and $sp_{r,s}(v_q)$ is the number of those paths passing through node v_q.

6.2.2.4 Degree Centrality (DC)

This metric quantifies the number of links, edges or one-hop neighbours a specific node has. For a given node $v_q \in V$, DC can be formally presented as in Eq. 6.4:

$$DC(v_q) = \frac{degree(v_q)}{N-1} \tag{6.4}$$

where $degree(v_q)$ denotes the number of links of v_q directly connected to other nodes and $N = |V|$.

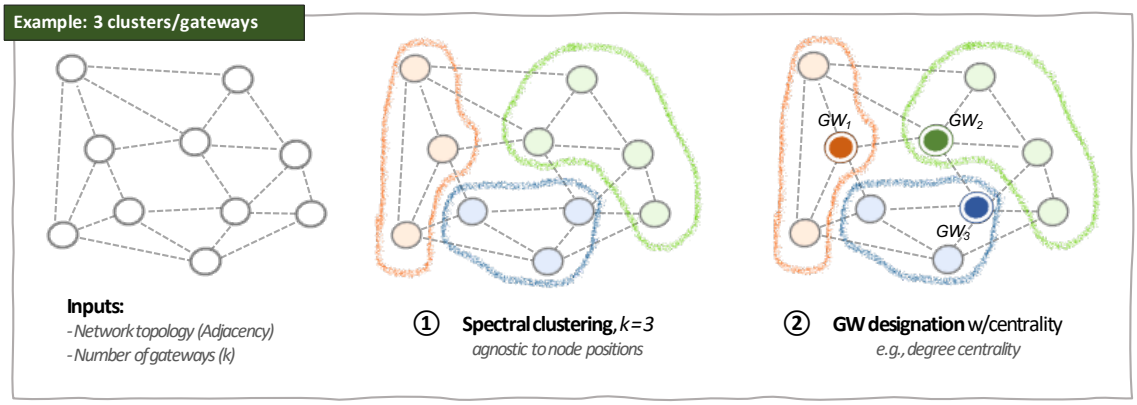

Figure 6.1: A toy example of the centrality-driven multi-gateway designation framework for $k = 3$ clusters/gateways.

6.2.3 Clustering-Assisted Multi-Gateway Designation

We advocate now for a multi-gateway designation framework in line with our centrality-driven strategy by further leveraging network science methods. Specifically, we generalize our prior approach to multiple gateways with the aid of the unsupervised learning method of *spectral clustering* [143]. While several clustering techniques exist in the literature [144], we resort to this method due to its superior performance as shown in comparative studies (e.g. [145]). More importantly for our research direction, we selected this class of clustering algorithm since it does not rely on the node's physical position but rather on the spectral (graph) properties of the network.

That being said, our clustering-aided approach consists in two main phases 1) first clustering the network with spectral clustering and 2) applying a centrality metric to designate one gateway inside each cluster. As an example, a graphical description of the approach when using spectral clustering combined with degree centrality is illustrated in Fig. 6.1.

6.2.3.1 Phase 1: Spectral Clustering

This phase consist in virtually partitioning the network G in a set of k disjoint and arbitrarily shaped clusters (or sub-graphs) using *spectral clustering*. The key idea behind this type of methods is to leverage the eigen-decomposition of the graph Laplacian matrix (L) to find solutions based on the relaxation of graph cut problems [146]. Specifically, we use the direct k-way spectral clustering algorithm proposed by Ng, Jordan, and Weiss [143] to identify groups of widely separated nodes represented by k connected subgraphs. Differently from other spectral clustering methods, the Ng-Jordan-Weiss (NJW) algorithm uses eigenvectors of the normalized Laplacian (L_{norm}) which can be computed as follows:

$$L_{norm} = D^{-1/2} \cdot L \cdot D^{-1/2} \tag{6.5}$$

where D is the degree matrix, i.e., the diagonal matrix with the degrees of the nodes, and $L = D - A$ is the Laplacian, with A being the adjacency matrix of the graph.

Algorithm 1 NJW Spectral Clustering [143]

Input: a graph G and the target number of clusters k

Output: a partition of k clusters $\Pi = \{G_1, G_2, ..., G_k\}$

1: Find the first k eigenvectors u_1,u_2,...,u_k of L_{norm} and sort them in the columns of U'
2: Build matrix $U = [u_{ij}]_{n\times k}$ based on U' by normalizing each row of U' using $u_{ij} = u'_{ij}/\sqrt{\sum_k u'^2_{ik}}$
3: Let the i^{th} row of the matrix U represent node v_i from graph G
4: Apply k-means algorithm (or an equivalent method) to U and find a k-way partitioning $\Pi' = \{G'_1, ..., G'_n\}$
5: Form the final partition Π assigning every node v_i to the cluster G_ℓ, if the i^{th} row of U belongs to G'_ℓ in Π'.

Algorithm 1 shows a high-level pseudo-code of the NJW spectral clustering. Note though this pseudo-code indicates the use of *k-means* clustering in step 4, it actually applies it to virtual distances, after normalization in step 2, thus keeping the independence from physical positions.

6.2.3.2 Phase 2: Clustering-Aided Multi-Gateway Designation

As shown in Fig. 6.1, we leverage a centrality-driven multi-gateway designation framework resorting spectral clustering to partitioning the network. The approach requires computing a centrality metric *per cluster* after a number of k clusters has been identified. This means selecting as gateway of a cluster the node with the highest centrality score. Note that since we are now dealing with *network centrality* expressions interpreted as *cluster centrality* metrics, we need to adapt the original definitions to this particular situation before applying them. This can be done by considering each cluster G_ℓ as a sub-graph of G, characterized by its (cluster) adjacency matrix A_ℓ and the number of nodes in the cluster N_ℓ, with $\sum_{l=1}^{k} N_\ell = N$. We formally summarize these adaptations for the *cluster centrality* [2] metrics being considered in Table 6.1.

6.3 Performance Evaluation

6.3.1 Centrality-Driven Single Gateway Designation

6.3.1.1 Simulation Setup

1) Network topologies. We consider a set of 100 mesh topologies generated from random graphs. Each graph is created using a sparse uniformly distributed random matrix of $N \times N$ and target node

[2] **Notation**: $degree(v_q)$ denotes the number of edges of node v_q that are directly connected to any of the rest $N_\ell - 1$ nodes in G_ℓ; $sp_{r,s}$ is the number of shortest paths between any pair of cluster nodes v_r and v_s, and $sp_{r,s}(v_q)$ is the number of those paths passing through node v_q; $distance(v_p, v_q)$ is the (hop-count) shortest path distance between nodes v_p and v_q, with $p \neq q$, $\forall\ v_p \in V_\ell$, where V_ℓ is the set of vertices or nodes of cluster G_ℓ; x_j is the j-th value of the eigenvector x of the subgraph G_ℓ, and $\lambda_{max}(A_\ell)$ is the largest eigenvalue of the cluster's adjacency matrix $A_\ell = [a_{j,q}]_{N_\ell \times N_\ell}$, with $a_{j,q}$ being the matrix element at the row j and column q.

Table 6.1: Cluster Centrality Metrics.

Metric	**Definition**
Degree	$DC(v_q) = \frac{degree(v_q)}{N_\ell - 1}$
Betweenness	$BC(v_q) = \sum_{q \neq r} \frac{sp_{r,s}(v_q)}{sp_{r,s}}$
Closeness	$CC(v_q) = \frac{1}{\sum_{p \neq q} distance(v_p, v_q)}$
Eigenvector	$EC(v_q) = \frac{1}{\lambda_{max}(A_k)} \cdot \sum_{j=1}^{N_k} a_{j,q} \cdot x_j$

density Λ, where $N = 80$ is the total number of nodes including the gateway. For each centrality metric, i.e. DC, CC, BC and EC, we choose the node with the highest score (i.e. centrality) as gateway. The remaining $N-1$ nodes act as field nodes, i.e. as sensors and/or relays.

2) Real-Time flows. A random subset of n field devices are assumed as sensors periodically transmitting sensing data toward one gateway. Each sensor node produces a single flow of real-time packets. We assume n varies within $[1,10]$ for all the cases. The result is a random set of n real-time flows for each network topology. For each flow, C_i is obtained directly from the multiplication of the route length of ϕ_i (in hops) and the length of the time slot (configured to 10ms). We assume implicit deadlines, thus $D_i = T_i$, where T_i is the flow period. Moreover, T_i is harmonically generated in the range $[2^4, 2^7]$ slots. This leads to a direct computation of the super-frame length, a.k.a. hyper-period (H), here considered its maximum value of 1280ms.

3) Real-time assessment. For the evaluation of schedulability we assume a worst-case factor $\Delta_{i,j}$ (as in [147]) and a time interval of evaluation $\ell = H$.

6.3.1.2 Simulation Results

Figure 6.2a shows the schedulability ratio achieved with a gateway designation based on degree centrality and on a random baseline. These results suggest that, under varying topologies and workload conditions, the degree centrality metric is always better than (or equal to) the baseline. Notably, the degree centrality achieves up to about 30% better schedulability under particular settings. These plots also suggest that higher gains are obtained under moderate workload, particularly at the low and high network connectivity levels. Note that connectivity is varied here through node density, where a value of 1 targets a fully linked network, i.e. with each node linked (in average) to every other node in the network.

Figure 6.2b shows the absolute deviation of the schedulability ratio achieved with the other types of centrality with respect to the degree centrality metric, which we consider as a reference for these plots. In all cases, our outcomes show that these other centrality criteria are always better than or equal to the degree centrality, achieving up to $\sim 18\%$ of additional improvement. However, none of these centrality metrics dominated the others in all the cases evaluated, thus exploring their synergy holds promise.

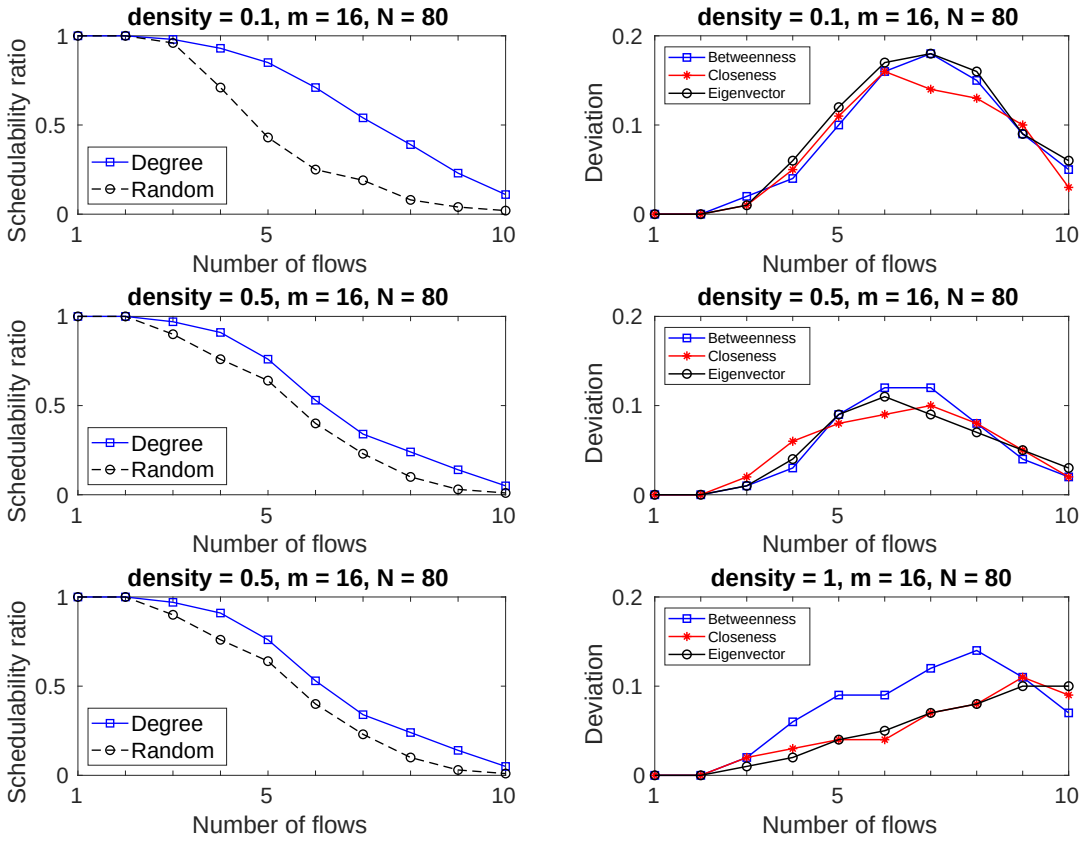

(a) (b)

Figure 6.2: The schedulability ratio under varying number of network flows $n \in [1,10]$; a) the comparison between the degree centrality and a random baseline when varying network density in $\{0.1, 0.5, 1.0\}$; b) the absolute deviation of the other centrality measures w.r.t. the degree centrality.

In particular, the betweenness centrality metric was able to achieve the largest gains for all densities, while eigenvector and closeness were better only under particular configurations. The eigenvector centrality was almost always equal or slightly better than the betweenness centrality for the lowest density case, but generally worse for the high and medium densities. Closeness centrality shows, in general, the smallest gains and a more unsteady performance, but still remarkably if compared to the random baseline. Degree centrality, though not dominant, remains the simplest, thus preferable from a complexity viewpoint.

6.3.2 Centrality-Driven Multi-Gateway Designation

6.3.2.1 Simulation Setup

1) Network topologies. We consider 1000 random topologies built upon the synthetic generation of network graphs. Each topology was generated with a target node density $d = 0.1$ using a sparse uniformly distributed binary random matrix of $N \times N$, i.e. assuming lossless links, where N is the total number of network nodes, including the k gateways. Without loss of generality, we use $k = \{1,3,5\}$ and $N = 75$ for all the simulation experiments.

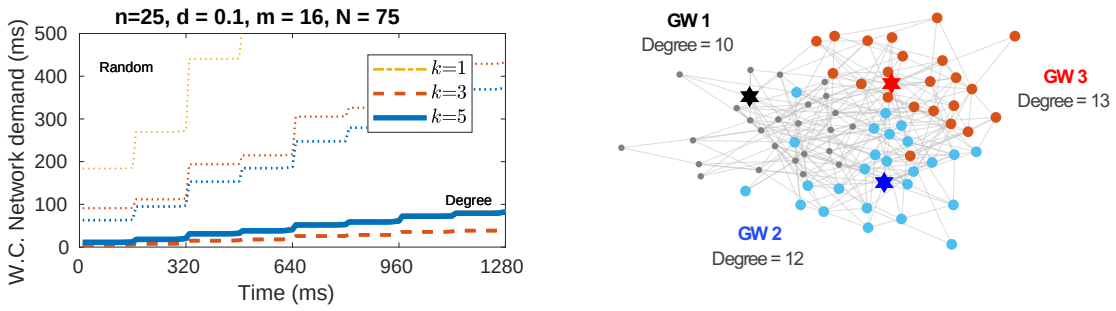

Figure 6.3: (Left) Worst-case network demand (ms) in one simulated case during a hyper-period. (Right) An illustrative example of joint clustering and gateway designation;

2) Gateway designation. After clusters have been created, a number of k nodes is selected as gateways using each of the cluster centrality metrics in Table 6.1. In the absence of a better solution to compare against, a random designation of k gateways is also considered, for benchmarking. Note the random designation is done before clusters are created.

3) Network flows. A subset of $n \in [1,30]$ vertices is selected randomly as sensor nodes, i.e. to periodically transmit deadline-constrained data toward one of the k gateways. Each C_i is computed directly by the product of the time slot, i.e., 10 ms, and the number of hops in the path ϕ_i. T_i is harmonic and randomly generated in the range of $[2^4, 2^7]$. This implies a super-frame length of $H = 1280$ms. Finally, D_i is set implicitly, i.e. $D_i = Ti$.

4) Real-time assessment. We assess schedulability over a time interval equal to the super-frame, i.e., $\ell = H$, and when all the $m = 16$ channels are available. Concerning $\Delta_{i,j}$, we use precise computation derived from the network topology.

6.3.2.2 Simulation Results

Fig. 6.3 and Fig. 6.4 show simulation results based on the setup described above. Fig. 6.4a presents the schedulability ratio over n flows for both the proposed multi-gateway designation framework (thicker lines) and a random baseline (thinner lines). As expected, results show that increasing the number of gateways improves schedulability in all cases. A schedulability ratio of 99% can be achieved with only 5, 5 and 6 flows using random designation with $k = 1, 3$ and 5, respectively. With our framework, these values increase to $11, 17$ and 21 flows, respectively, thus an improvement of 3.5 times in the number of schedulable flows with 5 gateways.

Fig. 6.3 (left) shows the network demand for one of the 1000 random topologies imposed by $n = 25$ flows over an interval equal to the hyperperiod H, for both approaches. These results confirm that our framework significantly reduces the worst-case demand bounds.

Fig. 6.3 (right) illustrates the clustering and gateway designation in a concrete topology when using our framework. The clustering is coded in different colours and the corresponding designated gateway is marked with a star.

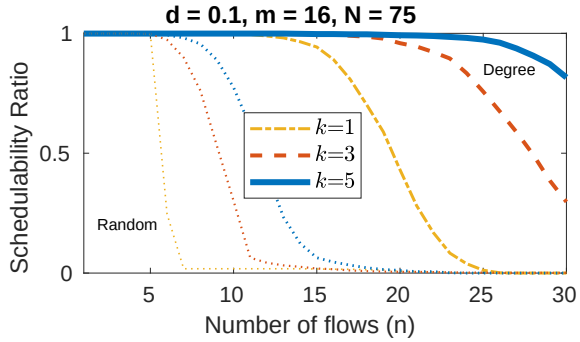

(a)

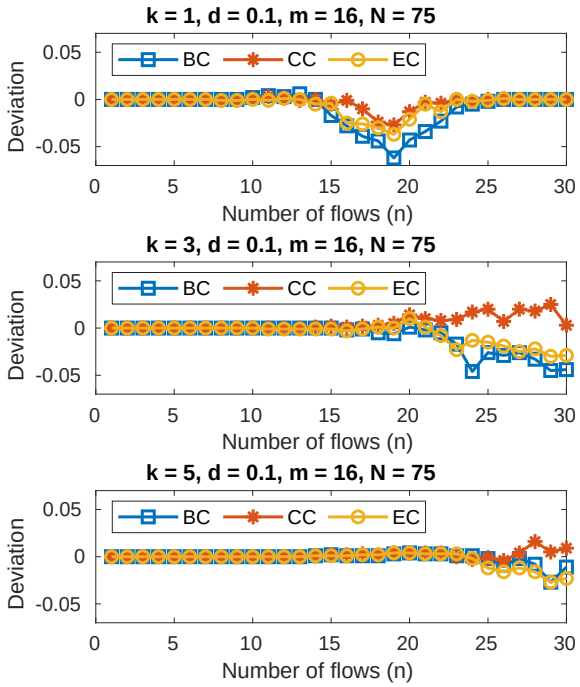

(b)

Figure 6.4: a) Schedulability ratio of 1000 random topologies with target density 0.1 and $k = \{1,3,5\}$, with *degree* centrality versus random designation, and b)schedulability ratio deviation of other centrality metrics w.r.t. degree centrality for $k \in \{1,3,5\}$

Figures 6.4b present the deviation (difference) in the schedulability ratio achieved by the other centrality metrics w.r.t. degree centrality, namely, betweenness centrality (BC), closeness centrality (CC) and eigenvector centrality (EC), for $k \in \{1,3,5\}$. These results should be correlated with those in Fig. 6.4a. All centrality metrics perform equally well for low loads, given the low mutual interference, with all flows meeting their deadlines (100% schedulability). With high loads, mutual interference grows and all metrics perform poorly, with few or no flows meeting their deadlines (0% schedulability). The differences, in any case small ($< 5\%$), appear when schedulability starts degrading, thus being of low interest from a system design point of view.

6.4 Summary & Concluding Remarks

This chapter has introduced the idea of centrality-driven gateway designation for enhanced traffic schedulability in real-time WSNs. Simulation results for the two case studies, single- and multi-gateway designation, have shown that centrality is an effective and promising approach to improve schedulability over an arbitrary (random) gateway designation.

The case of single-gateway designation showed larger deviations among the different centrality metrics evaluated, yet with considerably less amount of test cases evaluated, i.e. 100. The multi-gateway designation study with 1000 different topologies suggests these differences decrease as the number of test cases increases. In any case, both studies agree on the lack of a dominant or optimal criterion for gateway designation; the challenge to be addressed in the next chapter.

Interestingly, this chapter has emphasized the existence of an additional dimension for scheduling problems in real-time networks, i.e. gateway, sink or controller designation, with clear potential applicability to different types of infrastructures (e.g. 5G, time-sensitive or software-defined networks) which also rely on traffic schedulability guarantees as key performance indicators.

Similarly, we have shown that the novel combination of two well-established techniques, network centrality, and spectral clustering, can bring benefits as an efficient framework for finding positing-agnostic central nodes in complex structures, as alternative to the more common (position-dependent) k-means algorithm. While not declared as a major contribution of this thesis, it represents a research line to further validate and capitalize.

Finally, we recall this approach is intended to be used at systems design time, which is well suited for overwater WSNs with long-term network dynamics, i.e. stable topologies. We yet envision further research extending the centrality-driven gateway designation framework to dynamic topologies. We conjecture that in frameworks such as swarms of marine robots, a leader selection could be made based on centrality in order to facilitate real-time communication. This can be combined to our physical-layer positioning technique to find distance configurations for the swarm that can deal with both, real-time and overwater aspects simultaneously.

Chapter 7

Minimal-Overlap Centrality-Driven Gateway Designation

In this chapter, we aim to further enhancing *real-time* performance of globally synchronized wireless mesh networks (e.g. TSCH-based) by means of gateway designation. We continue advocating for a *judicious* centrality-driven method but this time by proposing a novel metric termed *minimal-overlap* network centrality. The new metric conveniently exploits the relationship between path node-overlaps and gateway designation for improved traffic schedulability. We thus make use of this metric to designate as gateway the node which produces the least overall number of overlaps. As in the previous chapter, we also extend the method to multiple gateways with the aid of the unsupervised learning method of *spectral clustering*. Extensive simulations with varying configurations evaluate the *real-time* performance of this new approach at system design time. Notably, these results show our methods are dominant over all classical network centrality criteria evaluated, both for single and multiple gateway designation.

The material included in this chapter is mostly derived from the following publications:

- M. G. Gaitán, P. d'Orey, P. Santos and L. Almeida, "Minimal-Overlap Centrality-Driven Gateway Designation for Real-Time TSCH Networks", in RAGE 2022 Workshop, co-located with DAC 2022. **[Best Paper Award]** [8].
- M. G. Gaitán, L. Almeida, P. d'Orey, P. Santos and T. Watteyne, "Minimal-Overlap Network Centrality for Multi-Gateway Designation in Real-Time TSCH Networks", in ACM Transactions on Embedded Computing Systems 2023 (Under Review) [1].

7.1 Problem Overview

In the context of IIoT, many networks are mesh WSNs[1] with a fixed set of field nodes gathering data from a process to support system-wide monitoring and control. The network flows are static, defined at design time, and converge to one or more gateways. Typically, gateways are deployed

[1] Further consider our use case of an overwater mesh WSN for real-time environmental monitoring as an example.

in some arbitrary positions. Conversely, gateway designation uses existing nodes for the gateway function without adding new ones, but their positions are constrained, instead.

The gateway – an essential node enabling seamless communication with external entities – also plays a role in *real-time* network operation. Proper gateway designation, routing, and scheduling are thus needed for real-time flows to meet their timing constraint. As shown in the previous chapter, the notion of network centrality – from network science – can effectively support gateway designation while facilitating real-time communication. Despite the promising results, none of the assessed metrics dominate the others and optimal performance is far from being achieved.

In this chapter, we address the challenge of proposing a new *dominant* network centrality metric specifically designed to reduce (worst-case) end-to-end deadline misses in WSNs. While classical centrality metrics have shown acceptable real-time network performance in some configurations, we observe these metrics were not tailored and engineered for *real-time communication* and as so do not explicitly take into account the following considerations:

1. **Conflicting transmissions**. In real-time WSNs, priority-based transmissions involving a common node can lead to the so-called *transmission conflicts*, which influence end-to-end delays, and consequently may cause violations of timing requirements (i.e. deadline misses). Shortest paths from sensor nodes toward a common gateway often involve several common nodes, thus leading to more transmission conflicts than e.g. disjoint but longer paths.

2. **Contention delays**. In time-triggered communication, contention can occur when a higher-priority transmission delays a lower-priority one. If more resources (i.e. channels) are available within the same slot, contention delays can occur when all of them are occupied by higher-priority transmissions. Shortest paths in WSNs use generally fewer transmissions (thus resources) than e.g. longer paths, leading potentially to lower contention delays.

In order to take into consideration these two factors, we propose a novel centrality metric for gateway designation which offer a good trade-off between contention and conflicts delays while improving traffic schedulability. Whereas a schedulability-optimal choice could be made using enough computational power, we advocate here for a less demanding method that does not require fully assessing network schedulability to achieve near-optimal real-time performance.

Organization. The remainder of this chapter is organized as follows. Section 7.2 formally presents our novel single- and multi-gateway designation methods. Section 7.3 offers an assessment of both case studies in terms of real-time performance under varying configurations. Section 7.4 summarizes and concludes the chapter.

7.2 Minimal-Overlap Network Centrality for Multi-Gateway Designation in Real-Time Wireless Sensor Networks

In this section, we present our novel *centrality-driven* single- and multi-gateway designation framework for real-time WSNs leading to improved real-time performance at system' design time.

We resort to alike fundamental concepts from our centrality-driven gateway designation in the previous chapter but we solve the gateway designation problem by proposing a new *flow-informed* metric termed *minimal-overlap centrality* based on the overall reduction of path node-overlaps in the network. We conjecture that by considering all flows' path information to reduce overlaps, we are simultaneously taking into account both conflict and contention factors *by design*. A lower overall number of path node-overlap reflects at the same time a lower amount of shared paths (potential conflicts), and a lower load (potential contention) allocated at the same node. Nevertheless, because less overlapping also implies having more disjoint but longer paths, an increase in overall contention is also expected. Yet, since transmission conflicts are deemed to be a major player on the worst-case end-to-end delays of mesh WSNs (see e.g., [148]), we also expect our trade-off heuristic approach leads to an improvement in traffic schedulability.

Note that we resort to equivalent network, flows, and performance models presented in the previous chapter. We do not further discuss this here for brevity reasons.

7.2.1 Minimal-Overlap Centrality-Driven Single-Gateway Designation

Given the network and real-time flow models presented earlier, we continue with the challenge of how to *judiciously* designate a node as gateway for improved WSN traffic schedulability. Here, since we are addressing first the case of single gateway designation, we consider $k = 1$ in the modeling framework. That being said, we opt now for a flow-informed gateway designation strategy which makes the network *aware* of the overall path-overlapping degree when considering all routing paths to be known beforehand[2]. To this purpose, we propose a novel network centrality metric termed *minimal-overlap* centrality which characterizes the relationship between the overall path node-overlaps and gateway designation. In this new perspective, a node with a higher centrality measure indicates a node with a lower number of shared paths, and thus with fewer node overlaps; ergo more "central". Similarly to the previous chapter, the resulting metric is then used to designate as a gateway the node with the highest score, here the one of *minimal-overlap* centrality. A graphical representation of the proposed gateway designation is presented in Fig. 7.1 for clarity.

Eq.7.1 formally presents our proposed metric:

$$MO(v_q) = \frac{1}{\sum_{i,j=1 \wedge i \neq j}^{n} \Delta_{i,j}^{q} + 1} \tag{7.1}$$

where the factor $\Delta_{i,j}^{q}$ is the node-path overlap contribution from flows f_i and f_j when their routes ϕ_i and ϕ_j are directed toward node v_q, and n is the number of flows in the set F.

In short, the new metric is built upon the computation of the overall *path overlapping* resulting from the superposition of all flow routes in the network when directed to a given node $v_q \in V$. Classical network centrality metrics are also considered for benchmarking purposes. We do not present them here for brevity reasons, since they have been formalized in the previous chapter.

[2] Although we have assumed here a hop-count-based shortest-path routing (e.g. Dijkstra) for simplicity, the selection of the routing algorithm is arbitrary, and thus does not challenge the validity of the approach. Note also that knowing the routing path of each flow beforehand is also a requirement of the real-time flow model adopted, i.e. ϕ_i

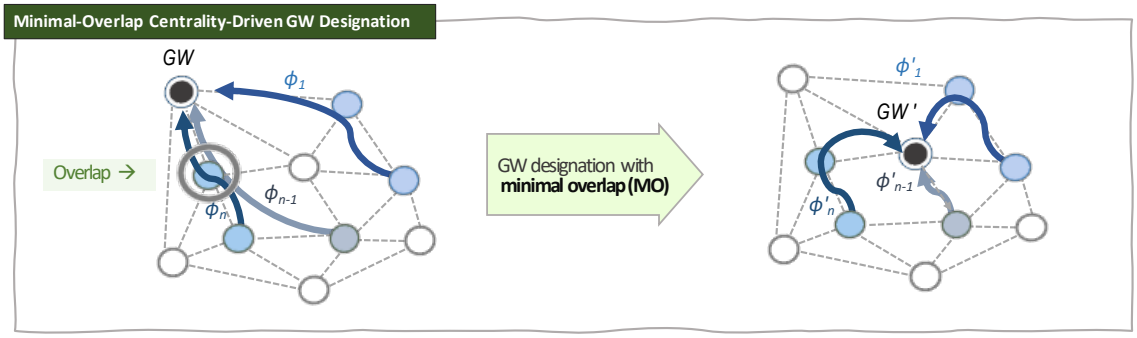

Figure 7.1: A graphical representation of the minimal-overlap centrality-driven single-gateway designation strategy applied to an arbitrary mesh network.

7.2.2 Minimal-Overlap Centrality-Driven Multi-Gateway Designation

Typically, increasing the parallelization of flows using multiple gateways may bring a number of benefits in terms of network performance, also from a *real-time* systems perspective. A higher number of gateways often means less congestion since all the flows do not need to converge to the same destination. This may reduce shared paths (fewer conflicts) and improve load balance (less contention), aspects of interest for this research. However, the question of how to *judiciously* designate multiple nodes as gateways for improved WSN traffic schedulability is not trivial, as it has common roots with the single-gateway designation problem. While prior work has shown schedulability improvements by multi-gateway placement (e.g. [124]), the problem of *designation* is different from *placement* since typically agnostic from nodes' positions, as in our case.

In this section, we leverage the multi-gateway extension of the combined *spectral clustering* and *centrality* framework presented in the previous chapter. The clear difference is that now in *phase* 2 we do not favor the use of a classical centrality metric but rather of our new flow-informed metric. We consider classical metrics for benchmarking. We recall that the overall approach allows us to keep freedom from node positions by only resorting to the spectral properties of the network. In this regard, the framework is intended to be used at system design time while only requiring two major inputs: *i*) the network topology (graph) in the form of an adjacency matrix and *ii*) the target number of gateways. We further remark that our multi-gateway designation is parametric, allowing exploring the trade-off between schedulability and k, the number of gateways, thus enabling efficient designs with the minimum number of gateways needed to guarantee traffic schedulability.

In the following, we elaborate on the differences the new approach has with *phase* 2 of the original framework. *Phase* 1 is the same, thus we do not cover it again for the sake of brevity.

7.2.2.1 Phase 2: Clustering-Aided Multi-Gateway Designation

This phase consists of first *i*) computing the centrality measure per sub-graph after the k clusters have been identified to then *ii*) selecting as gateway of each cluster the node with the highest centrality score. This reasoning applies to any other type of centrality being used for multi-gateway

designation. However, when computing the centrality score of each node, we need first to adapt the respective *network* centrality expression to the current interpretation of being a *cluster centrality* metric, as presented earlier in Table 6.1. Essentially, this adaptation is done by considering each cluster G_ℓ as a sub-graph of G characterized by its respective cluster adjacency matrix A_ℓ and the number of nodes in the cluster N_ℓ, with $\sum_{l=1}^{k} N_\ell = N$. In the case of Eq. 7.1 for the minimal-overlap centrality we reformule it as:

$$MO^{\ell}(v_q) = \frac{1}{\sum_{i,j=1 \wedge i \neq j}^{n_\ell} \Delta_{i,j}^{q} + 1} \tag{7.2}$$

where $n_\ell < n$ is the number of sources which flows are directed to node $v_q \in G_\ell$, $q \in [1, N_\ell]$, and thus $\mathrm{MO}^{\ell}(v_q)$ denotes the minimal-overlap (MO) cluster centrality for a given node $v_q \in G_\ell$. Note that when $k = 1$, the associated cluster corresponds to the whole network. Thus, this MO expression also generalizes Eq. 7.1 to multiple gateways.

7.3 Performance Evaluation

7.3.1 Simulation Setup

1) Wireless mesh networks. We consider 1000 network topologies built upon the synthetic generation of random graphs. Each graph is generated using a sparse uniformly distributed random matrix with a target (average) node density of $d = \{0.1, 0.5, 1.0\}$. The dimension of the random matrix is $N \times N$, where $N = 75$ is the total number of nodes in the network including $k = \{1, 3, 5\}$ gateways. All graphs represent TSCH-based WSNs in multi-channel operation, here using $m = 16$ channels and time slots of $t_{slot} = 10$ ms.

2) Real-time network flows. We consider a subset of $n \in [1, 30]$ nodes are source nodes while the rest acts as relays or gateways. Source nodes are selected randomly from the set of field nodes, i.e. excluding the k gateways. All flows are consistently generated according to the real-time model 4-tuple parameter (C_i, D_i, T_i, ϕ_i). Each flow is directed to only one of the k gateways through its shortest path ϕ_i. C_i is computed by multiplying the time slot duration t_{slot} with the length of the routing path (in number of hops). T_i is randomly generated in the form 2^{η}, with $\eta \in \mathbb{N}$ in the range $[4, 7]$, thus leading to harmonic periods. This implies a super-frame duration (or hyper-period) of $H = 2^7$ slots, i.e. $H = 1280$ ms. All the respective deadlines (D_i) are assumed to be equal to the respective flow periods, i.e. $D_i = Ti$, thus assuming an implicit-deadline model.

3) Real-time performance assessment. We resort to the supply/demand-bound based schedulability test introduced earlier. We recall this real-time performance assessment tool assumes all transmissions are scheduled under a global EDF scheduling policy. We consider an interval equal to the hyper-period ($\ell = H$) for evaluation, in all the cases. Concerning $\Delta_{i,j}$, we use precise computation of node-path overlaps derived directly from network topologies.

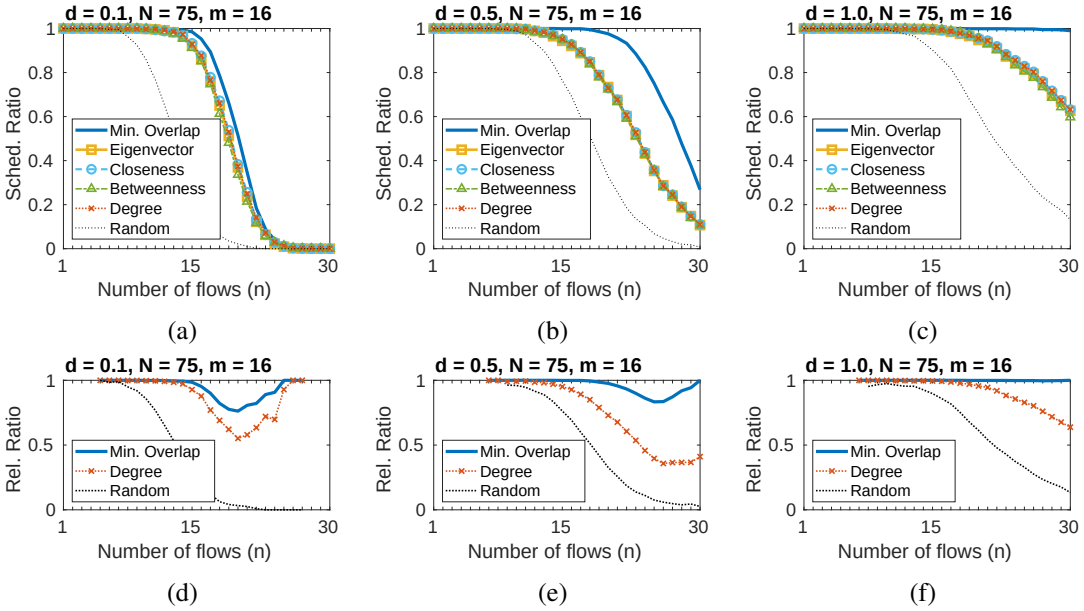

Figure 7.2: (Top) Schedulability ratio of 1000 random topologies for varying number of flows with target density 0.1 (*a*), 0.5 (*b*) and 1.0 (*b*) resorting to gateway designation methods based on *i*) classical network centrality metrics (e.g. eigenvector centrality) and *ii*) the proposed minimal-overlap network centrality. (Bottom) The relative ratio in terms of schedulability from the best and worst possible gateway assignments. A random selection is included as reference.

7.3.2 Simulation Results

7.3.2.1 Traffic Schedulability, $k = 1$

Fig. 7.2 (top-row) presents schedulability ratio results for the case of single-gateway designation, i.e. $k = 1$, when varying the number of network flows $n \in [1, 30]$ and when using different network densities $d = \{0.1, 0.5, 1.0\}$ (see left, middle and right plots of top row, respectively). These results correspond to different centrality metrics used as criteria to designate one gateway. Specifically, our minimal-overlap metric is compared against the classical eigenvector, closeness, betweenness and degree, as well as versus a random assignment for reference. As expected, it can be observed that the schedulability ratio decreases for larger numbers of flows in all configurations due to the larger channel contention and transmission conflicts. Conversely, higher network density increases the number of potential paths between any given pair of nodes, favoring schedulability.

The results also show that the minimal-overlap gateway designation method achieves higher schedulability for all numbers of flows and densities when compared with a non *flow-informed method* based on classical centrality metrics (e.g. betweenness or degree). We argue this is caused mostly by the minimal-overlap method's ability to decrease, by design, the number of overlapping paths. This, in turn, allows for reducing transmission conflicts, thus improving the timely delivery of data messages. As expected, the proposed *minimal-overlap* method is also clearly superior to the random selection, further demonstrating the significance of judicious gateway designation.

We also analyze how the proposed method deviates from the system's optimal gateway election

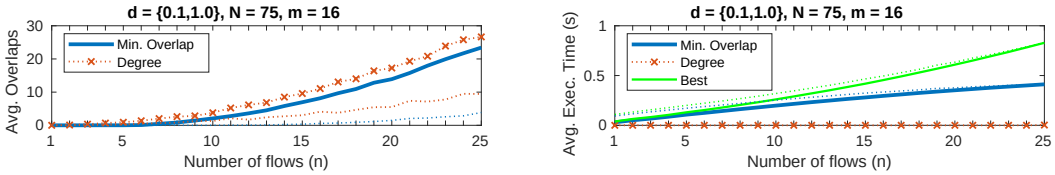

(a) (b)

Figure 7.3: (Left) Average number of overlaps of 100 random topologies when varying network flows for two gateway designation methods (minimal-overlap and degree) and two extreme densities, namely 0.1 (solid line) and 1.0 (dotted line). (Right) Execution time for different gateway designation methods, namely, minimal-overlap, degree and best, considering up to 25 network flows and two extreme target densities, namely 0.1 (solid line) and 1.0 (dotted line).

Fig. 7.2 (bottom-row). The metric *relative ratio* is defined as the ratio between the schedulability ratio of a given method to the schedulability ratio of the best and worst performing nodes in the network, with a value of 1 denoting best and 0 the worst performance. The results show the performance of the proposed method is only slightly below the best method, having the maximum degradation of $\sim$24% for a density of 0.1 and 20 simultaneous flows. We highlight that this degradation is lower for larger densities (e.g. $d = 0.5$), becoming negligible for highly connected networks (e.g. $d = 1.0$), because the overall overlapping degree decreases for increasing density; as shown also in [11]. Additionally, these results reveal that the performance improvements of the proposed method are, in general, able to increase for higher density and higher number of flows when compared with other centrality-based gateway designation methods or random gateway selection.

7.3.2.2 Computational Cost, $k = 1$

Fig. 7.3 depicts the average execution time for different gateway designation methods versus the optimal gateway designation. Regarding the classical centrality-based designation method, we solely present the result for degree centrality for visual clarity and because this has the lowest execution time among all metrics. We also present results for two extreme density values of 0.1 (solid line) and 1 (dashed lines). The setup for this experiment used MATLAB R2020b on Ubuntu 18.04 LTS on a laptop with an Intel Core i7-6500U CPU at 2.5GHz and 4GB of DD3 RAM.

These results confirm the low execution time of the degree-centrality gateway designation. On the other hand, minimal overlaps designation considerably decreases the execution time when compared against optimal gateway designation, particularly for higher number of flows. Note that the optimal method uses extensive search with full schedulability analysis for each case, while the MO metric just requires computing the number of overlaps in the network given a set of flows. The results also show that the density has a minimal impact on the average execution time. Overall, the proposed method provides a good trade-off between achievable schedulability ratio (near optimal) and computational cost (about half the value of the optimal method).

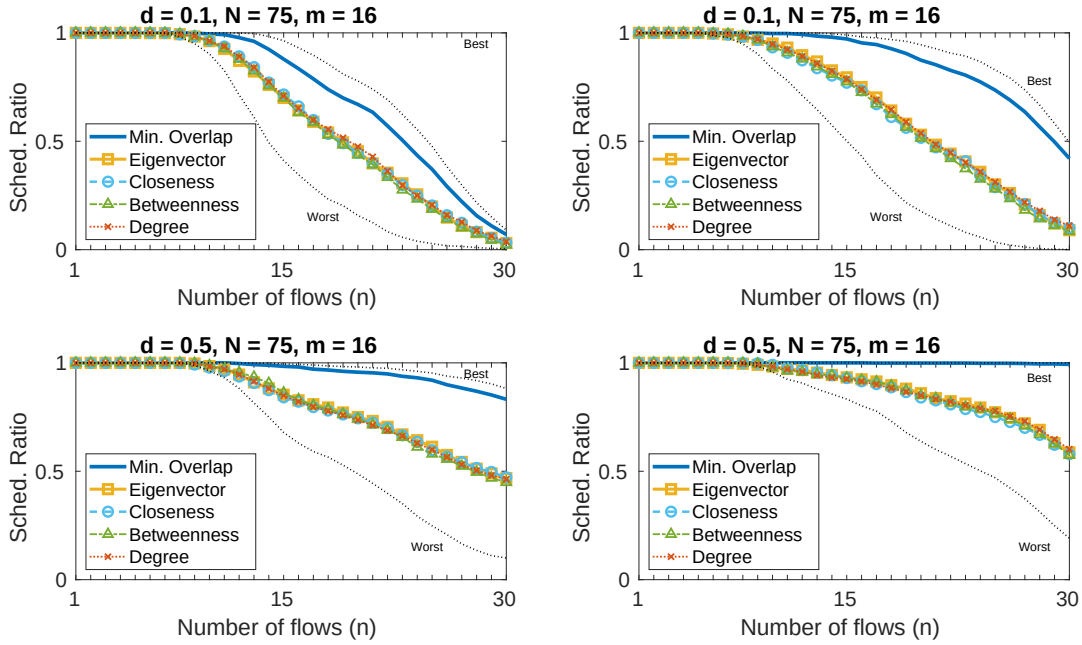

(a) $k = 2$ (b) $k = 3$

Figure 7.4: Average schedulability ratio of 1000 random topologies for varying number of flows when using (a) $k = 2$ and (b) $k = 3$ gateways. The solid blue line curves show the results for our minimal-overlap centrality used as a cluster centrality metric and when compared against classical centrality metrics. Best and worst performing nodes are also shown as benchmarks.

.

7.3.2.3 Schedulability Ratio, k>1

Fig. 7.4 presents different schedulability ratio results for the *minimal-overlap* multi-gateway designation framework when compared to classical centrality-driven methods. Also, both the best and worst possible gateway selections at each cluster are presented (in dotted lines) for comparison. Overall, these results show our minimal-overlap framework is always dominant over all the classical metrics assessed while achieving optimal (best) or near-optimal real-time performance, especially when the node density is increased. As expected, it is also shown to be clearly superior that the worst performing gateway selection at each cluster.

Fig. 7.4a shows the results for $k = 2$ gateways while Fig. 7.4b the case for $k = 3$. These results confirm the expectation that an increase in the number of gateways (and clusters) also favors schedulability. As shown in the previous chapter, a greater number of gateways significantly reduces network demand, positively impacting the overall network schedulability. This benefit can be observed here too, for example, in the case study with $d = 0.5$ (bottom-row), which allows passing from 10 to 30 schedulable flows with 99.9% of schedulability, which represents an improvement of 200% w.r.t. to the same framework, same configuration, but one more cluster/gateway. A similar effect can be observed when using $d = 0.1$ (top-row) but with lower gains, due to the reduced node density. Note that this density-related effect is consistent with the idea of having more diversity for paths favors schedulability, especially when using a *minimal-overlap*

approach.

7.4 Summary & Concluding Remarks

This chapter has provided a novel framework for designating nodes in real-time mesh WSNs. The end goal is to improve traffic schedulability by design by means of judicious gateway designation. The framework considers both single- and multi-gateway designation cases, both resorting to the notion of network centrality from social network analysis. As different from the previous chapter, we provide here a new centrality metric termed *minimal-overlap* centrality which characterizes the overall path-overlapping degree among any of the active flows in the network. This metric dominates over classical centrality metrics in terms of real-time performance, while offering considerable improvements in terms of schedulability. The multi-gateway version uses this metric at the cluster level, after partitioning the network in a set of k disjoint clusters using spectral clustering. Overall, this framework represents the first specific position-agnostic approach specifically designed to enhance traffic schedulability in real-time mesh WSNs.

In comparison with the previous chapter, this study has also evidenced the existence of an optimal (or best) solution among all the possible nodes in the gateway, for the single gateway case, or among all the nodes in each cluster, for the case of the clustering-assisted multi-gateway designation. We have used this option as ground truth while emphasizing its complexity from the computational point of view. This is visible not only in terms of time complexity estimation, but it is also clear analytically, by inspection. The minimal-overlap approach is simple in general, which means it can also be straightforwardly applied to a different context, e.g. energy consumption, or load balanced, while at the same time offering enhanced real-time behavior.

In the future, we are interested in further benefits from the use of this framework at run-time, equivalent to what was explained in the previous chapter, for example, as a potential solution for fast leader selection in dynamic networks with mobile robots, including swarms of small vessels in over-water environments, or vehicular platoons. We also aim to assess the validity of the framework in different scenarios in which topologies are not necessarily uniformly distributed as the ones evaluated, but with particular topological properties (e.g. network motifs), or in regular topologies (e.g. grids, hexagons, etc.). More importantly, we aim to verify the benefits of this framework in real-world testbeds.

Chapter 8

Minimal-Overlap Shortest-Path Routing

In this chapter, we focus on improving the *real-time* performance of globally synchronized wireless mesh networks (e.g. TSCH-based) regardless of gateway designation. To this purpose, we propose a novel scheme termed *minimal-overlap* shortest-path routing able to enhance traffic schedulability by means of *judicious* source routing design. The scheme is based on an original greedy meta-heuristic for minimizing the overall amount of flows' path-overlaps in the network. Simulation results with varying configurations show our flow-informed routing scheme effectively improves real-time network performance when compared to a conventional (hop-count) shortest-path routing. Additional experiments suggest our approach can lead to optimal or near-optimal traffic schedulability when combined with a centrality-driven gateway designation criterion, scheduling up to 3 times more flows than a naive real-time configuration.

The material included in this chapter is mostly derived from the following publications:

- M. G. Gaitán, L. Almeida, P. Santos and P. Yomsi, "EDF Scheduling and Minimal-Overlap Shortest-Path Routing for Real-Time TSCH Networks", in NG-RES 2021 Workshop, co-located with HiPEAC 2021 [11].
- M. G. Gaitán, L. Almeida, T. Watteyne, P. d'Orey, P. Santos and D. Dujovne, "Joint Scheduling, Routing and Gateway Designation in Real-time TSCH Networks", in JRWRTC 2022 Workshop, co-located with RTNS 2022 [9].

8.1 Problem Overview

The study of the real-time performance of mesh WSNs is multi-dimensional. Proper scheduling, routing, and gateway designation methods are needed for real-time flows to satisfy stringent timing constraints. Traditionally, priority-driven *real-time* scheduling have dominated research studies in this field, often assuming an arbitrary criterion for gateway designation and a standard routing operation. While plenty of specialized routing schemes for WSNs has been proposed in

the literature, only a few of them fit into the class of *real-time wireless routing* [134], i.e. routing methods specifically engineered to enhance and/or guarantee real-time performance in WSNs.

In this chapter, we aim to complement our prior findings on gateway designation by proposing a novel scheme for *source routing* able to improve traffic schedulability regardless of gateway designation. Similar to our prior research for minimal-overlap gateway designation, we take into account for the routing design the two dominant factors influencing worst-case end-to-end deadline misses in real-time (mesh) WSNs:

1. **Conflicting transmissions**. An optimal gateway designation can provide us with the “best" configuration", e.g. in terms of overlaps (thus potential conflicts), but this result is constrained to a given solution space imposed by the flows’ paths. Different routing methods provide different flow paths, and thereby different “best" configurations in terms of conflict delays, because of the different solution spaces being explored.

2. **Contention delays**. Any routing method has a particular contention “footprint" given by the overall number of transmissions resulting from the length of their flows’ paths. Longer paths increase worst-case contention delays and thus influence traffic schedulability. Shortest paths are preferred but they often increase transmission conflicts.

An approach that both reduces conflicts and contention delays is a non-trivial trade-off to achieve. Yet, resorting to the idea of path overlap minimization is still a compromise that can be exploited in further dimensions, e.g. routing. Therefore, as different from our prior research acting on the node to be designated as gateway, here we act on the routing dimension by offering a set of source routing paths of *minimal-overlap*. Concretely, we provide a novel greedy meta-heuristic-based scheme that generates a set of disjoint paths, which are “good enough" both in terms of reduced conflicts (i.e. minimal overlaps) and contention (i.e. shortest paths) delays; thus achieving better schedulability regardless of gateway designation.

Organization. The remainder of this Chapter is organized as follows. Section 8.2 formally presents our new method, formulating the problem and describing the proposed solution. Section 8.3 evaluates the performance of the proposed method under varying conditions, considering two main case studies. Finally, 8.4 offers a summary and concluding remarks.

8.2 Minimal-Overlap Shortest-Path Routing for Real-Time WSNs

Fig. 8.1 shows a graphical representation of the proposed *minimal-overlap* routing method. It clearly resemble Fig. 7.1 in the previous chapter due to the similar foundational questions both methods attempt to answer. Although, at first sight both problems may looks similar, a considerable difference is the fact that the routing problem here addressed has no straightforward optimal solution to which compare. A minimal-overlap gateway designation can be obtained by exhaustive search, by checking among all the nodes which of them provides the minimum overlapping degree. Alike with the optimal solution, i.e. the one which produces the best schedulability results. However, to find the set of flow paths which produces the minimal overlapping degree in the

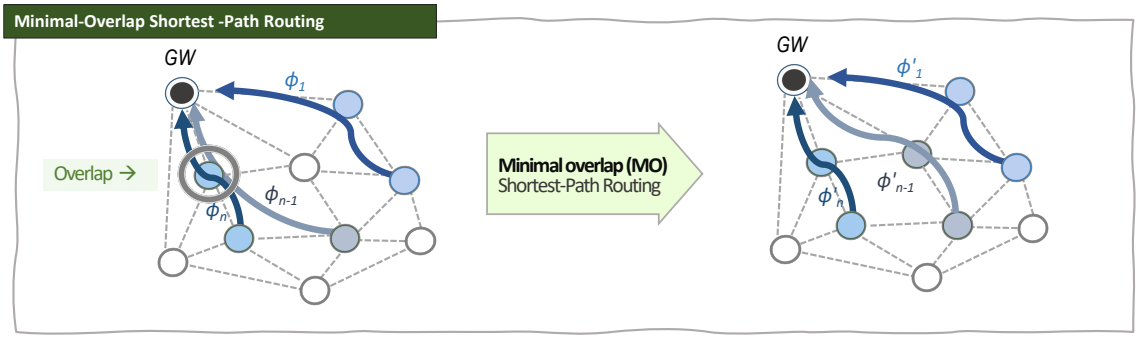

Figure 8.1: A graphical representation of the minimal-overlap shortest-path routing scheme applied to an arbitrary mesh network.

network is a combinatorial problem which escalates in computational complexity as the number of flows increases. Therefore, despite the common intuition of minimize path overlaps, the necessary techniques needed to solve each of the associated problems may differ significantly.

In this section, we present the challenge of finding a set of flows paths that minimize overlaps as an optimization problem. We then propose a solution for this problem by using a novel heuristic approach based on a greedy search algorithm. In short, this algorithm explores the solution space by providing a different set of flow paths at each iteration that depends on the previous set of paths found. Although the algorithm may recommend candidates than are worse than the initial or the current best solution among all the iterations explored, after few to several iterations the algorithm is able to find shortest-path combinations of considerably reduced overlapping; when compared to the initial solution. The output of the algorithm is the set of *minimal-overlap* shortest-paths.

8.2.1 Problem Formulation

We resort to the network and real-time flow models presented in the previous chapter but considering the case of single gateway designation only, $k = 1$. Given this framework, we consider the problem of finding the optimal set of flow paths $\Phi_{opt} \stackrel{\text{def}}{=} \{\phi_1^{opt}, \phi_2^{opt}, \ldots, \phi_n^{opt}\}$ that minimizes the *overall number of path overlaps* between any pair of flows in the network.

Definition 8.2.1. (Nominal Paths) We denote as $F_0 \stackrel{\text{def}}{=} \{f_1^0, f_2^0, \ldots, f_n^0\}$ the nominal (or initial) set of flows in the network which set of flow paths $\Phi_0 \stackrel{\text{def}}{=} \{\phi_1^0, \phi_2^0, \ldots, \phi_n^0\}$ is obtained using a conventional (hop-count) shortest-path algorithm.

Definition 8.2.2. (Candidate Paths) We denote as $F_k \stackrel{\text{def}}{=} \{f_1^k, f_2^k, \ldots, f_n^k\}$ (with $k \in \mathbb{N}$) the k^{th} variation of the nominal set of flows F_0 when a candidate set of routes $\Phi_k \stackrel{\text{def}}{=} \{\phi_1^k, \phi_2^k, \ldots, \phi_n^k\}$ is considered, instead. A method to generate candidate paths is proposed in the next subsection.

Definition 8.2.3. (Network Overlaps) We denote as Ω_k the *overall number of path overlaps* between any pair of flows in the set $F_k \stackrel{\text{def}}{=} \{f_1^k, f_2^k, \ldots, f_n^k\}$ with Ω_k computed as the sum of all the individual *node overlaps* δ_{ij}^k between the paths of any pair of flows f_i^k and f_j^k in the set F_k, where $i, j \in [1, n] \wedge i \neq j$; ergo Ω_0 is the respective overall number of path overlaps for F_0.

Given a network graph G, a nominal solution Φ_0 with respective Ω_0, and a number of $k_{max} \in \mathbb{N}$ candidate sets of routes Φ_k, we formulate the problem of minimizing Ω_k as follows:

$$\begin{aligned} \underset{\Omega_k}{\text{minimize}} \quad & \Omega_k = \sum_{\forall i,j \in [1,n] \wedge i \neq j} \delta_{i,j}(\Phi_k) \\ \text{subject to} \quad & k \in [1, k_{max}], \\ & \Phi_k \in [\Phi_1, \Phi_{k_{max}}] \end{aligned} \tag{8.1}$$

where $\delta_{i,j}(\Phi_k)$ denotes the number of *node overlaps* between the routes of the flows f_i^k and $f_j^k \in F_k$ (i.e. δ_{ij}^k), $\forall i,j \in [1,n] \wedge i \neq j$. The output result $\Omega_k = \Omega_k^{min}$ is the minimal *overall number of overlaps* within all the k_{max} possible sets of flow paths $[\Phi_1, \Phi_{k_{max}}]$. We call Φ_{opt} to the set of flow paths Φ_k that produces the optimal (or minimal-overlap) routes among all candidates.

Note. We make clear that each individual route ϕ_i^k in Φ_k is a sub-optimal version of the shortest-path ϕ_i^0 because its route length ζ_i^k is always greater than or equal to ζ_i^0, the route of the nominal (shortest) path. In the same way, the transmission time C_i^k associated with f_i^k is always a sub-optimal version of C_i^0, since C_i^k is always greater than or equal to C_i^0. We also clarify that a larger C_i^k does not necessarily imply a larger Ω_k, and vice-versa. Finally, note that although a larger C_i^k may lead to larger end-to-end delays, we conjecture that this impact is, in general, less detrimental than the impact of overlaps, thus we target to minimize this latter factor.

8.2.2 Greedy-Search Based Solution

We propose an approximate method to solve the problem formalized in (8.1). The approach is based on a greedy meta-heuristic that recommends a single candidate set Φ_k at each k^{th} iteration, and then computes the corresponding Ω_k. The smallest of the Ω_k after k_{max} iterations is designated as Ω_k^{min} which is reported at the last iteration. We detail the proposed method as follows:

Step 1 (Initial solution)

- At $k = 1$, $\Phi_k = \Phi_1$ is computed as a function of the path overlaps resulting from Φ_0, i.e., from the initial set of (hop count) shortest-paths, and from the graph $G = (V, E)$.
- Φ_1 is computed as the set of (weighted) shortest paths of $G^1 = (V, E^1)$, a modified version of the unitary-weighted G whose set of edges is weighted as a function of the node-overlapping degree derived from the set of flow paths Φ_0.
- The cost function $W_{i,j}(u,v)$ that weight any edge (u,v) in G whose nodes u and $v \in V$ are simultaneously in any pair of routes ϕ_i^0 and $\phi_j^0 \in \Phi_0$ is defined as follows:

$$W_{i,j}(u,v) = 1 + \sum_{e=1}^{\delta_{i,j}^0} \psi \tag{8.2}$$

where $\psi \in \mathbb{R}$ is an arbitrary factor[1], and $\delta^0_{i,j}$ is the number of *node overlaps* resulting from the routes ϕ^0_i and $\phi^0_j \in \Phi_0$, $\forall i, j \in [1,n] \wedge i \neq j$.

– Therefore, Φ_1 is the resulting set of (weighted) shortest-paths over G^1, and Ω_1 the corresponding *overall number of overlaps* for Φ_1.

– If $\Omega_1 < \Omega_0$, then $\Omega^{min}_k = \Omega_1$, else $\Omega^{min}_k = \Omega_0$.

Step 2 (Greedy search)

– For any $k \in]1, k_{max}]$, the search for a Ω^{min}_k is generalized.

– $G^k = (V, E^k)$ is defined as the modified version of $G^{(k-1)} = (V, E^{(k-1)})$ whose set of edges is weighted using the following cost function:

$$W^k_{i,j}(u,v) = 1 + \sum_{e=1}^{\delta^{(k-1)}_{i,j}} \psi \tag{8.3}$$

where $\delta^{(k-1)}_{i,j}$ results from the routes $\phi^{(k-1)}_i$ and $\phi^{(k-1)}_j \in \Phi_{(k-1)}, \forall i, j \in [1,n] \wedge i \neq j$.

– Φ_k is thus computed as function of the path overlaps resulting from the set $\Phi_{(k-1)}$.

– If $\Omega_k < \Omega^{min}_k$, then $\Omega^{min}_k = \Omega_k$, else $\Omega^{min}_k = \Omega^{min}_k$.

Step 3 (Best solution)

– At $k = k_{max}$, the algorithm finishes and provides Ω^{min}_k, i.e., the minimal *overall number of overlaps* within all the k_{max} Φ_k sets recommended. Note that the quality of Ω^{min}_k will depend on the quality of the generated Φ_k sets, as well as on the total number of iterations.

– The optimal set of routes Φ_{opt} is thus the Φ_k which provides Ω^{min}_k.

8.2.2.1 Pseudo Algorithm

Algorithm 2 presents a pseudo-code for the proposed method. The algorithm consists of three major procedures:

- EDGEUPDATE (lines 1-5),
- CALCOVERLAPS (lines 6-9) and
- MOGH (lines 10-27).

[1]The arbitrary factor Ψ is a user-defined parameter, here assumed as constant, but that can be optimized to provide better (e.g., faster) solutions for Ω^{min}_k. Yet, this aspect is not further explored in this dissertation.

Algorithm 2 Minimal-Overlap (MO) Routing

Input: G, F, k_{max}, ψ
Output: Φ_{opt}, Ω_{opt}

procedure EDGEUPDATE(G_{in}, Φ_{in})
  $W^k_{i,j}(u,v) = 1 + \sum_{e=1}^{\delta^{(k-1)}_{i,j}} \psi$
  $G^{out} \leftarrow G_{in}(V, E^{weighted})$
  return G^{out}
end procedure
procedure CALCOVERLAPS(Φ_{in})
  $\Omega_k = \sum_{i,j}^{n} \Delta_{ij}$
  return Ω^{out}
end procedure
procedure MOGH(G, F, k_{max})
  $k = 0$ ▷ Initial Solution Start
  $\Phi_0 \leftarrow$ SHORTESTPATH(G, F) ▷ Hop-count-based
  $G^0 \leftarrow G$
  while $k \leq k_{max}$ and $\Omega^{min}_k > 0$ **do** ▷ Greedy Search
    $G^k \leftarrow$ EDGEUPDATE(G^{k-1}, Φ_{k-1})
    $\Phi_k \leftarrow$ SHORTESTPATH(G^k, F) ▷ Weight-based
    $\Omega_k =$ CALCOVERLAPS(Φ_k)
    if $\Omega_k < \Omega_{min}$ **then**
      $\Omega^{min}_k = \Omega_k$
      $\Phi^{min}_k = \Phi_k$
    else
      $\Omega^{min}_k = \Omega^{min}_k$
    end if
    $k = k + 1$
  end while
  $\Phi_{opt} = \Phi^{min}_k$, $\Omega_{opt} = \Omega^{min}_k$. ▷ Best Solution
end procedure

The MOGH procedure is the main method. It determines a new set of flow paths Φ_k – and its corresponding overall number of overlaps Ω_k – at each k^{th} iteration. The method stops at the last iteration when it provides a set of paths of minimal overlapping degree (among the solution space explored). The procedure may stop first if the overall number of overlaps reaches zero, i.e. $\Omega_k = 0$.

The EDGEUPDATE procedure updates the weights of the link for the input topology G_{in} to then return a new weighted topology G_{out} over which the new paths and overlaps are calculated. It resorts to the cost function $W^k_{i,j}(u,v)$ to determine the weight of any edge (u,v) in G_{out} as a function of $\delta^k_{i,j}$ and ψ. We recall the former represents the number of overlaps between the paths of flows f^k_i and $f^k_j \in F_k$ at the graph G_{in}, while the latter is a user-defined parameter used to control the speed of convergence of the algorithm.

The SHORTESTPATH procedure provides the shortest sequence of edges between any pair of nodes in the graph, by resorting to a classical weighted or hop-count-based shortest-path mecha-

nism (e.g. Dijkstra). Finally, the CALCOVERLAPS procedure returns the total number of overlaps in the network by summing every $\Delta^k_{i,j}$ factors (as defined in Chapter 6) which denotes the overlapping degree experienced by the paths of any pair of flows f^k_i and $f^k_j \in F_k$.

8.3 Performance Evaluation

In this section, we report simulation results for two case studies. First, we evaluate the case when the *minimal-overlap* routing method assumes an arbitrary gateway designation, and we compare it against a naive shortest-path routing. Second, the case when the *minimal-overlap* routing scheme is used in conjunction with different centrality-driven gateway designation methods using classical network centrality metrics. We compared this latter case with a random gateway designation.

8.3.1 Case 1: Arbitrary Gateway Designation

8.3.1.1 Simulation setup

We break the setup up into two aspects allowing us to assess different workloads and topological conditions: *i*) network topologies and *ii*) network flows.

1) Network topologies. We consider 100 topologies built upon the generation of random graphs. Each graph was created based on a sparse uniformly distributed random matrix of size NxN and density Λ (with Λ in $[0,1] \in \mathbb{R}$). Each sparse matrix acted as an adjacency matrix for the graph generation. The size of the sparse matrix (NxN), and thus the number of vertices in the graph ($N = 66$), were fixed for all the simulation instances (as in [134]). We considered varying values of $\Lambda = \frac{\lambda}{N}$, with λ in the range $[4,12]$, where λ here indicates the median vertex degree of the graph. We justify this choice with practical deployments in which each node is typically required to be connected at least to other 3 nodes in the network (i.e., $\lambda \geq 3$). Note that, in general, this setup provided connected graphs but in the few cases nodes were disconnected we forced a random connection (edge) with any of the other connected vertices.

2) Network flows. For each topology, we consider a random subset of $n \in [2,22] \in N$ sensor nodes generating real-time flows toward the gateway (as in [134]). Arbitrarily, we select as gateway the node with the highest betweenness centrality [2]. Assuming (hop-count-based) shortest path routing, this configuration allows us to generate 100 instances of n shortest path each (for F_0). In alike fashion, we obtain the set of paths for the minimal-overlap routing scheme. This method requires k_{max}[3] and Ψ parameters as input, defined here as $k_{max} = 100$ and $\Psi = \Lambda$ for all the experiments.

Each flow generated has a real-time model representation characterized by the 4-parameter tuple (C_i, D_i, T_i, ϕ_i). Here, C_i represents the effective transmission time (in slots) for the path ϕ_i, obtained directly from the product of the number of hops (or links) traveled by the path ϕ_i from

[2] Note that at the time the experiments were performed, this metric was chosen only to avoid extreme designation conditions (e.g. at the border), but without awareness of their positive impact on the overall traffic schedulability.

[3] We observed empirically that, in general, a greater k_{max} may lead to better results in terms of a number of overlaps but at the cost of higher execution times. Thus, we did not further explore this aspect in this dissertation.

source to destination. This applies to both shortest-path and minimal-overlap routing algorithms. The T_i periods were assumed as random harmonically generated in the form of 2^{η} time slots, with $\eta \in \mathbb{N}$ in the range $[4,7]$ (as in [134]). This assumption leads to direct computation of the hyper-period $H \in \mathbb{N}$ (a.k.a, superframe length) as the maximum period within the range of harmonic periods, or as generally defined, the least common multiple of the set of periods, i.e., $H = lcm(T)$, where $T = \{T_1, T_2, \ldots, T_n\}$. In this case, $H = 2^7 = 128$ slots (or equivalently 1280ms). This value is used as the length of the time interval ℓ for the purposes of schedulability assessment. Traffic schedulability was evaluated using the test described in Chapter 3 yet when considering a worst-case $\Delta_{i,j}$ as in [147]. Finally, we assume $D_i = T_i$ for all the cases, i.e. in implicit-deadline model.

8.3.1.2 Results & Discussion

In the following, we present different performance results for our minimal-overlap (MO) shortest-path routing scheme when compared against a hop-count-based shortest path (SP) method. In all the cases we vary the working load by the parameter n, while considering the impact of other factors. In particular, we evaluate the impact of network density through λ, here representing the average number of neighbor (or links) each node is connected to, as well as the impact of the number of channels m. We recall TSCH allows up to $m = 16$ channels for frequency diversity.

The performance comparison of MO and SP in terms the overall (average) number of overlaps confirms the intuition behind the proposed method. The greedy heuristic search of the MO routing albeit sub-optimal is able to effectively reduce the node-overlapping degree in up to half (and more) of the baseline (see Fig. 8.2a). This, depending of the number of flows and/or the network density. The exponential growth of the number of overlaps as function of the number of flows justifies the need for its mitigation. This trend is also observable in the growth imposed on transmission conflicts, which directly depends on the number of overlaps (see Fig. 8.2c).

The compromise on the route lengths is marginal, whose impact is even negligible on more connected networks (see Fig. 8.2b). The influence on the channel contention is also minor, being discernible (in practice) only on networks with a lower number of active channels (Fig. 8.2d).

The benefits on the overall network schedulability are clear, regardless of the degree of connectivity (Fig. 8.2e) or the available radio channels (Fig. 8.2f), but suggesting superfluous effect on this latter parameter at a given point (see, e.g., $m = 8$ and $m = 16$ in Fig. 8.2f).

8.3.2 Case 2: Centrality-Driven Gateway Designation

8.3.2.1 Simulation Setup

1) Network topologies. We consider 100 mesh topologies generated from synthetic graphs. Each topology is created using a sparse uniformly distributed random matrix of $N \times N$ of zeros and ones, with target density d. N represents the total number of nodes, including the gateway; d is the portion of other nodes each vertex is linked to. We assume $N = 75$ and $d = 0.10$ for all topologies.

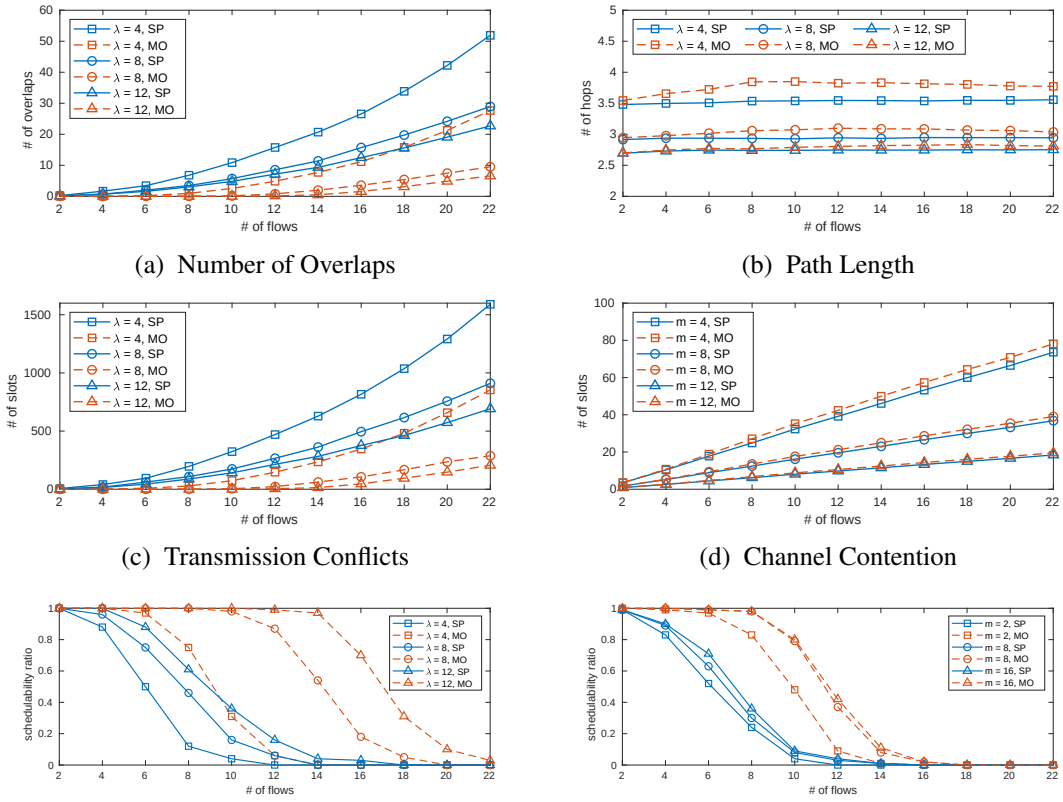

(a) Number of Overlaps

(b) Path Length

(c) Transmission Conflicts

(d) Channel Contention

(e) Schedulability ratio (λ)

(f) Schedulability ratio (m)

Figure 8.2: a) Number of overlaps, b) length of the paths and c) transmission conflicts demand under varying median vertex degree $\lambda = \{4,8,12\}$ and $m = 8$ channels; d) contention demand when varying # of channels $m = \{4,8,12\}$ and median vertex degree $\lambda = 4$; e) schedulability ratio for varying median vertex degree $\lambda = \{4,8,12\}$ and $m = 8$ channels, and f) varying # of channels $m = \{2,8,16\}$ and median vertex degree $\lambda = 4$. All plots consider average results when varying # of flows $n \in [2,22]$ with $N = 66$ nodes.

2) Network flows. A subset of $n \in [1,25]$ nodes is chosen randomly as sensor nodes which transmit periodically deadline-constrained data toward a single gateway. The rest of nodes act as relay. Each period is randomly generated as 2^{η}, with $\eta \in \mathbb{N} \in [2,7]$ slots. This implies a super-frame length of $H = 1280$ ms. C_i is computed directly from the number of hops in ϕ_i and $D_i = T_i$. As in the previous case study, we evaluate the schedulability over an interval equal to the super-frame length, $\ell = H$ using the same performance model. Similarly, we further assume network management is centralized, scheduling uses a global EDF policy, and routing can be either a hop-count-based shortest-path routing (Dijkstra) or the featured MO routing described in Algorithm 2 For MO, we further consider $\Psi = 0.1$ and $k_{max} = 100$.

8.3.2.2 Results & Discussion

Fig. 8.3a (top) presents the schedulability ratio when a gateway is designated based on the degree centrality while a hop-count-based shortest path routing is assumed. Fig. 8.3b (top) shows equiv-

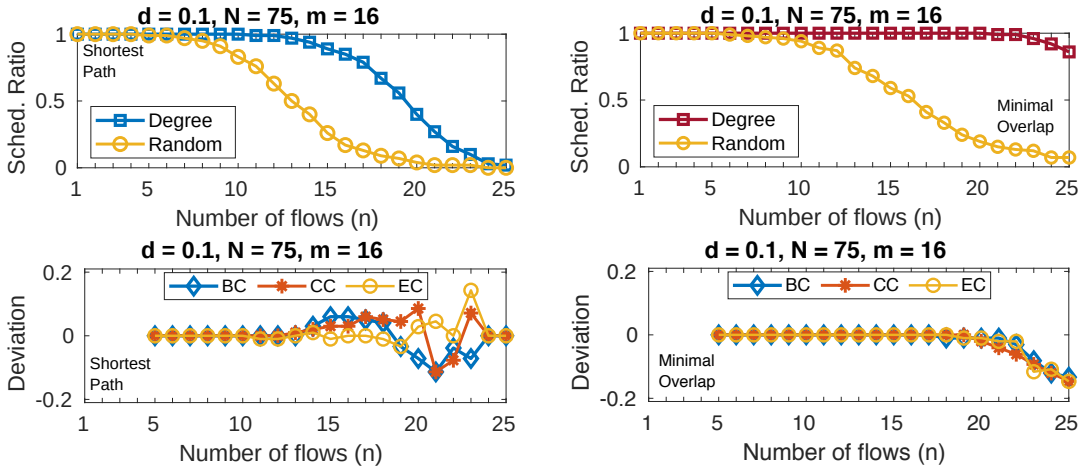

(a) Shortest Path Routing

(b) Minimal Overlap Routing.

Figure 8.3: (Top-row) Schedulability ratio under a varying number of network flows $n \in [1,25]$ for both a) shortest path routing and b) minimal-overlap routing when using the degree centrality metric for gateway designation compared to a random benchmark. (Bottom-row) Absolute deviation in terms of schedulability ratio of the other centrality metrics w.r.t. the degree centrality.

alent results for a gateway designation based on the degree centrality (DC) metric when the MO shortest-path routing is considered. Both configurations also include the case when the gateway is designated randomly. These results show that a joint MO-DC framework can schedule up to 3 times more flows than a basic routing configuration, and up to twice more than the MO only. Notably, achieving up to 80% better schedulability than a naive real-time setting.

Figs. 8.3a (bottom) and 8.3b (bottom) present the absolute deviation in terms of the schedulability ratio for the other centrality metrics (i.e. betweenness (BC), closeness (CC) and eigenvector (EC) types of centrality) with respect to degree centrality. These results suggest none of the metrics dominates over the others, regardless of the routing used. We also observe the deviation among the metrics remains larger (up to $\sim 20\%$) for the shortest path routing, and almost marginal ($< 3\%$) when MO is used; which suggests more predictable spectral properties MO. A random gateway designation is also included to complement the results presented in the previous case study.

8.4 Summary & Concluding Remarks

This chapter has described an original method for real-time wireless routing based on a greedy heuristic for path overlap minimization able to improve traffic schedulability regardless of gateway designation. Simulation results with varying configurations have shown considerable benefits in the two cases studies analyzed: *i*) when considering an arbitrary gateway designation, and *ii*) when used jointly with a centrality-driven gateway designation. Overall, both type of results highlight the importance of routing methods in the real-time performance of mesh WSNs. More importantly, they further stress the multi-dimensional nature of network design problem, showing both

gateway designation and routing dimensions can be complementary when aiming at improving WSNs traffic schedulability at systems design time.

As seen in the prior chapter, a gateway designation with reduced overlapping degree among network flows can considerably benefit real-time network performance. This situation has been further demonstrated by our minimal-overlap routing method which is driven by the same intuition. In this chapter, we have clearly shown that a reduction on path overlapping leads to a reduction in worst-case conflicts delays, and this in turn, to significant benefits in terms of traffic schedulability. Notably, our minimal-overlap routing achieves this with marginal impact on wort-case contention delays, mostly, due to its (weighted) shortest-path restriction.

In the future, we aim to further explore the opportunities for this new routing scheme. For example, it is a clearly open question to be verified if a joint approach with both minimal-overlap methods will lead or not to further improvement in terms traffic schedulability. Similar with the case of multiple-gateway in which flows are typically already balanced among gateways. Another interesting direction to explore is related to its (worst-case) energy-consumption efficiency, which can be driven by alike foundational basis in terms of deterministic guarantees.

Finally, showing its practical usefulness in real-world deployments is a must direction. Not only in arbitrary mesh WSNs replicating realistic situations, but especially in overwater WSNs, often characterized for long-term dynamics. In this direction, we envision an adaptive version of our minimal-overlap routing able to counteract possible changes on the network topology due to tides, by providing source routing paths of minimal-overlap at each point of the tide.

Chapter 9

Conclusions & Future Directions

9.1 Summary

This dissertation has addressed some of the most relevant challenges of wireless network design when dealing with real-time and overwater wireless networked systems. We have covered physical, data-link and network layer considerations, in overall, attempting to improve the performance of such kind of systems beyond the state of the art. Specifically, we have offered contributions with impact in terms of overwater RF propagation (physical), network schedulability (data-link) and routing (networking) under the viewpoint of providing novel solutions with cross-layer incidence.

We started designing each (physical) link of our networked systems taking into account the peculiarities of overwater propagation. In particular, we have addressed path loss performance only since directly related to signal strength, in turn, influencing practical metrics such as range and link stability. We also gave special emphasis to the impact of tides and related features such as intertidal zones, which although barely explored, can impact significantly impact link quality.

In general, we considered scenarios of short to medium range, i.e. between few tens of meters to (no more than) one kilometer, when operating with antennas close and/or very to the water surface. We justified and motivated those settings with two emerging but relevant use cases: IoT-driven environmental monitoring in water environments, and remote control of autonomous surface vehicles at near-shore scenarios. With this in mind, we have provided novel modeling and link design methods that effectively predict and/or improve path loss performance in shore-to-shore and shore-to-vessel configurations. Notably, we have demonstrated part of our findings using commercial wireless technologies, i.e. LoRa and WiFi, targeting sensor nodes in estuaries surroundings, and autonomous underwater vehicles operating at the surface, respectively.

After properly designing the network from the physical point of view, e.g. mitigating the detrimental impact of tidal fading and/or nulls, we have tackled challenges with impact on the upper layers of wireless communication. Concretely, we first introduced the idea of gateway designation in wireless mesh networks for enhanced traffic schedulability. We addressed both single and multi-gateway designation problem by offering straightforward criteria for the selection

of the gateway nodes, based on the notion of network centrality from graph mining. We first evaluate the use of classical metrics (e.g. eigenvector, betweenness, etc.) to then follow an akin insight by proposing a dominant metric, tailored engineered to improve real-time performance in mesh wireless sensor networks.

The novel gateway designation method leverage on the minimization of path node-overlaps, known to influence worst-case end-to-end delays and thus schedulability. The single metric takes advantage of this observation by choosing as gateway the node which leads to the least overall number of overlaps when routing paths are known. The same idea also shown to be useful when generalized to multiple gateways after a spectral clustering process is completed. The gateway designation then occurs at cluster level, offering a novel interpretation of cluster centrality for the proposed metric, as well as by offering a novel and fruitful combination for spectral clustering and centrality in the domain of real-time WSNs. A similar routing method was proposed to improve traffic schedulability by design, regardless of gateway designation. This method was also inspired by the idea of minimize overlaps but using a novel greedy search heuristic to generate source routes of minimal overlaps. Notably, offering complementary benefits in terms of real-time performance when used jointly with a centrality-driven gateway designation.

9.2 Thesis Validation

We aim to verify if the work done so far allow us to validate the following:

> A *judicious* wireless network design which takes into account both *real-time* and *overwater* factors of wireless communication has the potential to significantly improve the performance of *real-time* wireless networked systems operating *over water* environments.

We accompany this thesis statement with the list of our main contributions:

Part I: Overwater Communication

- ✓ A set of novel *tidal-informed* link design methods for improved communication quality with static and mobile surface nodes based on both antenna height and positioning.
- ✓ A novel methodology for *overwater* path-loss prediction based on the non-trivial integration of the *two-ray* propagation model and precise location-dependent *hydrodynamics* modeling.

Part II: Real-Time Communication

- ✓ A new metric termed *minimal overlap centrality* that exploits the relationship between path-node overlaps and gateway designation for improved traffic schedulability.
- ✓ A novel *routing* scheme based on a new greedy heuristic for *minimizing overlaps* that improves schedulability regardless of the gateway designation criterion.

Illustrative example. An integrated panorama of both overwater and real-time communication contributions can be better communicated through our first target use-case: real-time environmental monitoring. We can imagine, for instance, an overwater WSN deployment for dependable water quality monitoring, or for the real-time monitoring of parking slots at a smart marina. This implies a set of sensor nodes transmitting deadline-constrained data with certain periodicity. We can consider a small scale network with tens to one hundred nodes, with one or multiple gateways. At physical level, we can assume each of the network link operate at 2.4 GHz, one of the RF bands used to validate our propagation model. We can further assume the existence of two type of links shore-to-shore (e.g. among two onshore node) and shore-to-vessel (e.g. among a node onshore and another on the water, e.g. a buoy), which are mostly deployed over water, with few of them deployed over an intertidal zone. Consistenly, at data-link level we can assume a MAC sub-layer operation with TSCH operating e.g. over the IEEE 802.15.4 PHY layer (which uses 2.4 GHz). At the network level, we consider a mesh, and the use of source routing. All of these features provide a set of realistic conditions for the network operation.

Discussion. All the research methods proposed in this thesis are strongly aligned with the thesis statement. We provide methods which either use *overwater* or *real-time* factors to provide a *judicious* wireless network design. We consider the illustrative example to further explain how each of the declared contributions is consistent with the thesis direction.

- **1) Tidal-Informed 2-ray-Based Link Design and Positioning**. In the context of the illustrative example, we can benefit from this method to provide a link design that mitigates tidal fading for both S2S and S2V scenarios. Considering the particular feasibility of each link, we can either act on the position or the antenna height to provide links which experience minimal attenuation for a given tidal range. We can even use more than one antenna to further improve the chances to counteract tidal fading. The end goal is to avoid situations in which the signal strength gets reduced to values in which connectivity is lost; thus, improving reliability. By doing this, we argue our method effectively provides a *judicious* link design which contributes to improve the performance of the overall system. Thus, in alignment with the thesis statement.

- **2) Path Loss Prediction Methodology for Intertidal Zones**. For the few links we assumed deployed over an intertidal zone, we need to take care where the reflection point is falling, e.g. if on water or on soil. We then can estimate the expected link quality. If the impact of the intertidal zones is beyond the sensitivity level of the receiver, we can then study alternative to further increase reception, e.g. by controlling antenna height or other parameter depending on the technology. We did not covered specific solutions for this case in our dissertation, but we argue our methodology enables a *judicious* link design over intertidal zones. Thereby, in alignment with the thesis statement.

- **3) Minimal Overlap Gateway Designation**. Once an stable or stationary topology design has been engineered by means of the prior two methods, we can act on different parameters.

In particular, we can select one or multiple nodes to play the role of gateway so as to improve real-time performance with respect to an arbitrary (thus, not *judicious*) gateway designation. We can have the case in which only one gateway is possible and need to be selected among few or many available positions. Our method also enable the study of how many gateway are needed given a network topology, a particular periodicity of nodes and routing behavior. This, therefore contribute to improve performance by (*judicious*) network design.

- **4) Minimal Overlap Shortest-Path Routing**. In the case gateway designation is not possible (or it is not enough), we can further improve performance by means of (*judicious*) routing. We argue that a naive approach which is not aware on the impact of node-overlaps in (worst-case) end-to-end network will lead to sub-optimal paths. We, instead, can offer a set of path of minimal overlaps which facilitate real-time communication. Thus, improving overall performance at systems' design time.

While several limitations and works to be done in the thesis direction can still be mentioned, we believe our research contribution has established a promising path for future work toward the enhancement of real-time and overwater wireless networks by design.

9.3 Future Directions

We envision general and specific future directions for our work. First, after the discussion on the thesis validation, it is clear that work needs to be done to further integrate the methods, and demonstrate the impact of all them working together. Second, and individually for each method, further validation, extensions and related studies are also need to better understand the practical validity of the proposal in different but related contexts, i.e. using different technologies, in different environments, weather conditions, etc. Third, the studies here conducted, although specific for the overwater/real-time communication problems being addressed, have for sure similarities with other problems in related domains, and thus can serve of further inspiration or applicability in those domains. e.g. vehicular, time-sensitive and/or 5G networks.

Despite the many possibilities, we consider the following directions as the more clear and immediate since not covered in the thesis but in which some work still can be done:

- **1) Antenna-Height Design and Positioning Over Intertidal Zones**. As we mentioned earlier, our methodology for path loss prediction over intertidal zones could also be extended to provide antenna-height- and positioning-based methods alike to those we proposed for links deployed over water only. This is not only necessary to further justify the practical utility of our methods but also to further tune the real-world application scenarios.

- **2) Channel Modeling and Characterization for Autonomous Surface Vehicles**. We have provided a novel validation for the two-ray model in challenged scenarios, particularly for AUVs with antenna heights in the order of the wavelength. These studies and methods yet did not consider further observations we did more recently [10], e.g. in terms of the position

of the vessel. We believe this opens a new research line with several potential opportunities for improved channel modeling in these particular scenarios.

- **3) Joint Scheduling, Routing and Gateway Designation**. We have provided results for a centrality-driven gateway designation operating in conjunction with our minimal-overlap routing, but only when considering classical metrics for network centrality. Thus, it is yet to be further clarified in which situations a joint operation of both our minimal-overlap routing and gateway designation together can provide further benefits over the case already evaluated. Additionally, although we have preferred a heuristic-based approach to tackle this problem, an optimality-driven schedulability analysis that considers gateway designation, routing and schedulability together is an open challenge that could also be addressed.

References

[1] Miguel Gutiérrez Gaitán, Pedro M Almeida, Luís d'Orey, Pedro Santos, and Thomas Watteyne. Minimal-overlap network centrality for multi-gateway designation in real-time wireless sensor networks. *ACM Transactions on Embedded Computing Systems*, 2023 (Under Review).

[2] Miguel Gutiérrez Gaitán, Pedro M d'Orey, José Cecílio, Marta Rodrigues, Pedro M Santos, Luis Pinto, Anabela Oliveira, António Casimiro, and Luís Almeida. Modeling LoRa communications in estuaries for IoT environmental monitoring systems. *IEEE Sensors Journal*, 2022.

[3] Miguel Gutiérrez Gaitán, Diego Dujovne, Julián Zuñiga, Alejandro Figueroa, and Luís Almeida. Multi-gateway designation for real-time TSCH networks using spectral clustering and centrality. *IEEE Embedded Systems Letters*, 2022.

[4] Miguel Gutiérrez Gaitán, Pedro M d'Orey, Pedro M Santos, Manuel Ribeiro, Luis Pinto, Luís Almeida, and J Borges De Sousa. Wireless radio link design to improve near-shore communication with surface nodes on tidal waters. In *OCEANS 2021: San Diego–Porto*, pages 1–8. IEEE, 2021.

[5] Miguel Gutiérrez Gaitán, Pedro M Santos, Luis R Pinto, and Luís Almeida. Optimal antenna-height design for improved capacity on over-water radio links affected by tides. In *Global OCEANS 2020: Singapore–US Gulf Coast*, pages 1–7. IEEE, 2020.

[6] Miguel Gutiérrez Gaitán, Pedro M Santos, Luis R Pinto, and Luís Almeida. Experimental evaluation of the two-ray model for near-shore WiFi-based network systems design. In *2020 IEEE 91st Vehicular Technology Conference (VTC2020-Spring)*, pages 1–3. IEEE, 2020.

[7] Miguel Gutiérrez Gaitán, Luis Pinto, Pedro Miguel Santos, and Luís Almeida. On the two-ray model analysis for overwater links with tidal variations. In *11º Simpósio de Informática*, 2019.

[8] Miguel Gutiérrez Gaitán, Pedro d'Orey, Pedro M Santos, and Luis Almeida. Minimal-overlap centrality-driven gateway designation for real-time TSCH networks. In *Real-time And intelliGent Edge computing workshop (RAGE), co-located with 59th Design and Automation Conference (DAC 2022)*, 2022.

[9] Miguel Gutiérrez Gaitán, Luis Almeida, Thomas Watteyne, Pedro M d'Orey, Pedro M Santos, and Diego Dujovne. Joint scheduling, routing and gateway designation in real-time TSCH networks. In *RTNS 2022-30th International Conference on Real-Time Networks and Systems*, 2022.

[10] Pedro M d'Orey, Miguel Gutiérrez Gaitán, Pedro M Santos, Manuel Ribeiro, João B Sousa, and Luís Almeida. Empirical evaluation of short-range wifi vessel-to-shore overwater communications. In *Proceedings of the 16th ACM Workshop on Wireless Network Testbeds, Experimental evaluation & CHaracterization*, pages 77–84, 2022.

[11] Miguel Gutiérrez Gaitán, Luís Almeida, Pedro M Santos, and Patrick Meumeu Yomsi. EDF scheduling and minimal-overlap shortest-path routing for real-time TSCH networks. In *Proceedings of the 2nd Workshop on Next Generation Real-Time Embedded Systems (NG-RES 2021)*, volume 87, pages 2–1. Schloss Dagstuhl–Leibniz-Zentrum für Informatik, 2021.

[12] Miguel Gutiérrez Gaitán, Luís Almeida, Alejandro Figueroa, and Diego Dujovne. Impact of network centrality on the gateway designation of real-time TSCH networks. In *2021 17th IEEE International Conference on Factory Communication Systems (WFCS)*, pages 139–142. IEEE, 2021.

[13] Miguel Gutiérrez Gaitán, Pedro M d'Orey, Pedro M Santos, Manuel Ribeiro, Luıs Pinto, Luıs Almeida, and J Borges de Sousa. Improving WiFi communication with surface nodes at near-shore on tidal waters. In *31º Seminário Rede Temática de Comunicações Móveis (RTCM 2022)*, 2022.

[14] Diogo Almeida, Miguel Gutiérrez Gaitán, Pedro d'Orey, Pedro Miguel Santos, Luis Pinto, and Luís Almeida. Demonstrating RA-TDMAs+ for robust communication in WiFi mesh networks. In *42nd IEEE Real-Time Systems Symposium*, 2021.

[15] Miguel Gutiérrez Gaitán, Luís Almeida, Alejandro Figueroa, and Diego Dujovne. Network centrality: An insight for gateway designation in real-time wireless sensor networks. In *4th Doctoral Congress in Engineering*, 2021.

[16] Miguel Gutiérrez Gaitán, Pedro M d'Orey, Pedro M Santos, Manuel Ribeiro, Luıs Pinto, Luıs Almeida, and J Borges de Sousa. Improving short to medium range communication over water tides: Why does height matters? In *29º Seminário Rede Temática de Comunicações Móveis (RTCM 2021)*, 2022.

[17] Miguel Gutiérrez Gaitán, Pedro Miguel Santos, and Luís Almeida. Real-time communication support for over-water wireless multi-hop networks. In *7th Barcelona Supercomputing Center Severo Ochoa Doctoral Symposium*, pages 51–52, 2020.

[18] Miguel Gutiérrez Gaitán, Pedro M Santos, Luis R Pinto, and Luis Almeida. Wi-Fi-based network systems design over freshwater: Experimental evaluation using COTS devices. In *15th Doctoral Symposium*, page 64, 2020.

[19] Miguel Gutiérrez Gaitán, Luis Pinto, Pedro Miguel Santos, and Luís Almeida. An analysis of the two-ray propagation model to support near-surface overwater wireless sensor networks design. In *Proceedings of the 3rd Doctoral Congress in Engineering (DCE 2019)*, 2019.

[20] Miguel Gutiérrez Gaitán and Patrick Meumeu Yomsi. Multiprocessor scheduling meets the industrial wireless. *U. Porto Journal of Engineering*, 5(1):59–76, 2019a.

[21] Miguel Gutiérrez Gaitán, Ramiro Samano-Robles, and Jonathan Fernández. Outage probability of v2v multiple-antenna rice fading links with explicit ground reflection. In *IEEE Global Communication Conference (GLOBECOM 2022)*, 2022.

[22] Miguel Gutiérrez Gaitán and Ramiro Samano-Robles. Orthogonal space-time block coding for V2V LOS links with ground reflections. In *24th International Microwave and Radar Conference (MIKON 2022)*, 2022.

[23] Esteban De La Fuente Rubio and Miguel Gutiérrez Gaitán. Libredte: Software tools and support for electronic invoicing in chile. In *2021 40th International Conference of the Chilean Computer Science Society (SCCC)*, pages 1–6. IEEE, 2021.

[24] Radha Reddy, Luís Almeida, Miguel Gutiérrez Gaitán, Pedro Miguel Santos, and Eduardo Tovar. Synchronous framework extended for complex intersections. In *24th Euro Working Group on Transportation Meeting*, 2021.

[25] Miguel Gutiérrez Gaitán and Ramiro Sámano-Robles. In-tunnel multi-ray analysis for los V2V links with multiple antennas. In *2021 IEEE 7th World Forum on Internet of Things (WF-IoT)*, pages 783–788. IEEE, 2021.

[26] Miguel Gutiérrez Gaitán, Ramiro Sámano-Robles, and Amir Hossein Farzamiyan. On the optimum number of antennas for V2V LOS links with ground reflection. In *2020 IEEE MTT-S Latin America Microwave Conference (LAMC 2020)*, pages 1–3. IEEE, 2021.

[27] Fernando Lizana, Ricardo Tello, Miguel Gutiérrez Gaitán, David Ruete, and Carlos Gómez-Pantoja. Building a text messaging-based system to support low-cost automation in household agriculture. In *2020 Congreso Estudiantil de Electrónica y Electricidad (INGELECTRA)*, pages 1–5. IEEE, 2020.

[28] Amir Hossein Farzamiyan, Miguel Gutiérrez Gaitán, and Ramiro Sámano-Robles. A multi-ray analysis of LOS V2V links for multiple antennas with ground reflection. In *2020 AEIT International Annual Conference (AEIT)*, pages 1–6. IEEE, 2020.

[29] Radha Reddy, Luís Almeida, Miguel Gaitan, Harrison Kurunathan, Pedro Santos, and Eduardo Tovar. Work-in-progress: Worst-case response time of intersection management protocols. In *2021 IEEE Real-Time Systems Symposium (RTSS)*, pages 556–559. IEEE, 2021.

[30] Miguel Gutiérrez Gaitán, Patrick M Yoms, Pedro M Santo, and Luís Almeida. Work-in-progress: Assessing supply/demand-bound based schedulability tests for wireless sensor-actuator networks. In *2020 16th IEEE International Conference on Factory Communication Systems (WFCS)*, pages 1–4. IEEE, 2020.

[31] Miguel Gutiérrez and Patrick Meumeu Yomsi. Ff-dbf-win: On the forced-forward demand-bound function analysis for wireless industrial networks. *Proceedings of the Work-in-Progress Session (ECRTS 2018)*, pages 13–15, 2018.

[32] Radha Reddy, Luís Almeida, Miguel Gutiérrez Gaitán, Pedro Miguel Santos, and Eduardo Tovar. Sustainability analysis of complex multi-lane intelligent signalized intersections. In *Doctoral Congress in Engineering*, 2021.

[33] Radha Reddy, Luis Almeida, Miguel Gutiérrez Gaitán, Pedro Miguel Santos, and Eduardo Tovar. Impact of intersection management on energy-efficiency when mixing electric and combustion vehicles. In *23rd EURO Working Group on Transportation Meeting*, 2020.

[34] Christopher Haslett. *Essentials of Radio Wave Propagation*. Cambridge University Press, USA, 1st edition, 2008.

[35] Artur Zolich, David Palma, Kimmo Kansanen, Kay Fjørtoft, João Sousa, Karl H Johansson, Yuming Jiang, Hefeng Dong, and Tor A Johansen. Survey on communication and networks for autonomous marine systems. *Journal of Intelligent & Robotic Systems*, pages 1–25, 2018.

[36] Te Wei, Wei Feng, Yunfei Chen, Cheng-Xiang Wang, Ning Ge, and Jianhua Lu. Hybrid satellite-terrestrial communication networks for the maritime Internet of Things: Key technologies, opportunities, and challenges. *IEEE Internet of Things Journal*, 8(11):8910–8934, 2021.

[37] Jue Wang, Haifeng Zhou, Ye Li, Qiang Sun, Yongpeng Wu, Shi Jin, Tony QS Quek, and Chen Xu. Wireless channel models for maritime communications. *IEEE Access*, 6:68070–68088, 2018.

[38] Wei Chen, Changzhen Li, Junyi Yu, et al. A survey of maritime communications: From the wireless channel measurements and modeling perspective. *Regional Studies in Marine Science*, 48:102031, 2021.

[39] O Mendoza-Cano, R Aquino-Santos, J López-De La Cruz, Robert M Edwards, A Khouakhi, I Pattison, V Rangel-Licea, E Castellanos-Berjan, MA Martinez-Preciado, P Rincón-Avalos, et al. Experiments of an IoT-based wireless sensor network for flood monitoring in Colima, Mexico. *Journal of Hydroinformatics*, 23(3):385–401, 2021.

[40] José Cecílio, Pedro M Ferreira, and António Casimiro. Evaluation of LoRa technology in flooding prevention scenarios. *Sensors*, 20(14):4034, 2020.

[41] Roberto Girau, Matteo Anedda, Mauro Fadda, Massimo Farina, Alessandro Floris, Mariella Sole, and Daniele Giusto. Coastal monitoring system based on social Internet of Things platform. *IEEE Internet of Things Journal*, 7(2):1260–1272, 2019.

[42] Tommaso Zugno, Filippo Campagnaro, and Michele Zorzi. Controlling in real-time an ASV-carried ROV for quay wall and ship hull inspection through wireless links in harbor environments. In *Global Oceans 2020: Singapore–US Gulf Coast*, pages 1–9. IEEE, 2020.

[43] UN General Assembly. Transforming our world: The 2030 agenda for sustainable development. 2015.

[44] Oratile Khutsoane, Bassey Isong, Naison Gasela, and Adnan M Abu-Mahfouz. Watergridsense: A LoRa-based sensor node for industrial iot applications. *IEEE Sensors Journal*, 20(5):2722–2729, 2019.

[45] Yujae Song, Huicheol Shin, Sungmin Koo, Seungjae Baek, Jungmin Seo, Hyoun Kang, and Yongjae Kim. Internet of maritime things platform for remote marine water quality monitoring. *IEEE Internet of Things Journal*, pages 1–1, 2021.

[46] Usman Raza, Parag Kulkarni, and Mahesh Sooriyabandara. Low power wide area networks: An overview. *IEEE Communications Surveys & Tutorials*, 19(2):855–873, 2017.

[47] Lorenzo Parri, Stefano Parrino, Giacomo Peruzzi, and Alessandro Pozzebon. Low power wide area networks (LPWAN) at sea: Performance analysis of offshore data transmission by means of LoRaWAN connectivity for marine monitoring applications. *Sensors*, 19(14):3239, 2019.

[48] Yuting Wang, Xiaolong Zheng, Liang Liu, and Huadong Ma. PolarTracker: Attitude-aware channel access for floating low power wide area networks. In *IEEE Conference on Computer Communications*, pages 1–10. IEEE, 2021.

[49] Lalit Baghel, Sukriti Gautam, Vikas Malav, and Suman Kumar. TEMPSENSE: LoRa enabled integrated sensing & localization solution for water quality monitoring. *IEEE Trans. on Instrumentation and Measurement*, 2022.

[50] António Casimiro, J Cecılio, Pedro Ferreira, Anabela Oliveira, Paula Freire, Marta Rodrigues, and Luís Almeida. AQUAMON–a dependable monitoring platform based on wireless sensor networks for water environments. In *Proceedings of the 38th International Conference on Computer Safety, Reliability and Security*, 2019.

[51] Jose Pinto, Maria Costa, Renato Mendes, Keila Lima, Paulo Dias, João Pereira, Manuel Ribeiro, Renato Campos, Maria Paola Tomasino, Catarina Magalhães, Francisco López-Castejón, Javier Gilabert, Adriana M. Santos-Ferreira, José Silva, Paulo Relvas, Trent Lukaczyk, Kay Skarpnes, Emlyn Davies, Alexander Chekalyuk, and Kanna Rajan. Coordinated robotic exploration of dynamic open ocean phenomena. *Field Robotics*, 2:843–871, 2022.

[52] Emir Cem Gezer, Lin Zhao, Jordan Beason, and Mingxi Zhou. Towards seafloor mapping using an affordable micro-UUV. In *IEEE OCEANS*, pages 1–5, San Diego, USA, 2021. IEEE.

[53] Benedetto Allotta, Riccardo Costanzi, Francesco Fanelli, Niccolò Monni, Libero Paolucci, and Alessandro Ridolfi. Sea currents estimation during AUV navigation using unscented Kalman filter. *IFAC World Congress*, 50(1):13668–13673, 2017.

[54] Hongwei Zhang, Shitong Zhang, Yanhui Wang, Yuhong Liu, Yanan Yang, Tian Zhou, and Hongyu Bian. Subsea pipeline leak inspection by autonomous underwater vehicle. *Applied Ocean Research*, 107:102321, 2021.

[55] Yiming Huo, Xiaodai Dong, and Scott Beatty. Cellular communications in ocean waves for maritime Internet of Things. *IEEE Internet of Things Journal*, 7(10):9965–9979, 2020.

[56] Sanghai Guan, Jingjing Wang, Chunxiao Jiang, Ruiyang Duan, Yong Ren, and Tony Q. S. Quek. MagicNet: the maritime giant cellular network. *IEEE Communications Magazine*, 59(3):117–123, 2021.

[57] Ruinan Li Li, Xiaolong Zheng, Yuting Wang, Liang Liu, and Huadong Ma. Polarscheduler: Dynamic transmission control for floating lora networks. In *IEEE International Conference on Computer Communications (INFOCOM)*, pages 550–559, virtual, 2022. IEEE.

[58] Filipe B Teixeira, Tiago Oliveira, Mário Lopes, José Ruela, Rui Campos, and Manuel Ricardo. Tethered balloons and tv white spaces: A solution for real-time marine data transfer at remote ocean areas. In *IEEE Third Underwater Communications and Networking Conference (UComms)*, pages 1–5, Lerici, Italy, 2016. IEEE.

[59] Gianluca Antonelli, Giovanni Indiveri, Carlos Barrera, Massimo Caccia, Gerard Dooly, Niamh Flavin, Fausto Ferreira, Nikola Mišković, Maaten Furlong, Achim Kopf, et al. Advancing the EU marine robotics research infrastructure network: the EU marine robots project. In *OCEANS 2021: San Diego–Porto*, pages 1–10. IEEE, 2021.

[60] David Pugh and Philip Woodworth. *Sea-level science: understanding tides, surges, tsunamis and mean sea-level changes*. Cambridge University Press, 2014.

[61] Giorgio C Buttazzo. *Hard real-time computing systems: predictable scheduling algorithms and applications*, volume 24. Springer Science & Business Media, 2011.

[62] Scott Bainbridge, Damien Eggeling, and Geoff Page. Lessons from the field—two years of deploying operational wireless sensor networks on the great barrier reef. *Sensors*, 11(7):6842–6855, 2011.

[63] Yoshio Karasawa and Takayasu Shiokawa. Characteristics of L-band multipath fading due to sea surface reflection. *IEEE transactions on antennas and propagation*, 32(6):618–623, 1984.

[64] Wei Wang, Thomas Jost, and Ronald Raulefs. A semi-deterministic path loss model for in-harbor LoS and NLoS environment. *IEEE Transactions on Antennas and Propagation*, 65(12):7399–7404, 2017.

[65] Changzhen Li, Junyi Yu, Wei Chen, Kun Yang, and Fang Li. Shadowing correlation and a novel statistical model for inland river radio channel. In *ICC 2019-2019 IEEE International Conference on Communications (ICC)*, pages 1–6. IEEE, 2019.

[66] Wei Wang, Gerald Hoerack, Thomas Jost, Ronald Raulefs, Michael Walter, and Uwe-Carsten Fiebig. Propagation channel at 5.2 GHz in baltic sea with focus on scattering phenomena. In *2015 9th European Conference on Antennas and Propagation (EuCAP)*, pages 1–5. IEEE, 2015.

[67] Alex Macmillan, Mahesh K Marina, and Jhair Tocancipa Triana. Slow frequency hopping for mitigating tidal fading on rural long distance over-water wireless links. In *IEEE Conference on Computer Communications (INFOCOM) Workshops*, pages 1–5. IEEE, 2010.

[68] DW Taplin. Tidal fading on short oversea paths elliptical, vertical and horizontal polarisation compared. *NASA STI/Recon Technical Report N*, 76:15328, 1975.

[69] Giacomo Bernardi, Peter Buneman, and Mahesh K Marina. Tegola tiered mesh network testbed in rural scotland. In *ACM Workshop on Wireless networks and systems for developing regions*, pages 9–16, 2008.

[70] Khurram Shabih Zaidi, Varun Jeoti, Micheal Drieberg, Azlan Awang, and Asif Iqbal. Fading characteristics in evaporation duct: Fade margin for a wireless link in the south china sea. *IEEE Access*, 6:11038–11045, 2018.

[71] Brennan Yamamoto, Allison Wong, Peter Joseph Agcanas, Kai Jones, Dominic Gaspar, Raymond Andrade, and A Zachary Trimble. Received signal strength indication (RSSI) of 2.4 GHz and 5 GHz wireless local area network systems projected over land and sea for near-shore maritime robot operations. *Journal of Marine Science and Engineering*, 7(9):290, 2019.

[72] André Coelho, Mário Lopes, Bruno Ferreira, Rui Campos, and Manuel Ricardo. Experimental evaluation of shore to unmanned surface vehicle Wi-Fi communications. In *2018 Wireless Days (WD)*, pages 86–91. IEEE, 2018.

[73] Chee-Wei Ang and Su Wen. Signal strength sensitivity and its effects on routing in maritime wireless networks. In *2008 33rd IEEE Conference on Local Computer Networks (LCN)*, pages 192–199. IEEE, 2008.

[74] Changzhen Li, Junyi Yu, Wei Chen, Kehao Wang, Shoufeng Wang, Kun Yang, and Xiaofeng Wu. Measurement-based wireless channel analysis and modelling for shipping environments. *IET Microwaves, Antennas & Propagation*, 14(8):812–820, 2020.

[75] Liuguo Yin, Chuanao Jiang, Chunxiao Jiang, and Yi Qian. Collaborative spectrum managements and sharing in coordinated space, terrestrial and ocean networks. *IEEE Network*, 34(1):182–187, 2019.

[76] Deji Chen, Mark Nixon, Song Han, Aloysius K Mok, and Xiuming Zhu. WirelessHART and IEEE 802.15. 4e. In *2014 IEEE International conference on industrial technology (ICIT)*, pages 760–765. IEEE, 2014.

[77] Diego Dujovne, Thomas Watteyne, Xavier Vilajosana, and Pascal Thubert. 6TiSCH: deterministic IP-enabled industrial internet (of things). *IEEE Communications Magazine*, 52(12):36–41, 2014.

[78] Chung Laung Liu and James W Layland. Scheduling algorithms for multiprogramming in a hard-real-time environment. *Journal of the ACM (JACM)*, 20(1):46–61, 1973.

[79] Andrea Goldsmith. *Wireless Communications*. Cambridge Univ. Press, 2005.

[80] Theodore S Rappaport. *Wireless Communications: Principles and practice*. Prentice Hall Communications Engineering and Emerging Technologies Series. Prentice Hall, 2nd edition, 2002.

[81] Chengjie Wu, Mo Sha, Dolvara Gunatilaka, Abusayeed Saifullah, Chenyang Lu, and Yixin Chen. Analysis of EDF scheduling for wireless sensor-actuator networks. In *2014 IEEE 22nd International Symposium of Quality of Service (IWQoS)*, pages 31–40. IEEE, 2014.

[82] Abusayeed Saifullah, You Xu, Chenyang Lu, and Yixin Chen. Priority assignment for real-time flows in wirelesshart networks. In *2011 23rd Euromicro Conference on Real-Time Systems*, pages 35–44. IEEE, 2011.

[83] Laurent Chasserat, Nicola Accettura, and Pascal Berthou. Short: Achieving energy efficiency in dense lorawans through tdma. In *2020 IEEE 21st International Symposium on" A World of Wireless, Mobile and Multimedia Networks"(WoWMoM)*, pages 26–29. IEEE, 2020.

[84] Vasileios Asteriou, Anastasios Valkanis, Georgia Beletsioti, Konstantinos Kantelis, Georgios Papadimitriou, and Petros Nicopolitidis. Lorawan-based adaptive macs for event response applications. *IEEE Access*, 10:97465–97480, 2022.

[85] Dolvara Gunatilaka, Mo Sha, and Chenyang Lu. Impacts of channel selection on industrial wireless sensor-actuator networks. In *IEEE INFOCOM 2017-IEEE Conference on Computer Communications*, pages 1–9. IEEE, 2017.

[86] Frederico Santos, Luís Almeida, and Luís Seabra Lopes. Self-configuration of an adaptive TDMA wireless communication protocol for teams of mobile robots. In *2008 IEEE International Conference on Emerging Technologies and Factory Automation*, pages 1197–1204. IEEE, 2008.

[87] Aqsa Aslam, Luís Almeida, and Frederico Santos. A flexible tdma overlay protocol for vehicles platooning. In *International Workshop on Communication Technologies for Vehicles*, pages 169–180. Springer, 2018.

[88] Luis Ramos Pinto, Luis Almeida, Hassan Alizadeh, and Anthony Rowe. Aerial video stream over multi-hop using adaptive tdma slots. In *2017 IEEE Real-Time Systems Symposium (RTSS)*, pages 157–166. IEEE, 2017.

[89] Luis Oliveira, Luís Almeida, and Daniel Mossé. A clockless synchronisation framework for cooperating mobile robots. In *2018 IEEE Real-Time and Embedded Technology and Applications Symposium (RTAS)*, pages 305–315. IEEE, 2018.

[90] Federico Terraneo, Federico Amedeo Izzo, Alberto Leva, and William Fornaciari. Tdmh: A communication stack for real-time wireless mesh networks. *arXiv preprint arXiv:2006.03554*, 2020.

[91] DA Robinson, JD Cooper, and CMK Gardner. Modelling the relative permittivity of soils using soil hygroscopic water content. *Journal of Hydrology*, 255(1-4):39–49, 2002.

[92] JR Wang. The dielectric properties of soil-water mixtures at microwave frequencies. *Radio Science*, 15(05):977–985, 1980.

[93] Recommendation ITU. Electrical characteristics of the surface of the earth. *ITU-R P.527-4*, 2017.

[94] Giulio Maria Bianco, Romeo Giuliano, Gaetano Marrocco, Franco Mazzenga, and Abraham Mejia-Aguilar. LoRa system for search and rescue: path-loss models and procedures in mountain scenarios. *IEEE Internet of Things Journal*, 8(3):1985–1999, 2020.

[95] Carlos A Oroza, Ziran Zhang, Thomas Watteyne, and Steven D Glaser. A machine-learning-based connectivity model for complex terrain large-scale low-power wireless deployments. *IEEE Transactions on Cognitive Communications and Networking*, 3(4):576–584, 2017.

[96] A Mondloch. Overwater propagation of millimeter waves. *IEEE Trans. on Antennas and Propagation*, 17(1):82–85, 1969.

[97] Miguel Pereira. Spread spectrum techniques in wireless communication part 2: Transmission issues in free space. *IEEE instrumentation & measurement magazine*, 13(1):8–14, 2010.

[98] Naoki Fuke, Keizo Sugiyama, and Hideyuki Shinonaga. Long-range oversea wireless network using 2.4 GHz wireless LAN installation and performance. In *Proc. of the International Conference on Computer Communications and Networks (ICCCN)*, pages 351–356. IEEE, 2003.

[99] Yvon-Marie Le Roux, Jacky Ménard, Claude Toquin, Jean-Pierre Jolivet, and Fabien Nicolas. Experimental measurements of propagation characteristics for maritime radio links. In *International Conference on Intelligent Transport Systems Telecommunications (ITST)*, pages 364–369. IEEE, 2009.

[100] Gilles Callebaut and Liesbet Van der Perre. Characterization of LoRa point-to-point path loss: measurement campaigns and modeling considering censored data. *IEEE Internet of Things Journal*, 7(3):1910–1918, 2019.

[101] Amado Gutiérrez-Gómez, Víctor Rangel, Robert Edwards, et al. A Propagation Study of LoRa P2P Links for IoT Applications: The Case of Near-Surface Measurements over Semitropical Rivers. *Sensors*, 21(20), 2021.

[102] Xinyan Zhou, Xiaoyu Ji, Yi-chao Chen, et al. LESS: Link estimation with sparse sampling in intertidal WSNs. *Sensors*, 18(3):747, 2018.

[103] Xinyan Zhou, Yongjie Li, Di He, Chengyi Zhang, and Xiaoyu Ji. Energy-efficient channel allocation based data aggregation for intertidal wireless sensor networks. *IEEE Sensors Journal*, 2021.

[104] Miao Xu and Wenyuan Xu. Taco: Temperature-aware compensation for time synchronization in wireless sensor networks. In *IEEE International Conference on Mobile Ad-Hoc and Sensor Systems*, pages 122–130. IEEE, 2013.

[105] Allan Braga, Hugo Da Cruz, Leslye Eras, et al. Radio Propagation Models Based on Machine Learning Using Geometric Parameters for a Mixed City-River Path. *IEEE Access*, 8:146395–146407, 2020.

[106] Alex Macedo, Leslye Castro, Diego da Silva, et al. Mixed Path Model for Urban and Suburban City-River Path for 1,400 MHz. In *IEEE International Microwave and Optoelectronics Conference*, pages 1–3. IEEE, 2019.

[107] Thiago da Silva, Alaim Costa, Diego da Silva, Leslye Castro, Jasmine Araujo, and Gervásio Cavalcante. Radio propagation for the amazon region considering the river level. In *Workshop on Communication Networks and Power Systems (WCNPS)*, pages 1–4. IEEE, 2019.

[108] LJ Carter. UHF propagation over a cluttered, mixed land/water path. In *1991 Sixth International Conference on Mobile and Personal Communications*, pages 1–6. IET, 1993.

[109] Sanjoy Baruah, Vincenzo Bonifaci, Alberto Marchetti-Spaccamela, and Sebastian Stiller. Improved multiprocessor global schedulability analysis. *Real-Time Systems*, 46(1):3–24, 2010.

[110] Changqing Xia, Xi Jin, and Peng Zeng. Resource analysis for wireless industrial networks. In *International Conference on Mobile Ad-Hoc and Sensor Networks (MSN)*, pages 424–428. IEEE, 2016.

[111] Rebiha Souadih and Fouzi Semchedine. Energy-efficient coverage and connectivity of wireless sensor network in the framework of hybrid sensor and vehicular network. *International Journal of Computers and Applications*, 44(5):444–454, 2022.

[112] Bo Xing, Mayur Deshpande, Sharad Mehrotra, and Nalini Venkatasubramanian. Gateway designation for timely communications in instant mesh networks. In *2010 8th IEEE International Conference on Pervasive Computing and Communications Workshops (PERCOM Workshops)*, pages 564–569. IEEE, 2010.

[113] Wei Liu, Hiroki Nishiyama, Nei Kato, Yoshitaka Shimizu, and Tomoaki Kumagai. A novel gateway selection method to maximize the system throughput of wireless mesh network deployed in disaster areas. In *2012 IEEE 23rd International Symposium on Personal, Indoor and Mobile Radio Communications-(PIMRC)*, pages 771–776. IEEE, 2012.

[114] Usman Ashraf, Slim Abdellatif, and Guy Juanole. Gateway selection in backbone wireless mesh networks. In *2009 IEEE Wireless Communications and Networking Conference*, pages 1–6. IEEE, 2009.

[115] Sylia Mekhmoukh Taleb, Yassine Meraihi, Asma Benmessaoud Gabis, Seyedali Mirjalili, and Amar Ramdane-Cherif. Nodes placement in wireless mesh networks using optimization approaches: A survey. *Neural Computing and Applications*, pages 1–37, 2022.

[116] Naércio Magaia, Alexandre P Francisco, Paulo Pereira, and Miguel Correia. Betweenness centrality in delay tolerant networks: A survey. *Ad Hoc Networks*, 33:284–305, 2015.

[117] Wei Koong Chai, Diliang He, Ioannis Psaras, and George Pavlou. Cache "less for mmore" in information-centric networks. *Computer Communications*, 36(7):758–770, 2013.

[118] Eduardo MR Oliveira, Heitor S Ramos, and Antonio AF Loureiro. Centrality-based routing for wireless sensor networks. In *2010 IFIP Wireless Days*, pages 1–5. IEEE, 2010.

[119] Andrés Vázquez-Rodas and J Luis. A centrality-based topology control protocol for wireless mesh networks. *Ad Hoc Networks*, 24:34–54, 2015.

[120] Leonardo Maccari, Quynh Nguyen, and Renato Lo Cigno. On the computation of centrality metrics for network security in mesh networks. In *2016 IEEE Global Communications Conference (GLOBECOM)*, pages 1–6. IEEE, 2016.

[121] Maryam Vahabi, Hamid Reza Faragardi, and Hossein Fotouhi. An analytical model for deploying mobile sinks in Industrial Internet of Things. In *IEEE Wireless Communications and Networking Conference Workshops*, pages 155–160. IEEE, 2018.

[122] Arvind Kumar, Rakesh Matam, and Mithun Mukherjee. Time optimal concurrent data collection trees for iot applications. In *2021 IEEE International Systems Conference (SysCon)*, pages 1–7. IEEE, 2021.

[123] Yu-Shu Chen, Shih-Ying Chang, Tzu-Wen Chang, and Ming-Jer Tsai. Multiple sink placement with latency and reliability guarantee in lossy wireless sensor networks. In *IEEE Global Communications Conference (GLOBECOM)*, pages 1–7. IEEE, 2018.

[124] Felix Dobslaw, Tingting Zhang, and Mikael Gidlund. QoS-aware cross-layer configuration for industrial wireless sensor networks. *IEEE Transactions on Industrial Informatics*, 12(5):1679–1691, 2016.

[125] Nicola Accettura, Elvis Vogli, Maria Rita Palattella, Luigi Alfredo Grieco, Gennaro Boggia, and Mischa Dohler. Decentralized traffic aware scheduling in 6tisch networks: Design and experimental evaluation. *IEEE Internet of Things Journal*, 2(6):455–470, 2015.

[126] Luca Mottola and Gian Pietro Picco. Muster: Adaptive energy-aware multisink routing in wireless sensor networks. *IEEE Transactions on Mobile Computing*, 10(12):1694–1709, 2010.

[127] Adrian Lang, Yi Wang, Cheng Feng, Eleni Stai, and Gabriela Hug. Data aggregation point placement for smart meters in the smart grid. *IEEE Transactions on Smart Grid*, 13(1):541–554, 2021.

[128] Abusayeed Saifullah, You Xu, Chenyang Lu, and Yixin Chen. Real-time scheduling for WirelessHART networks. In *2010 31st IEEE Real-Time Systems Symposium (RTSS)*, pages 150–159. IEEE, 2010.

[129] Giuliana Alderisi, Svetlana Girs, Lucia Lo Bello, Elisabeth Uhlemann, and Mats Björkman. Probabilistic scheduling and adaptive relaying for WirelessHART networks. In *2015 IEEE 20th Conference on Emerging Technologies & Factory Automation (ETFA)*, pages 1–4. IEEE, 2015.

[130] Keoma Brun-Laguna, Pascale Minet, and Yasuyuki Tanaka. Optimized scheduling for time-critical industrial IoT. In *2019 IEEE Global Communications Conference (GLOBECOM)*, pages 1–6. IEEE, 2019.

[131] Stefano Scanzio, Mohammad Ghazi Vakili, Gianluca Cena, Claudio Giovanni Demartini, Bartolomeo Montrucchio, Adriano Valenzano, and Claudio Zunino. Wireless sensor networks and TSCH: A compromise between reliability, power consumption, and latency. *IEEE Access*, 8:167042–167058, 2020.

[132] Harrison Kurunathan, Ricardo Severino, Anis Koubâa, and Eduardo Tovar. Worst-case bound analysis for the time-critical MAC behaviors of IEEE 802.15. 4e. In *2017 IEEE 13th International Workshop on Factory Communication Systems (WFCS)*, pages 1–9. IEEE, 2017.

[133] Marcelo Nobre, Ivanovitch Silva, and Luiz Affonso Guedes. Routing and scheduling algorithms for WirelessHART networks: A survey. *Sensors*, 15(5):9703–9740, 2015.

[134] Chengjie Wu, Dolvara Gunatilaka, Mo Sha, and Chenyang Lu. Real-time wireless routing for Industrial Internet of Things. In *2018 IEEE/ACM Third International Conference on Internet-of-Things Design and Implementation (IoTDI)*, pages 261–266. IEEE, 2018.

[135] Alexandre Sousa, Luis Madureira, Jorge Coelho, José Pinto, João Pereira, João Borges Sousa, and Paulo Dias. Lauv: The man-portable autonomous underwater vehicle. *IFAC Proceedings Volumes*, 45(5):268–274, 2012.

[136] Christopher Haslett. *Essentials of Radio Wave Propagation*. Cambridge University Press, New York, NY, USA, 1st edition, 2008.

[137] Ehab Salahat, Ahmed Kulaib, Nazar Ali, and Raed Shubair. Exploring symmetry in wireless propagation channels. In *2017 European Conference on Networks and Communications (EuCNC)*, pages 1–6, 2017.

[138] Marta Rodrigues and André Fortunato. Assessment of a three-dimensional baroclinic circulation model of the tagus estuary (Portugal). *AIMS Environmental Science*, 4(6):763–787, 2017.

[139] M. Rodrigues, R. Martins, J. Rogeiro, A. B. Fortunato, A. Oliveira, A. Cravo, J. Jacob, A. Rosa, A. Azevedo, and P. Freire. A Web-Based Observatory for Biogeochemical Assessment in Coastal Regions. *Journal of Environmental Informatics*, 38(1), 2021.

[140] LEE Yee Hui, Feng Dong, and Yu Song Meng. Near sea-surface mobile radiowave propagation at 5 GHz: measurements and modeling. *Radioengineering*, 23(3):824–830, 2014.

[141] Ergin Dinc and Ozgur B. Akan. Channel model for the surface ducts: Large-scale path-loss, delay spread, and AOA. *IEEE Transactions on Antennas and Propagation*, 63(6):2728–2738, 2015.

[142] Thomas W Valente, Kathryn Coronges, Cynthia Lakon, and Elizabeth Costenbader. How correlated are network centrality measures? *Connections*, 28(1):16, 2008.

[143] Andrew Ng, Michael Jordan, and Yair Weiss. On spectral clustering: Analysis and an algorithm. *Advances in Neural Information Processing Systems*, 14, 2001.

[144] Dongkuan Xu and Yingjie Tian. A comprehensive survey of clustering algorithms. *Annals of Data Science*, 2(2):165–193, 2015.

[145] Mayra Z. Rodriguez, Cesar H. Comin, Dalcimar Casanova, Odemir M. Bruno, Diego R. Amancio, Luciano da F. Costa, and Francisco A. Rodrigues. Clustering algorithms: A comparative approach. *PLOS ONE*, 14(1):1–34, 01 2019.

[146] Maria Nascimento and Andre De Carvalho. Spectral methods for graph clustering– a survey. *European Journal of Operational Research*, 211(2):221–231, 2011.

[147] Venkata Prashant Modekurthy, Dali Ismail, Mahbubur Rahman, and Abusayeed Saifullah. A utilization-based approach for schedulability analysis in wireless control systems. In *2018 IEEE International Conference on Industrial Internet (ICII)*, pages 49–58. IEEE, 2018.

[148] Abusayeed Saifullah, You Xu, Chenyang Lu, and Yixin Chen. End-to-end communication delay analysis in industrial wireless networks. *IEEE Transactions on Computers*, 64(5):1361–1374, 2014.